Modeling Active Perception Sensors for Real-Time Virtual Validation of Automated Driving Systems

Vom Fachbereich Maschinenbau an der
Technischen Universität Darmstadt
zur Erlangung des Grades eines
Doktor-Ingenieurs (Dr.-Ing.)
genehmigte

Dissertation

vorgelegt von

Peng Cao, M. Sc.
aus Shanghai

Berichterstatter:	Prof. Dr. rer. nat. Hermann Winner
Mitberichterstatter:	Prof. Dr. techn. Arno Eichberger
Tag der Einreichung:	18.10.2017
Tag der mündlichen Prüfung:	20.12.2017

Darmstadt 2017
D 17

Preface

This work was written during my work as a research associate of the Institute of Automotive Engineering (FZD) at Technical University Darmstadt. The contents of this work were developed in the research project “ModUs A²”. “ModUs A²” was funded by the Federal Ministry of Economic Affairs and Energy (BMWI) in cooperation with the company, IPG Automotive GmbH, within the framework of “Central Innovation Program for Medium-sized Companies (ZIM)”.

I would like to thank Mr. Prof. Dr. rer. nat. Hermann Winner for his excellent guidance and support during my work. He is always available and willing to answer my queries. The countless expert discussions have always inspired me and made a lasting impression.

I would like to thank Mr. Prof. Dr. techn. Arno Eichberger for taking over the co-supervision and the professional exchange, which were very constructive for solving research questions.

I would like to thank the BMWi for its funding and the possibility of investigating an exciting scientific topic. For the implementation of the project “ModUs A²”, I would like to thank all the project colleagues in IPG Automotive GmbH for their support in the integration of the models.

To my other colleagues at FZD: I would like to thank you for your wonderful cooperation and support as well. Without this, many attempts would not have been possible. The competent support from the secretariat and the workshops has always helped me as well.

I also benefitted from debating issues with my friends and family. Your kind suggestions and encouragement kept me moving forwards. My parents deserve a particular note of thanks: your wise counsel and kind words have, as always, served me well.

Last but not least, I would like to thank my wife Ruochen. Not only in the daily life but also in the scientific work, she has supported and helped me so much that I can have enough strength, courage and determination to overcome all the challenges.

Peng Cao Darmstadt, October 2017

List of Contents

List of Abbreviations

Abbreviation	Description
ACC	Adaptive Cruise Control
ADAS	Advanced Driver Assistance System
ADS	Automated Driving System
CPU	Central Processing Unit
CVC	Cell-Volume Concept
DAS	Driver Assistance System
Exper.	Experiment
FDTD	Finite Difference Time Domain
FMCW	Frequency Modulated Continuous Wave
FSK	Frequency-Shift-Keying
GbV	Grad-based-View
GPU	Graphics Processing Unit
GUI	Graphical User Interface
HCVC	Hybrid Cell-Volume Concept
HiL	Hardware-in-the-Loop
ISO	International Organization for Standardization
LFMCW/FSK	Linear Frequency Modulation Shift Keying
Lidar	Light detection and ranging
OuT	Object under Test
PSD	Power Spectral Density
Radar	Radio detection and ranging
RCS	Radar Cross Section
RT	Real Time
SAE	Society of Automotive Engineers
SiL	Software-in-the-Loop
SNR	Signal-to-the-Noise Ratio
ToF	Time of Flight
VeP	Vector-Projection

List of Symbols and Indices

Symbol	Unit	Description
A	Miscellaneous; m^2; m	amplitude; area; ray (distance) between sensor and object
B	m	ray (distance) between object and reflection point on road
c	m/s	velocity of light
C	m	ray (distance) between sensor and reflection point on road
D	m; dB	radial distance between sensor and the geometric center of a certain object; RCS at peak boundary
E	J	Energy
f	Hz	frequency
G	1	antenna gain
h	m	height
i	1	numeration; imaginary unit
j	1	numeration
k	1	numeration; scale factor
L	1; m	loss; diagonal dimension of corner reflector
l	m	optical path length
m	1	slope of linear frequency change
n	1	numeration
N	W; m; °	noise power density; normal direction; peak width
P	W; dB	power
r	m	range
R	m	radial distance between sensor and a certain reflecting point
RCS	m^2, dB	radar cross section
S	miscellaneous	integral
t	s	time
T	s	cycle time
ToF	s	Time of Flight
u	bin-width	distance between cell center and vector position
U	1	ramdom variable
v	m/s	velocity
V	1	Fresnel reflection coefficient
W	m	width
x	miscellaneous	coordinate in x direction
y	miscellaneous	coordinate in y direction
z	miscellaneous	coordinate in z direction
α	1; °, rad	mathematical term; angle
β	1	mathematical term
γ	1	mathematical term
Γ	1	mathematical term
δ	miscellaneous	Dirac impulse
ε	1	relative permittivity
θ	°, rad	angle (e. g. incidence angle, heading angle)
ϑ	°, rad	elevation angle

Symbol	Unit	Description
κ	dB/km	attenuation coefficient
λ	m	wave length
ξ	rad/m	spatial frequency
σ	1; m²	standard deviation; reflectivity (Radar Cross Section)
τ	1	mathematical term
φ	°, rad	phase
ϕ	°, rad	azimuth angle
ω	rad/s	angular frequency

Index	Description
0	initial; peak position; boundary
2ref	second reflecting point on road surface
atm	atmosphere
A	ray A
AA	in wave propagation direction A-A
ABC	triangle ABC; in wave propagation direction A-B-C
B	ray B
chirp	chirp sequence modulation
cell	cell size
cor	corner of vehicle
C	ray C
CBA	in wave propagation direction C-B-A
CBBC	in wave propagation direction C-B-B-C
d	difference
e	effective
f	frequency
ground	ground-truth
Gauss	Gaussian distribution
H	horizontal
Hanning	Hanning window
i	numeration
j	numeration
max	maximum
min	minimum
M	modulation
noise	noise
obj	object
of	of flight
p	peak
Poisson	Poisson window
r	range
road	road surface
rec	receiver
ref	reflecting
rel	relative
rgate	in the same range-gate
R	repeat; received; reflector
sensor	sensor
signal	signal
s	sensor
t	transmit; time
total	totally
trans	transmitter
v	vehicle

V	vertical
width	width of a peak
x	in x direction
y	in y direction
ϕ	azimuth angle

Summary

The validation of the functionality is up to now always an insolvable problem for the development of automated driving systems (ADS), although customers' demands on safer and easier drivable vehicles are being raised. The simulation-based test methods (e.g. X-in-the-Loop test) with sensor models are nowadays being developed and considered by the most players in the automotive industry as an economically feasible solution for the validation of ADS. However, in order to ensure the reality and the validity of test results, the sensor performances and the driving environment should be modeled realistically. This reality presents a challenge for modeling technology.

The current sensor models are either white-box models that focus on representating every step in the workflow of a certain sensor, or black-box models that describe the general properties of perception sensors without considering physical phenomenon or physical structures.

In this dissertation, a novel grey-box method for modeling the active automotive perception sensors with neither the efficiency disadvantages of the white-box methods nor the the reality disadvantages of black-box methods. This grey-box method can offer a necessary reality and efficiency for the ADS validations, which will also be demonstrated by some verification test cases in this dissertation finally.

The main body of this dissertation proceeds as follows. To begin with, a brief background on the working principles of the existing driver assistance systems (DAS), active automotive perception sensors will be provided in Chapter 2 as a basis for the subsequent modeling. Additionally, the current methods for modeling active perception sensors will be introduced briefly.

In the next chapter (Chapter 3), after a statement of the basic problems in the modeling, the general workflow of the active perception sensors will be summarized and a framework for its grey-box modeling will be introduced. According to this framework, the sensor model to be developed should consist of the following parts: sensor performance model, wave propagation model and environment model.

For modeling the sensor performances, a novel modeling method, so-called Cell-Volume Concept (CVC), is developed. Three kinds of variants of this method are introduced and compared in Chapter 4. In this dissertation, the modeling of automotive radars is considered as focus. On this account after an analysis of the advantages and disadvantages of the variants, the so-called vector-projection variant is chosen and implemented exemplarily.

Based on the vector-projection Cell-Volume Concept, a wave propagation model, which simulates the propagation of the electromagnetic waves from the sensor into the atmosphere, is developed and introduced in Chapter 5. The possible physical phenomenon during wave propagation are analyzed and selectively modeled regarding the modeling necessity. The sensor radiation pattern that decides the initial wave status (angle-selective power density distribution of the radiation) will also be modeled as a part of the wave propagation model in this chapter. Furthermore, to ensure simulation efficiency and avoid unnecessary computing effort, an ergodic method is developed and introduced.

In Chapter 6, as one of the most important parts of the environment model, a model for representing the reflectivity (distribution) of different vehicles at different aspect angles is developed and introduced. This model plays an essential role in calculating the performance of waves reflected by different points on vehicle surfaces in driving environment. The modeling of reflectivity distribution is especially meaningful for the simulation of the detection and measurement in short range. Furthermore, compared to the other current methods with similar fidelity, the modeling method in this dissertation is based on macroscopic vehicle characteristics and therefore has advantages regarding calibration and representation efforts.

Finally, the developed sensor model should be verified via comparing simulation results with real sensor outputs. For this purpose, some evaluation criteria are utilized in Chapter 7. The simulation efficiency is also taken into consideration. By using these evaluation criteria, the developed sensor model has shown the capability of representing sensor performances dynamically and efficiently in the verification test cases.

In summary, the developed sensor model in this dissertation is appropriate to be applied for radar modeling. The simulation efficiency and fidelity can be ensured simultaneously. For finding the application possibility of this sensor model in modeling the other types of active perception sensors, some discussions and suggestions are also given and summarized in Chapter 8.

1 Introduction

1.1 Motivation and Goal

Due to the increasing traffic density and traffic jams in the last decades, customers' demands on traffic safety and easily operatable vehicles are rising. In order to fulfill these demands, the most automotive manufactures have increased research and development activities in driver assistance systems (DAS) and automated driving systems (ADS). With the rising level of driving automation (defined by SAE, Figure 1.1), this kind of systems can support drivers more and more in driving and eventually take over completely the driving tasks. On the one hand, it is believed that the reaction time in some emergency cases can be reduced and some human mistakes in driving can be avoided by these systems, so that driving safety can be raised[1]. On the other hand, the reduction of drivers' tasks can improve driving comfort.

SAE level	Name	Narrative Definition	Execution of Steering and Acceleration/ Deceleration	*Monitoring* of Driving Environment	Fallback Performance of *Dynamic Driving Task*	System Capability *(Driving Modes)*	
***Human driver* monitors the driving environment**							
0	**No Automation**	the full-time performance by the *human driver* of all aspects of the *dynamic driving task*, even when enhanced by warning or intervention systems	Human driver	Human driver	Human driver	n/a	DAS
1	**Driver Assistance**	the *driving mode*-specific execution by a driver assistance system of either steering or acceleration/deceleration using information about the driving environment and with the expectation that the *human driver* perform all remaining aspects of the *dynamic driving task*	Human driver and system	Human driver	Human driver	Some driving modes	
2	**Partial Automation**	the *driving mode*-specific execution by one or more driver assistance systems of both steering and acceleration/ deceleration using information about the driving environment and with the expectation that the *human driver* perform all remaining aspects of the *dynamic driving task*	**System**	Human driver	Human driver	Some driving modes	
***Automated driving system* ("system") monitors the driving environment**							
3	**Conditional Automation**	the *driving mode*-specific performance by an *automated driving system* of all aspects of the dynamic driving task with the expectation that the *human driver* will respond appropriately to a *request to intervene*	System	**System**	Human driver	Some driving modes	ADS
4	**High Automation**	the *driving mode*-specific performance by an automated driving system of all aspects of the *dynamic driving task*, even if a *human driver* does not respond appropriately to a *request to intervene*	System	System	**System**	Some driving modes	
5	**Full Automation**	the full-time performance by an *automated driving system* of all aspects of the *dynamic driving task* under all roadway and environmental conditions that can be managed by a *human driver*	System	System	System	**All driving modes**	

Figure 1.1 Level of automation (SAE)[2]

[1] Kühn, M.; Hannawald, L.: Driver Assistance and Road Safety (2016).

[2] SAE: Levels of Driving Automation (2017).

Nowadays, various DAS have already been produced and equipped on production vehicles[3] [4] [5] [6], meanwhile many demo ADS (L3-L5 driving automation, SAE (Figure 1.1)) have been developed as well[7] [8] [9] [10]. However, compared to the validation of functional safety (correctness of operation in response to inputs[11]) for DAS, the validation for ADS reveals a new challenge. Unlike in DAS, drivers do not have to play an inevitable role in ADS. They are not obliged to be occupant, when the systems cannot either monitor driving environment well or make a right decision for further driving behaviors in the next moment. According to SAE, an ADS should at least be able to monitor the driving environment by itself without a driver. This raises the requirement not only on the system functional safety, but also on the validation of functional safety.

According to Wachenfeld[12], in order to solve the challenges, which is brought on by the ADS validation test as well as the requirements on its effectivity and efficiency, two approaches can be applied:

1. Reusing the validated and released functions and
2. Accelerating the test execution.

This dissertation focuses on a method that enables the realization of the second approach, the acceleration of test execution.

There are two ways to accelerate the test execution. The first one is parallel execution of various test process steps. However, this method requires more test persons, test vehicles at the same time for the same few test cases, which raises no only the monetary effort but also the costs of prototyping.

The other way is the simulation-based validation method. This method models and represents virtually the ego vehicle, driving environment and other traffic participants in a virtual simulation. This simulation instead of real world offers various test cases to ADS under test. This method has two major advantages: On the one hand, the accelerating of

[3] Winner, H. et al.: Handbook of Driver Assistance Systems (2016), pp. 917–1396.

[4] Daimler: Mercedes-Benz Intelligent Drive (2017).

[5] BMW: BMW 7er Limousine : Fahrerassistenz (2017).

[6] Lincoln: 2017 Lincoln MKZ Technology Features (2017).

[7] Aeberhard, M. et al.: Lessons Learned from Automated Driving (2015).

[8] Kammel, S. et al.: Team AnnieWAY's autonomous system (2008).

[9] Thrun, S. et al.: Stanley - The robot that won (2006).

[10] Waymo: Journey – Waymo (2017).

[11] TÜV SÜD: Functional Safety (2018).

[12] Wachenfeld, W.; Winner, H.: Die Freigabe des autonomen Fahrens (2015).

test execution is much easier in simulation than in real world. On the other hand, the modeled environment or vehicle can be changed by parameterization artificially, so that test cases can be built more economically than in real world. Because of these advantages, the simulation-based validation methods are an economically feasible solution for the validation of ADS.

However, a drawback of losing fidelity comes with these advantages of this method. When the real world is simulated as a model, some differences between the model and the reality exist. When the differences change some behaviors of the object under test (OuT) and furthermore the results of these behaviors, the test results are questionable. A simulation-based homologation shows the existence possibility of software models, which are sufficiently accurate for certain cases[13] [15]. (e.g. for some vehicle characteristics, such as vehicle dynamics, and some vehicle components, such as inertial sensors) However, software models for environmental sensing with active perception sensors[14] [15], which are an important components in ADS, are not included. This motivates the further discussion in this dissertation on perception sensor modeling, which permits efficient (at least real-time) and sufficiently accurate test execution.

1.2 Basic Methodology

In order to develop a novel active perception sensor modeling method for the purpose described above, the advantages and disadvantages of the current modeling methods are analyzed. After that, the detailed requirements on active perception sensor models for virtual validation of ADS are created. Based on these requirements, a novel modeling concept is established.

As the first step in using the novel modeling concept, the inputs and outputs of the model are to be determined. For this purpose, the working principle of active perception sensors is analyzed and the sensor parts that can be modeled by the novel modeling concept are identified.

When modeling, a top down methodology is used to structure the model. Sensor performance model, wave propagation model and environment model are considered as components of the sensor model, and developed one after another. In order to fulfill the validity requirements on the model, the sensor performance model is developed at first, as this submodel decides if the whole model can describe the required sensor behaviors and

[13] Baake, U. et al.: Testing and Simulation-based Validation (2014).

[14] Schöner, H.-P.: Challenges and Approaches for Testing (2016).

[15] Schubert, R. et al.: Simulation of Sensor Models (2014).

their results realistically. The further development of wave propagation model and environment model focuses on describing the relationship between the required sensor behaviors and the influence factors on them.

Finally, sensor performance model, wave propagation model and environment model are combined with each other, and verified via comparing simulation results with real sensor outputs in test field tests. For this purpose, some test cases and evaluation metrics are created.

Figure 1.2 presents the basic methodology applied for developing the modeling method.

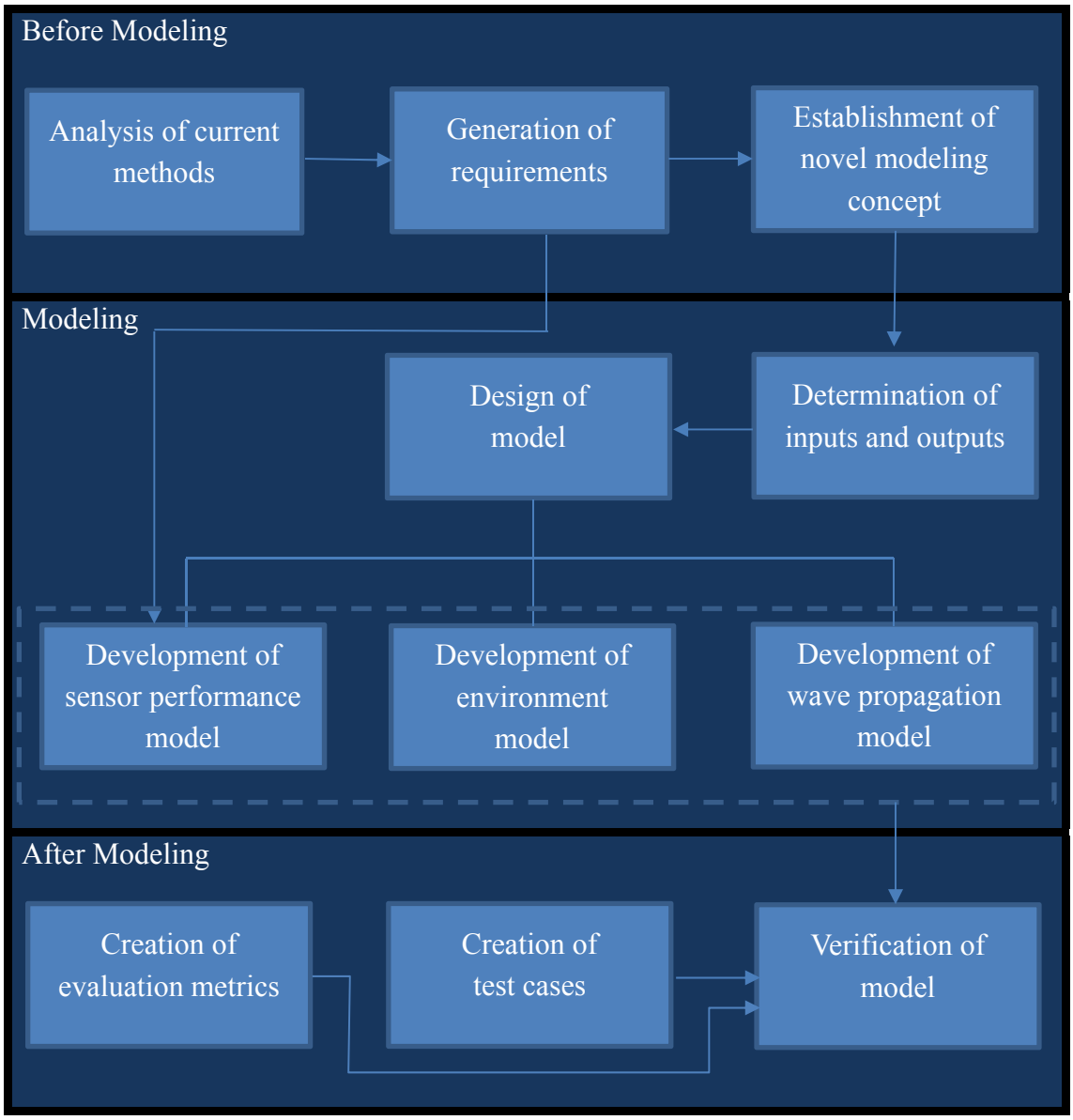

Figure 1.2 Basic methodology applied for developing the modeling method

1.3 Structure of the Thesis

The present work consists of seven sections. They are structured according to the order of the introduced methodology.

Chapter 2. State of the Art:

This section starts with a brief background on the working principles of existing DAS and active automotive perception sensors. This information is used as a basis

for the subsequent modeling. Additionally, the current methods for modeling active perception sensors are introduced briefly.

Chapter 3. Generic grey-box modeling:

After comparing the advantages and disadvantages of the current methods, a statement of the basic problems in the modeling is given. Based on it, the detailed requirements on active perception sensor modeling are generated. A so-called generic grey-box modeling method is introduced as novel modeling concept. The general working principle of the active perception sensors is analyzed, and the inputs and outputs of the model to be developed are determined. A framework for the grey-box modeling concept is established. According to this framework, the sensor model to be developed consists of the following parts: sensor performance model, wave propagation model and environment model.

Chapter 4. Sensor performance model:

A novel modeling method, so-called Cell-Volume Concept (CVC), which can fulfill the requirements on perception sensor models, is developed. Three kinds of variants of this method are introduced and compared. The so-called vector-projection variant is chosen and implemented exemplarily for radar sensor modeling.

Chapter 5. Wave propagation model:

Based on the vector-projection Cell-Volume Concept, a wave propagation model, which simulates the propagation of the electromagnetic wave from the sensors into the atmosphere, is developed and introduced. An ergodic method is developed and introduced for ensuring simulation efficiency and avoiding unnecessary computing effort. In this model, a modeling of the necessary physical phenomenon during wave propagation and the radiation pattern of the sensor is included.

Chapter 6. Environment model:

A model for representing the reflectivities of different vehicles and their distribution over azimuth angle at different aspect angles, which plays an essential role in the simulation of the detection and measurement in short range, is developed and introduced.

Chapter 7. Model verification

The developed sensor model is verified via comparing simulation results with real sensor outputs. The simulation efficiency is used for evaluating the model as well. Some representative test cases are developed and used in the verification tests.

Chapter 8. Conclusion and outlook:

This section summarizes the developed modeling method, the validation results and the advantages of the developed method in comparison with the current methods. To extend the sensor model to other active perception sensors types, some discussions and suggestions are given and summarized.

2 State of the Art

2.1 Definitions and Basics

2.1.1 Perception Sensor

Perception is “the way in which something is regarded, understood, or interpreted”[16]. Accordingly, perception sensors in vehicles are the way in which the vehicle regards, understands and interprets the driving environment. Principally, perception sensors are one of the most important parts in DAS and ADS. They can be divided into two main types: active perception sensors and passive perception sensors.

The sensing of passive perception sensors relies on external radiation sources. A typical example is camera. Normally, this kind of perception sensors cannot achieve object information from the modulation of received waves. The object ranging and detection are mostly based on graphic processing and classification[17] [18].

The active perception sensor works based on the waves, which the sensor transmits and receives. Modulation and demodulation of the transmitted waves are a typical way for active perception sensors to get object information. Typical examples of active perception sensors are radar, lidar and ultrasonic sensors. As this dissertation focuses on the modeling of this kind of perception sensors, the work principles of various active perception sensor are described here in detail. Unlike the others, ultrasonic sensors use mechanical wave as signal carrier, which causes some different characteristics (e.g. higher latency, higher sensitivity to wind or different reflectivities of same materials) in wave propagation. Therefore, this dissertation does not take ultrasonic sensors into discussion and focuses only on radar and lidar.

Radar

Radar (Radio Detection and Ranging) is originally a military technology developed in the Second World War. It can be used for object detection, range and velocity measurement. Nowadays, it is also used in civil applications, such as DAS and ADS. The bandwidths of

[16] Oxford Dictionaries: Definition of perception (2017).

[17] Khammari, A. et al.: Vehicle detection combining gradient analysis (2005).

[18] Gupte, S. et al.: Detection and classification of vehicles (2002).

the electromagnetic wave currently used by radars in road traffic are 24.0-24.25 GHz, 76-77 GHz and 77-81 GHz. Short-range radars use 24.0-24.25 GHz, whereas long-range radars normally use 76-77 GHz and 77-81 GHz[20].

Radar detection works by using the waves reflected from objects. An object detection is achieved under two conditions: 1) The transmitted radar wave is reflected on the surface of the object and finally reaches the radar receiver. (See Figure 2.1). 2) The received wave power is higher than the detection threshold, which is preset in some radars or can be set dynamically by some radars themselves. (Detailed explanation of the detection threshold is given in Section 3.1.1.)

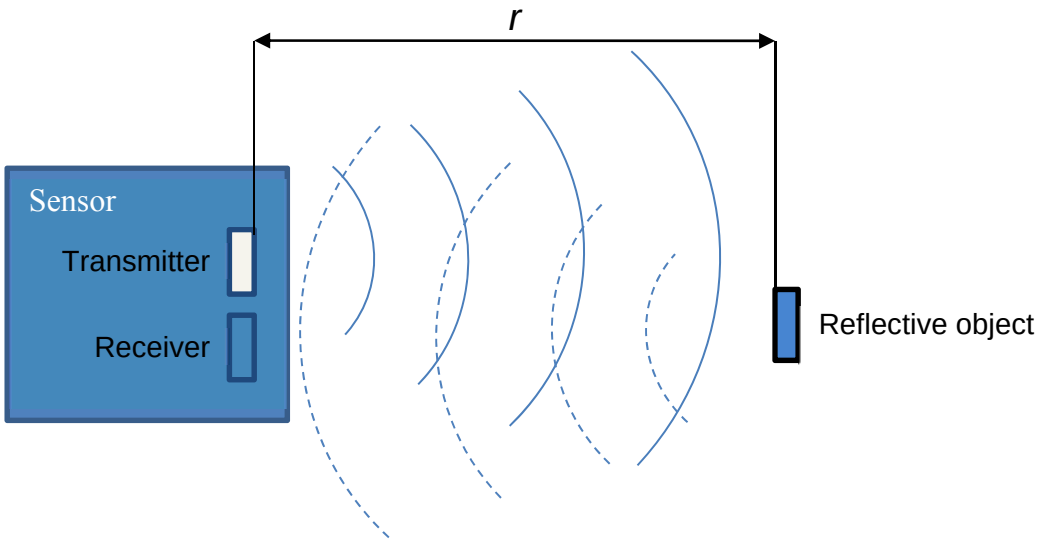

Figure 2.1 Work principle of radar detection

1) States measurement

In principle, radar counts the propagation time of radar wave between sensor and objects for calculating the range. After the duration between transmit and receive of a signal t_{of} is measured, the range r between sensor and the object that reflects this signal can be calculated by:

$$r = 0.5c \cdot t_{\mathrm{of}}, \tag{2-1}$$

where c is velocity of light.

The duration between transmittion and receiving of a signal Δt is called Time of Flight (ToF).

Radar uses Doppler Effect to measure the radial relative velocity of objects. In comparison with the transmitted wave, the relative movement between sensor and objects can cause a frequency shift of the received wave (Doppler Effect). The relationship between

the relative velocity v_{rel} and the frequency shift Δf caused by it can be presented as follows[19]:

$$\Delta f = -2\frac{v_{\mathrm{rel}}}{c} \cdot f_0, \tag{2-2}$$

where c is light speed, f_0 is the frequency of signal carrier.

Beside range and relative velocity of objects, radars are also able to measure azimuth angles of objects. According to Winner[20], various methods like scanning, monopulse principle, multibeam concept, dual sensor concept and planar antenna array concept can make the azimuth angle measurement possible. Among them, the planar antenna array concept and monopulse principle are introduced here in detail, because the sensor modeled exemplarily in this dissertation uses planar antenna array for azimuth angle measurement, meanwhile the monopulse principle is the basis of the azimuth angle measurement in planar antenna array concept.

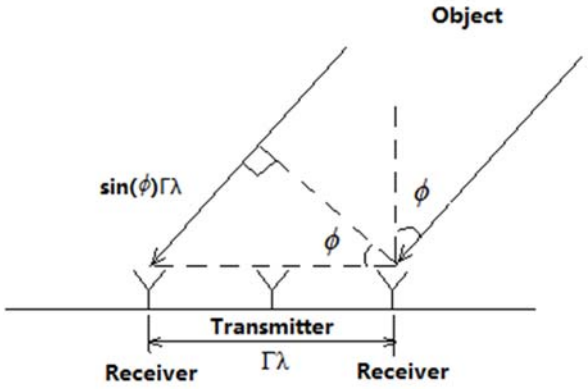

Figure 2.2 Azimuth angle measurement by monopulse principle

Figure 2.2 explains how the azimuth angle ϕ of an object in sensor view can be measured by monopulse principle. According to Winner[20], as shown in Figure 2.2, monopulse principle uses two receivers to measure the direction in which the reflected wave is coming. Due to the distance $\Gamma\lambda$ between the two receivers (where Γ is a dimensionless value; λ is the wavelength), the wave from object has to travel for $\sin(\phi)\ \Gamma\lambda$ more to reach the receiver on the left side than on the right side. This leads to a phase difference $\Delta\varphi$ between the waves received on the left and right sides. Monopulse principle measures the phase difference $\Delta\varphi$ and calculates the azimuth angle ϕ as follows:

$$\phi = \arcsin\frac{\Delta\varphi}{2\pi\Gamma}, \tag{2-3}$$

[19] Only valid when $v_{\mathrm{rel}} \ll c$.

Obviously, the monopulse principle cannot offer a multi-target capability in azimuth angle measurement. This means, the monopulse principle cannot measure the azimuth angles of multiple objects at the same time. The planar antenna array concept can compensate for this weakness of the monopulse principle.

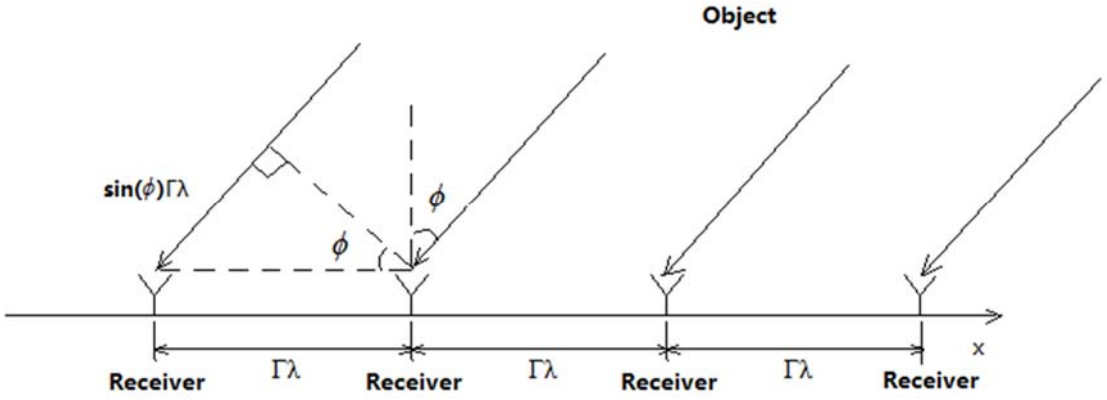

Figure 2.3 Azimuth angle measurement by planar antenna array

As shown in Figure 2.3, planar antenna array principle uses an array of receiver antennas to receive the waves reflected from objects. However, the underlying working principle is the same as that of monopulse principle: It relies on the phase differences between the waves received by different receiver antennas.

The working principle of planar antenna array radar can be derived from Winner[20] as follows:

Suppose the direction in which the antenna array arranged is the *x*-direction (see Figure 2.3). When *i* objects with different azimuth angles ϕ_j exist, the amplitude $A(x)$ of the overlaid waves received at a certain position on the *x*-axis can be presented as follows:

$$A(x) = \sum_{j=1}^{i} \sin\left(2\pi f_0 t + \frac{\sin(\phi_j)x}{\lambda}\right), \tag{2-4}$$

where f_0 is the frequency of signal carrier.

After a Fourier transformation over *x*, a spectral power distribution can be described as follows:

$$\left|\hat{A}(\xi)\right| = \sum_{j=1}^{i}\left(\left|\sqrt{2\pi}\frac{\delta\left(\xi - \frac{\sin(\phi_j)}{\lambda}\right)}{2}\right|\right). \tag{2-5}$$

[20] Winner, H.: Automotive Radar (2016).

Obviously, in the spectral power distribution, there will be Dirac impulses at the positions where $\xi = \frac{\sin(\phi_j)}{\lambda}$. Thus, by searching for Dirac impulses, azimuth angles ϕ_j of different objects can be obtained. In practice, due to the limited number of receiver antennas (a spatial discretization), the spectral power distribution is a periodic function.

Due to the wide beam width, the most automotive radars cannot measure elevation angles of objects well. According to Diewald[21], that elevation angle measurement is also possible by means of an analysis on interference effect. However, this method is considered as a special application of radar in this dissertation, and therefore will not be further discussed.

2) Modulation methods

Radar sensors can be classified according to their modulation methods, amplitude modulation, frequency modulation and phase modulation. In these three kinds of modulation methods, radar changes the amplitudes, the frequency, and the phase of the transmitted waves respectively, in order to measure object states or transfer information. Typical frequency modulation methods are, for example, Frequency-Shift-Keying (FSK), Linear Frequency Modulation Shift Keying (LFMCW/FSK), Frequency Modulated Continuous Wave (FMCW), Chirp Sequence Modulation[22]. The Chirp Sequence Modulation will be introduced here in detail, because the sensor to be modeled as example in this dissertation is using this modulation. The FMCW is introduced as the technology of the beginning of the automotive radars.

Principally, FMCW radar uses ToF for range measurement and Doppler Effect for velocity measurement. However, it does not count the time between the transmission and receiving of the signal. Instead of that, it changes the carrier frequency linearly at first. After that, as Figure 2.4 (a) shows, FMCW radar measures the frequency shift between the transmitted wave and the received wave, which is, in this case, caused by both Doppler Effect and time delay on signal receiving (ToF). In this way, the sensor can receive informations about object velocity and range at the same time.

---

[21] Diewald, F.: Diss., Objektklassifikation und Freiraumdetektion (2013).

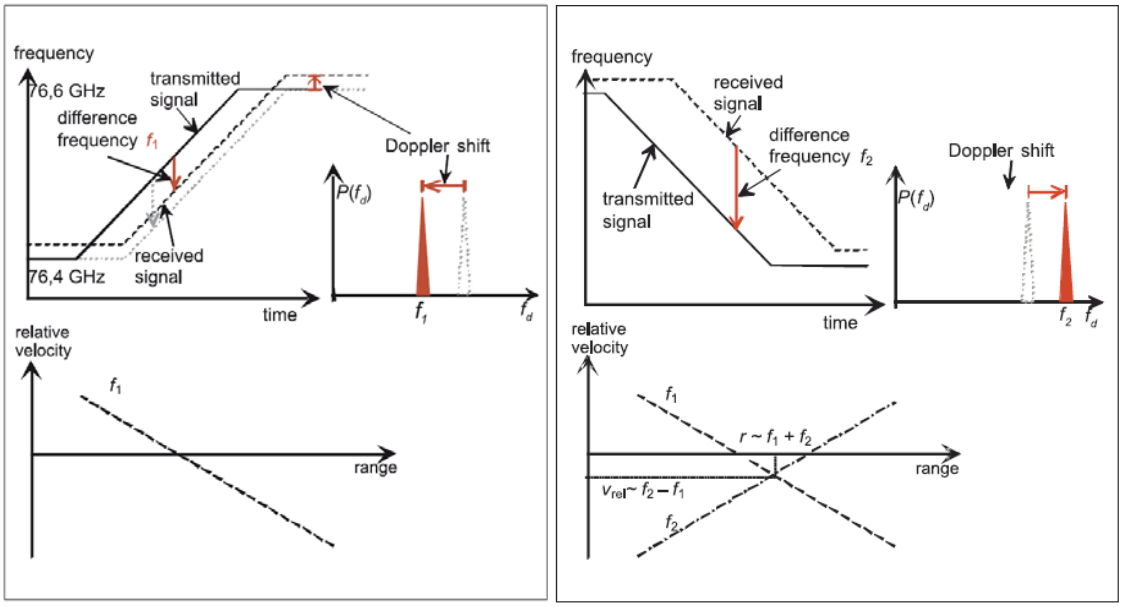

(a) (b)

Figure 2.4 Working principle of FMCW radar[22]

The relationship among the frequency shift f_d, the range r and the velocity v_rel is as follows:

$$v_\mathrm{rel} = \frac{c}{2}\frac{f_\mathrm{d}}{f_0} - \frac{m}{f_0} \cdot r \tag{2-6}$$

where c is the light speed; m is the slope of linear frequency change; f_0 is start frequency before change.

However, this function is underdetermined and therefore unsolvable. For achieving the range and velocity, a linear change of the frequency with another, e.g. negative slope is needed, as Figure 2.4 (b) shows. Thus, the range and velocity can be obtained by solving the equations (2-6) with positive and negative slope. For multi-target detection, more slopes are required.

Chirp Sequence Modulation is based on FMCW. As Figure 2.5 shows, it changes the transmission frequency linearly as well, and repeats the changing in sequence of cycles.

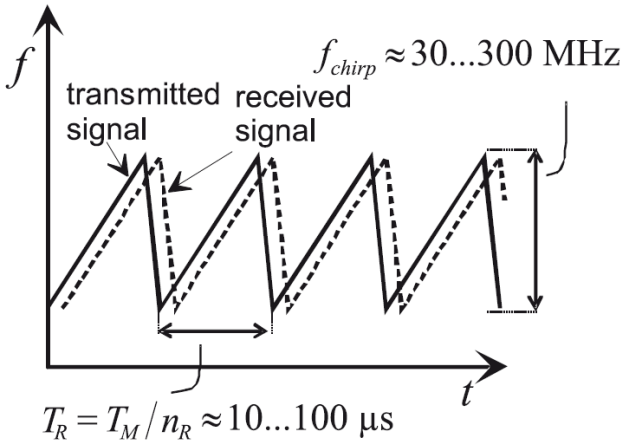

Figure 2.5 Working principle of Chirp Sequence Modulation[22]

However, the slope is steeper, and the frequency change cycle is much shorter than FMCW. Thus, the Doppler shift in each cycle can be neglected. Based on frequency shift, an explicit expression of the object range value can be obtained.

After that, the following process describes how to get the relative velocity.

The received signal $A(t)$ in the n-th cycle is as follows:

$$A(t) = A_0 \sin(\omega_0 t + \omega_\mathrm{r} t + \omega_\mathrm{rel} n T_\mathrm{R}) \tag{2-7}$$

where A_0 is the transmitted signal amplitude; ω_0 is the frequency of the transmitted wave at the time t; ω_r is the frequency shift induced by ToF; ω_rel is the frequency shift induced by Doppler effect; T_R is the cycle time.

As explained above, because of the short cycle time, the Doppler shift is neglected. However, when considering more cycles, the Doppler shift effects like a phase shift among different cycles.

At first, the signals from different ranges of the object range values (range-gates) are processed separately. This means principally a grouping of the signals with similar ω_r.

Through a Fourier transformation of the signals over time, an expression as follows can be obtained:

$$\frac{\hat{\mathrm{A}}(\omega)}{A_0} = \frac{\sqrt{2\pi}}{2} \sin(\omega_\mathrm{rel} n T_\mathrm{R}) \left(\delta\big(\omega + (\omega_0 + \omega_\mathrm{r})\big) + \delta\big(\omega - (\omega_0 + \omega_\mathrm{r})\big)\right) +$$
$$\frac{\sqrt{2\pi}}{2} \cos(\omega_\mathrm{rel} n T_\mathrm{R})(\delta\big(\omega + (\omega_0 + \omega_\mathrm{r})\big) - \delta\big(\omega - (\omega_0 + \omega_\mathrm{r})\big))i \tag{2-8}$$

[22] Winner, H.: Radarsensorik (2009).

Obviously, this expression is meaningful, only when $\omega = \pm(\omega_0 + \omega_r)$. At these points, a complex amplitude with a phase shift of $\omega_{rel} n T_R$ can be obtained. This phase shift is induced by Doppler shift in a cycle time.

Through a Fourier transformation of the complex amplitudes

$$\frac{\hat{A}_{rgate}(\omega)}{A_0} = \frac{\sqrt{2\pi}}{2}\sin(\omega_{rel} n T_R) + \frac{\sqrt{2\pi}}{2}\cos(\omega_{rel} n T_R) i \tag{2-9}$$

in the same range-gate of all the cycles, the rotational speed of the amplitude in the complex plane $\frac{d(\omega_{rel} n T_R)}{d T_R n}$, which indicates the Doppler shift ω_{rel}, can be obtained. Thus, the relative velocity can be measured according to Doppler effect.

Lidar

Lidar (Light Detection and Ranging) uses also a measurement principle based on electromagnetic waves for measuring the range and the relative velocity between objects and sensor. Compared to the radar, Lidar uses electromagnetic waves in another band like ultraviolet, infrared, or visible light rather than microwaves[23].

Like radar, lidar receives the waves reflected on object surfaces to detect objects and measures their range by determining ToF as well. However, the velocity measurement method based on the Doppler shift for automotive lidar is unknown. Lidar measures relative velocity normally by means of differential calculation of measured range values. In practice, relative velocity can also be calculated on the average of several differential values, in order to reduce stochastic measurement errors.

Thanks to the shorter wavelength used by lidar, narrower beams can be generated by lidar than by radar, which makes both of azimuth angle and elevation angle measurements possible. As introduced by Geduld[23], lidar uses either multibeam rigid, multibeam SWEEP, multibeam spread or single beam scan to measure the azimuth angles of objects (see Figure 2.6). When one of the beams has reached an object and reflected back, the existence of this object will be comfirmed, and at the same time, its azimuth angle will be determined by the sending direction of this beam. In principle, the methods in Figure 2.6 can all be used for elevation angle measurements.

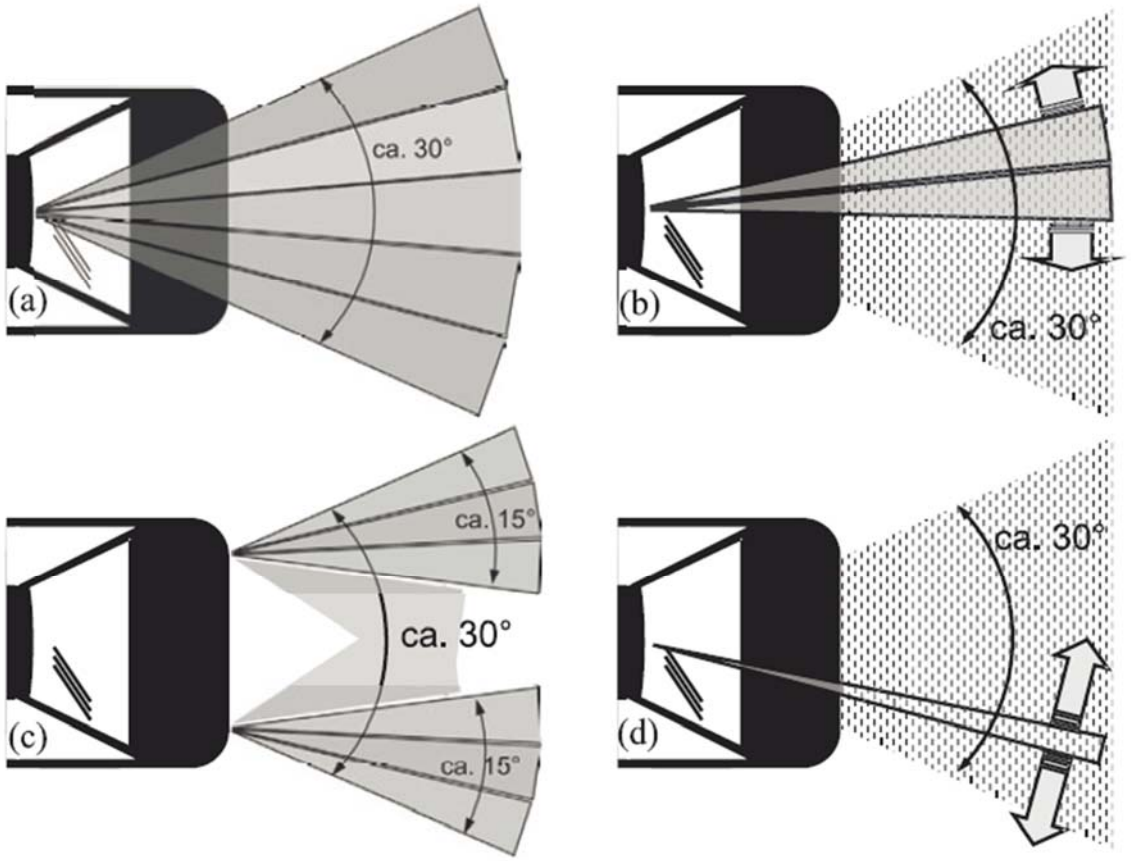

Figure 2.6 Examples of different beam sensors: (a) Multibeam Rigid, (b) Multibeam SWEEP, (c) Multibeam Spread, (d) Single Beam Scan[23]

2.1.2 Driver Assistance System (DAS)

According to the three-level hierarchy of the driving task by Donges (see Figure 2.7)[24], the driving tasks can be classified into three levels: navigation level, path guiding (or guidance) level and stabilization level.

[23] Geduld, G.: Lidarsensorik (2012).

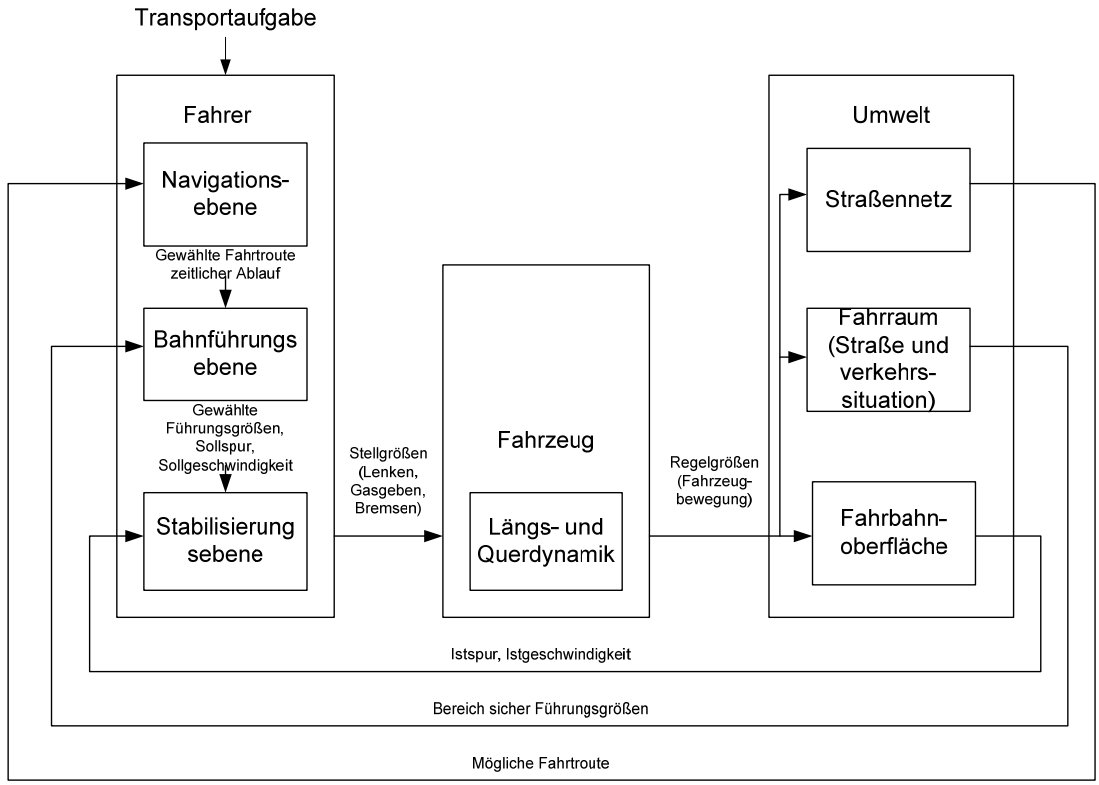

Figure 2.7 Three-level hierarchy of the driving task by Donges[24]

With a road network and a specific destination, the driver (navigation level) can select a driving route at first. Thereafter, according to the instantaneous traffic situation, the driver can decide his desires in the vehicle guidance, e.g. the desired track, the desired speed, etc. (path guiding level). Finally, according to the actual state of the vehicle, the driver outputs some appropriate values for vehicle action actuating variables, e.g. steering wheel angle, gas / brake pedal angle, to the vehicle (stabilization level).

Driving safety and vehicle control quality are mostly depending on how well drivers can finish the tasks on these three levels, which is restricted by driver's experience and traction limit when driving conventional vehicles. The objective of DAS is to support drivers or take the place of drivers to finish some driving tasks in certain situations, so that the tasks can be accomplished more effectively and efficiently. For example, on the navigation level, digital maps in navigation system can help to inform the driver of the circumstance changes or the potential danger in one minute or more ahead; on the stabilization level, some chassis control systems can observe and control steering angles, individual wheel speeds, and brake or acceleration to stabilize the vehicle like a reflex-like stimulus-response mechanisms. Besides, on the path guiding level, some systems can assist drivers

[24] Donges, E.: Aspekte der aktiven Sicherheit (1982).

by completing his knowledge and recognition of surrounding driving situation[25]. In this case, the perception sensors like radar and lidar mentioned previously are required. However, how much a driver can be assisted depends on the driving situations and the system capability. This will be explained later in this section.

The major current DAS based on active perception sensors (radar and lidar) are briefly described as follows:

Adaptive Cruise Control (ACC)[26]

ACC enables the ego-vehicle to follow the vehicle in front and keep a certain time gap. For the functionality of this system, the position and the relative velocity of the vehicle in front should be measured. Nowadays, it works normally based on long-range radars.

Collision Protection System[27]

Collision Protection System can execute an emergency brake for the driver, when a collision tendence is occurred. For this system, the position and relative velocity of objects in front are required as well. The current systems use normally short-range radars, cameras and lidars.

Lane Change Assistance[28]

Lane Change Assistance detectes the objects in the blind spot on the left and right side of the ego-vehicle, or even the objects that are closing from behind, in order to warn the driver, when a collision tendence exists in lane changing. Such detections are normally based on radars or ultrasonic sensors.

Beside these systems, there are some Level 2 systems like Traffic jam Assistance and Automation, which are using active perception sensors as well. These systems can be considered as an integration of different Level 1 systems. The functionality of these systems will not be further introduced.

2.1.3 Automated Driving System (ADS)

Figure 1.1 gives a definition of the boundary between advanced driver assistance system and automated driving system. According to this definition, the most important characteristic of ADS, which differs ADS from systems with lower automation level, is that the driving environment is monitored by the ADS systems themselves alone.

---

[25] Donges, E.: Driver Behavior Models (2016).

[26] ISO/TC 204: ISO 15622:2010 (2010).

[27] ISO/TC 204: ISO 15623:2013 (2013).

[28] ISO/TC 204: ISO 17387:2008 (2008).

According to SAE, ADS can be classified into three categories: conditional automation, high automation and full automation.

As introduced above, all the three categories of ADS should be able to monitor the driving environment by themselves without any supports from the drivers. However, the driver should be ready to intervene appropriately at any time when driving a conditional automation system, as the system has such an expectation after giving the driver a request for it.

Compared to conditional automation system, high automation has not such an expectation, even when driver's intervention is desired. If the desired intervention is either not present or not appropriate, the system should be capable of taking the vehicle to a safe status, e.g. driving slowly or parking the vehicle on roadside.

According to the definition of SAE, the full automation systems should be able to drive the vehicle in any driving situations or under any conditions, which are manageable for human drivers. An intervention is needed by the full automation systems. Such a system can totally release the driver.

2.2 Current Modeling Methods for Active Perception Sensors

2.2.1 Current Modeling Methods

According to modeling methods, the current existing for active perception sensor models can be classified into two groups: "white-box model" and "black-box model".

White-Box Model

White-box model focuses on representating every step in the workflow of a certain sensor. It comprises normally two kinds of models: sensor electronic models and wave propagation models.

In the sensor electronic models of this type, the electronic components in sensors are modeled according to their working principles. Usually, the sensor manufacturers create these models by themselves. These models are used internally by the sensor manufacturers or their potential customers for testing and validation of a certain sensor or the functionality of a certain DAS based on this sensor.

Numerous methods for creating such electronic models are introduced in the literatures. For example, various modeling methods for different transmitters, receivers, antennas,

detectors, filters, and modulation/demodulation processors are introduced in Skolnik[29] and Ludloff[30]. Due to the huge amount of the models, they will not be introduced here in detail. The most of them are just restatements of the working principles of the object to be modeled.

In wave propagation models of this type, the propagation of the electromagnetic waves between active perception sensor and objects is normally modeled based on physical laws.

Such a model is for example:

Finite Difference Time Domain Model

According to Fuchs[31], Finite Difference Time Domain (FDTD) method can model the wave propagation in atmosphere. This method discretizes the time and the space where the wave propagates, in order to simulate the wave propagation by time-discrete simulation of electromagnetic induction in every discretized element of space, as Figure 2.8 shows. The edges of the space elements indicate either electrical field or magnetical field. The electrical field of a space element in a certain time interval can induct the magnetical field of the neighboring space elements in the next time interval, meanwhile the magnetical field can induct the electrical field in the same manner. Thus, the wave propagation is simulated. In accordance with this method, the strength of the electromagnetic field at anytime and anywhere can be calculated exactly, including the places where the sensor receiver and the object surfaces are. Thus, the information carried in wave modulation, like phase and frequency shift, can be represented. In addition, this method can mesh the object surfaces into elements, so that the dielectric coefficients in different element can be defined separately and arbitrary geometric form of object surfaces can be modeled discretely. In this way, a physical modeling of the influence factors on object reflectivity, like material, angle of incidence and angle of reflection is possible.

---

[29] Skolnik, M. I.: Radar Handbook (2008).

[30] Ludloff, A.: Praxiswissen Radar und Radarsignalverarbeitung (2008).

[31] Fuchs, F.: Diss., Entwicklung und Verifikation eines RCS-Rechenmodells (2001).

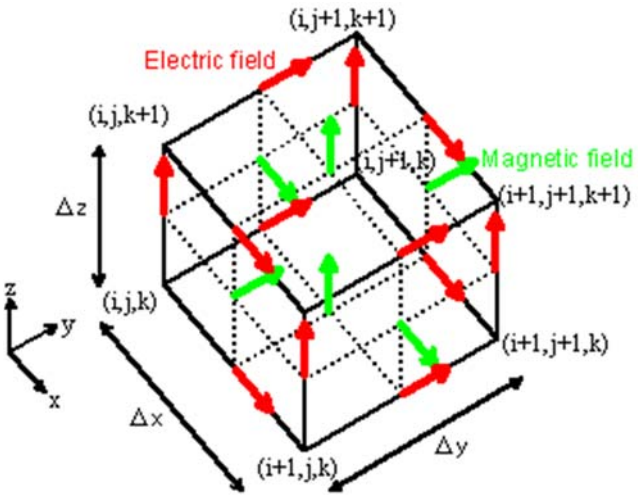

Figure 2.8 Working principle of FDTD[32]

However, on the one hand, the modeling of wave propagation in atmosphere can be complicated. Due to the long coherence time of some radars (e. g. frequency modulated continuous wave radar (FMCW-radar)), this method sometimes has to simulate a long time period, over which the model has to calculate the phase of wave in every time frame prospectively based on the wave frequency. In addition, in order to simulate the interference of the waves reflected from different directions without aliasing errors (Nyquist–Shannon sampling theorem), it is necessary to discretize the space around the propagation paths into extreme small elements. For example, according to Nyquist-Shannon sampling theorem, the space element size must reach at least 1.95 mm to simulate the propagation of 77 GHz automotive radar wave. This means, the electromagnetic induction in millions of elements must be simulated at the same time, in order to cover the pavement within the detection area of an automotive long-range radar (e.g. with a detection range of 200 m). On the other hand, the modeling of reflection by this method is complicated. As mentioned above, the reflection surfaces have to be meshed for modeling reflection. However, if the surfaces are not made from metal, they must be meshed in the dimension of depth as well, due to the penetration of radar waves.

For reaching a higher validity, finer meshing could be required, which makes the model built by this method more complex.

Ray tracing method

[32] Hirano, T.: FDTD (2017).

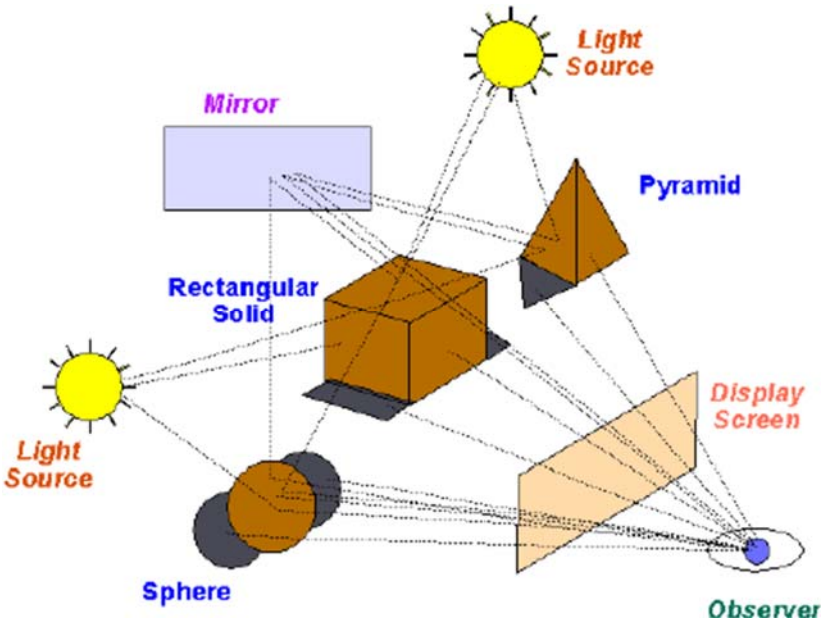

Figure 2.9 Working principle of ray tracing method[33]

Unlike the FDTD model that is based on the physical optics, the ray tracing method is based on geometric optics. Initially, this method is used for 3D image rendering. As Figure 2.9 show, the ray-tracing algorithm starts from the point of observer, and "shoots" a ray through each pixel of the display screen into the virtual world. In the graphic processing, the color and the brightness of each pixel shown on the display screen are decided by what the corresponding ray meets during its propagation. In the propagation, different phenomenon such as reflection and refraction could happen. Every reflection and refraction can influence the original pixel, because they changes the power and frequency range of the light that reaches the pixel at last. A ray must propagate until it find a light source, which indicates the sending power and frequency range of the light ray. For modeling shadows, shadow rays, which can go through objects, are used. Due to the limitation of geometric optics, the original ray tracing method is not able to simulate some physic phenomenon like diffuse reflection, caustic, interference or diffraction. However, with the development of this model, approaches like distributed ray tracing (for modeling diffuse reflection)[34], path tracing (for modeling caustic and global illumination)[35] and modification of object model (for modeling interference and diffraction)[36] are used for solving these problems.

[33] Villa-Martinez, H.: Accelerating Algorithms for Ray Tracing (2006).

[34] Cook, R. L. et al.: Distributed Ray Tracing (NY : ACM, 1984).

[35] Kajiya, J. T.: The Rendering Equation (NY : ACM, 1986).

[36] Johnston, D. V.; Tarjan, P. N.: CS348b Final Project (2006).

In this decade, the ray tracing method is also used for modeling perception sensors like camera[37], lidar[38] as well as simple pulse radar[39]. However, these descriptions are all created by simplifications, for example, without considering wave interference and reflection capability in detail[39] [40]. However, for modeling active perception sensors, the wave interference and the detailed reflection capability of every object are necessary, because the detection and measurement of the active sensors can be influenced by them significantly, unlike image rendering[41]. Meanwhile, unlike the camera, the active perception sensors have also separation capability in the dimensions of range and relative velocity, which cannot be described by ray-tracing method without modification. A grey-box modeling method, named hybrid Cell-Volume-Concept (HCVC), which presents a solution for this problem, is introduced in Section 4.2.3.

In summary, the advantages of the white-box sensor models are:

- A complete detailed representation of the internal structure of an perception sensor and the wave propagation on a physical level is present;
- The measurement results of an perception sensor can be reproduced with high accuracy due to the high modeling depth;
- When testing and validating a sensor or a driver assistance system by these models, each individual characteristic can be manipulated and analyzed.

The disadvantages of the white-box sensor models are:

- High computational complexity during simulation can be expected, especially when a complex environment is to be simulated;
- Low suitability for modeling different perception sensors exists;
- High model maintenance and model expansion effort can be expected;
- These models are principally not suitable for the conception and validation of a DAS or ADS in the early development phase, e.g. for the selection of perception sensors.

Generally, the models of this group are too complex and difficult to be adapted to different sensor variants, which makes it difficult for them to meet the requirements of the ADS validation.

---

[37] Liu, D. S.-M.; Hsu, C.-W.: Ray-Tracing Based Interactive Camera Simulation (2013).

[38] Majek, K.; Bedkowski, J.: Range Sensors Simulation (2016).

[39] Gubelli, D. et al.: Ray-tracing Simulator for Radar (2013).

[40] Buddendick, H.; Eibert, T. F.: Radio Channel Simulations (2005).

[41] Johnston, D. V.; Tarjan, P. N.: CS348b Final Project (2006).

Black-Box Model

The second group of perception sensor models includes the models that describe the general properties of perception sensors, without considering physical phenomenon or physical structures. This group of models is called "black-box model". Black-box modeling can be executed not only for modeling an entire sensor, but also for modeling a specific part of sensor workflow, like wave propagation or data processing. However, unlike the white-box modeling, it models in terms of the relationship between the inputs and the outputs of the object to be modeled (or transfer characteristics), without knowing its internal implementation. Black-box models are normally simple and efficient. Moreover, a black-box model can adapt itself to the modeling of different sensors by parametrization, if it is developed based on some generic characteristics.

Examples for such a model are:

1. **The Radar Equation**
   The radar equation is a basic model for modeling the propagation of radar wave, which is useful not only for estimating the range of a radar, but also for radar system design[42]. It provides a simplified mathematic relationship between transmitting power and receiving power of a radar sensor as follows[44a]:

$$P_{\mathrm{R}} = \frac{P_{\mathrm{total}} \cdot G \cdot \sigma \cdot A_{\mathrm{e}}}{(4\pi)^2 r^4} \cdot \frac{1}{L_{\mathrm{t}} \cdot L_{\mathrm{atm}}} \tag{2-10}$$

   where
   P_{R}: Received Power
   r: Radial Distance
   σ: Radar Cross Section (RCS)
   G: Antenna Gain
   P_{total}: Radiated Power
   A_{e}: Effective Area of Radar Antenna
   L_{t}: Losses in the Transmit Antenna
   L_{atm}: Losses in the Atmosphere
   As the equation shows, the radar equation only represents a relationship between transmitting power and receiving power based on an ideal wave propagation. The influences of wave propagation and sensor data processing on the receiving power are summarized as some simplified parameters like losses.
2. **Swerling Target Model[43]**

[42] Skolnik, M. I.: Radar Handbook (2008), p.1.11.

[43] Barton, D. K.: Radar system analysis and modeling (2004), p.94.

Swerling target model tries to provide a statistic (black-box) description for the fluctuation of radar targets reflection capability σ, as
Table 2.1 shows.

Table 2.1 Swerling target model[44b]

Model	Probability density p function of RCS σ	Fluctuation
Swerling 0	$\sigma = \bar{\sigma} = \text{const}$	None
Swerling 1	$p(\sigma) = \frac{1}{\bar{\sigma}} e^{-\frac{\sigma}{\bar{\sigma}}}$	From target illumination to target illumination
Swerling 2		From pulse to pulse or from burst to burst
Swerling 3	$p(\sigma) = \frac{4\sigma}{\bar{\sigma}^2} e^{-\frac{2\sigma}{\bar{\sigma}}}$	From target illumination to target illumination
Swerling 4		From pulse to pulse or from burst to burst

Swerling model 1 and 2 are used for representing the reflection capability of the targets, which consist of many reflectors in a similar size. Swerling model 3 and 4 are used for representing the reflection capability of the targets, which consist of a main reflector and some smaller ones. Swerling model 2 and 4 are specialized for modeling the sensors, which change their transmission frequency from pulse to pulse, or from pulse group to pulse group. The target fluctuation in such cases is quicker than in the other cases.
Obviously, such a statistic description cannot represent the relationship between the incidence angle of radar wave and the reflection capability physically.

3. **Statistic Estimation for Measurement Errors**[44c]
   According to Ludloff[44d], an empiric relationship between measurement errors and SNR (Signal-to-the-Noise Ratio) exists as follows.

$$\sigma_{t,\min} = \frac{1}{\beta\sqrt{2E/N_0}}$$

$$\sigma_{\phi,\min} = \frac{1}{\gamma\sqrt{2E/N_0}}$$

[44] Ludloff, A.: Praxiswissen Radar und Radarsignalverarbeitung (2008), a: p. 2-31; b: p. 3-17; c: p. 10-1; d: p. 10-4 - p.10-10.

$$\sigma_{f,\min} = \frac{1}{\alpha\sqrt{2E/N_0}} \tag{2-11}$$

where $\sigma_{t,\min}$ indicates the minimum standard deviation of measured time of flight (range); $\sigma_{\phi,\min}$ indicates the minimum standard deviation of measured azimuth angle; $\sigma_{f,\min}$ indicates the minimum standard deviation of measured Doppler shift (relative velocity); E is the signal energy; N_0 is the noise power density; α, β, γ should be respectively defined by an empirical formula according to some basic information from modulation, e.g. pulse duration, radiation pattern, or residence time of beam on target.

The equations can only be used to estimate the minimum standard deviation of measurement quantities. Due to the different data processing algorithms, the concrete relationship between measurement errors and SNR is more complicated than this description.

4. **Statistical Model for Sensor Behaviors**
   Hanke et al.[45], Hirsenkorn et al.[46], Hirsenkorn et al.[47] show some statistical sensor models. The representations of sensor behaviors in these models are principally created based on the statistics of sensor data. The concrete data processing is not taken into consideration.

Obviously, the most black-box models can only statically or statistically describe the performance of the sensors in a certain time frame. They cannot represent the performance exactly in every specific case.

In summary, the advantages of black-box models are:

- Simple structure and parameterizable interface
- Efficient simulation
- Representation possibility for the properties of the perception sensors of the same type

The disadvantages of black-box models are:

- Simulated measurement results with lower accuracy
- Less representation possibility for the different characteristics between different sensor versions of the same type.
- High difficulty in identifying their parameters (mostly statistical without physical meaning).

[45] Hanke, T. et al.: Generic Architecture for Simulation (2013).

[46] Hirsenkorn, N. et al.: A Non-parametric Approach (2015).

[47] Hirsenkorn, N. et al.: Virtual Sensor Models (2016).

- Unavoidable deviation from reality. These models cannot represent exactly the sensor performances or rather the sensor outputs in every specific case, therefore, they have less suitability for the usage in a HiL or SiL test, for example as signal inputs for a control unit or other hardware components of a DAS or ADS.

2.2.2 Current Simulation Products on the Market

Up to now, there are already some simulation products on the market in Europe: VIRES VTD, IPG CarMaker® , TASS PreScan, dSPACE ASM Traffic and Tesis DYNA4 Driver Assistance.

VIRES VTD – VIRTUAL TEST DRIVE[48]

VIRES VTD is a specific simulation software for testing ADAS, active safety and automated driving systems, in which very complex driving situations can be generated and simulated. (see Figure 2.10)

Figure 2.10 Simulated driving situation by VTD[48]

According to its user manual[49], a ray-tracing interface is provided in this software. However, neither sensor model nor wave propagation model has been provided to customers as product based on this interface.

[48] VIRES: VTD - VIRES Virtual Test Drive (2017).

[49] VIRES: Virtual Test Drive User Manual (2017).

IPG CarMaker®[50]

IPG CarMaker® is a simulation software developed by IPG Automotive GmbH. It enables a computer-aided virtual vehicle test, in which not only the driving situation, but also the parameters of vehicles and vehicle components, such as vehicle geometry, tire and chassis, the parameters of road model and automatic driver can be varied. In this way, various test cases for automated driving and vehicle dynamics tests can be generated. (see Figure 2.11)

Figure 2.11 Simulated driving situation by IPG CarMaker®[50]

During the test execution, various vehicle state variables, e.g. velocity, distance traveled, engine rotation speed or lateral acceleration on each wheel, can be calculated, recorded and displayed in diagrams.

Three kinds of active perception sensor models are provided in the current version of this software[51]:

1) Free Space Sensor+
   It is a generic geometry sensor interface, which can provide detailed virtual scenario with high resolution in 3-D and detect free space. This model can be considered as an ideal object model.
2) HiFi Radar Sensor
   This model simulates the detection based on SNR and describes the detection errors with probability of existence (false negatives/positives), which can be considered as a black-box sensor model.
3) Radar Raw Signal Interface
   In this model, the raw signal is provided. This means, the ToF, the amplitude and the relative frequency shift of the waves reflected by different reflecting points

[50] IPG: CarMaker (2017).

[51] IPG: Complex Scenarios for the Future (2017).

can be present as outputs. Therefore, this model is basically a white-box wave propagation model.

TASS PreScan[52]

PreScan of TASS is also a simulation platform for ADAS and active safety, which enables the representation of different driving scenarios as test cases for ADAS. By this software, various passive perception sensors such as camera, fisheye camera and the corresponding light effects can be modeled realistically. (see Figure 2.12)

Figure 2.12 Simulated driving situation by TASS PreScan[52]

For modeling active perception sensors like radar, lidar or ultrasonic sensors, this software can use GPU to provide a visualization of sensor beams, by which the field of view of sensor, range and scan patterns can be visualized[53]. This part of the software is principally also a kind of white-box modeling for light propagation in the atmosphere, which can be considered as an interface and extended for further sensor performance modeling.

In active perception sensor modeling, some research investigations have already been carried out by TASS and models for this purpose exist on the market as add-on product for PreScan as well[54]. These models can model different types of sensor errors such as white/colored sensor noise, false positive/negative detections[55]. However they are principally based on a probabilistic model (see Figure 2.13), which is a typic black-box model. Therefore, they inherit most disadvantages of black-box models described in Section 2.2.1.

[52] TASS: PreScan (2017).

[53] TASS: New in PreScan (2017).

[54] wendweb: BASELABS Models in PreScan (2017).

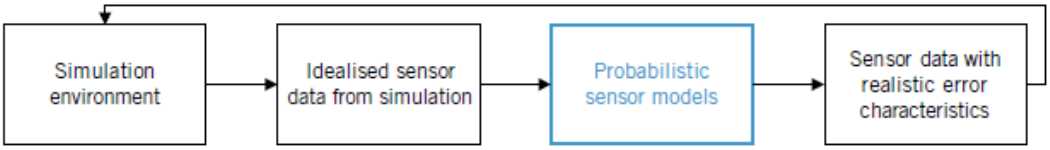

Figure 2.13 General structure of an add-on black-box sensor model for PreScan[55]

dSPACE ASM Traffic[56]

ASM Traffic of dSPACE is a simulation tool suite for supporting the development and test of ADAS and autonomous driving features as well. This software can offer models of multiple sensors for object detection and recognition. Beside the detection of other traffic vehcles and traffic objects, the sensor models in ASM Traffic can principally provide the contours of cars and humans, traffic signs, and obstacles.

For modeling active perception sensor, the sensor model uses only a purely geometrical approach. The nearest point of each detected vehicle or object can be calculated by this approach (see Figure 2.14). The distance, relative velocity, relative acceleration, and relative horizontal and vertical angles for this point can be calculated as well[56]. The sensor model here can be considered as an ideal data interface from sensors. It can be used as a basis for the further sensor modeling.

---

[55] Schubert, R. et al.: Simulation of Sensor Models (2014).

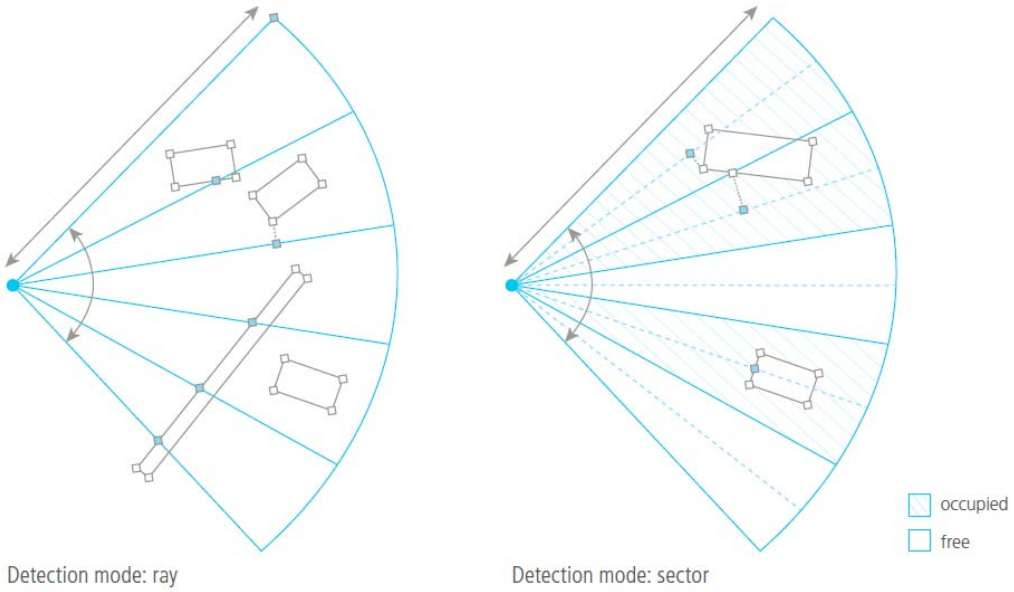

Figure 2.14 Object detection in dSPACE ASM Traffic[56]

Tesis DYNA4 Driver Assistance[57]

DYNA4 Driver Assistance is also a simulation framework for ADAS-Tests. It can provide a physical sensor simulation for the pulse-echo-method based sensors (e. g. ultrasonic sensor and lidar). In this sensor simulation, a ray tracing interface is principally provided. The ToF and signal strength of each reflected ray are represented as outputs (see Figure 2.15). When modeling the signal strength of the rays, the attenuation caused by radial propagation, the atmospheric attenuation, the absorption and reflection of objects and the sensor radiation pattern are taken into consideration. However, the representation of sensor performance, phase shift and interference of the rays is not included in the model. Therefore, this model is basically a white-box wave propagation model, which is not suitable for radar modeling without extension.

[56] dSPACE: ASM Traffic (2017).

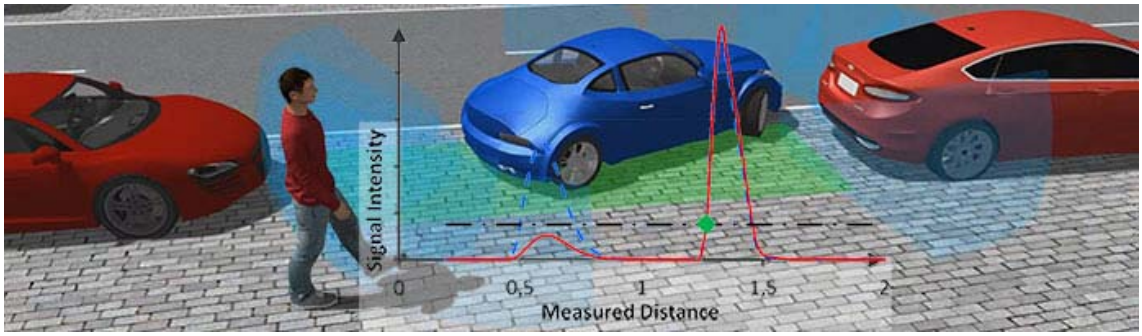

Figure 2.15 Signal intensity simulation in Tesis DYNA4 Driver Assistance[57]

Summary

In summary, various simulation products are present for virtual validation of ADAS and have the potential for ADS. However, in these well-known simulation products, a complete and realistic model for the active perception sensor modeling does not exist. The current models in these produces are partly black-box models, which can only offer a limited validity; partly only interfaces, which have to be extended by the users before utilization.

[57] TESIS: Sensorsimulation (2017).

3 Generic Grey-Box Modeling

As discussed in Chapter 2.2.1, both white-box models and black-box models have their disadvantages. This represents the common dilemma in the simulation-based test methods. In order to ensure the validity of test results, high requirement must be set on the quality of driving environment representation and vehicle component simulation. The white-box models, which are based on sensor working principles or physic laws of electromagnetic waves, can describe the characteristics of sensors in high fidelity. From this point of view, the white-box models can be considered the best solution for simulation-based methods. Nevertheless, these models are not usually used in virtual validation of ADS for two reasons. On one hand, the increasing fidelity in white-box modeling can affect the testing efficiency easily (e.g. by simulating more optical phenomena or using finer meshing in Finite Difference Time Domain method (see Chapter 2.2.1)). On the other hand, a model of this kind is normally developed for a certain specific individual sensor. The low reusability of these models limits their application in the early development phase of ADS, while simulation-based test methods because of their low monetary effort and time exposure should have a wide range of applications[58], for example in perception sensor selection.

Under this circumstance, black-box modeling methods like stochastic modeling method find their application in environment perception sensor modeling. However, as mentioned in the Chapter 2.2.1, black-box models can only offer a static or statistic description of the sensor performance in a certain time frame, and therefore cannot represent exactly the performance in every specific case. This makes it almost impossible to be used for error analysis or system identification, which are essential for system validation. According to Bernsteiner[59], by using the phenomenological method, black-box models can be extended to represent some sensor performances in some specific cases. However, this method is principally also based on a priori knowledge, therefore, it cannot be applied to identify the unknown problems of the object under test (OuT), either.

In summary, in order to extend the usage of simulation-based methods in ADS validation, a novel modeling method that can

1. describe the different sensor performances in every specific case (dynamic sensor performance description);
2. be reused generically for modeling different sensors;
3. permit efficient (at least real-time) test execution,

[58] ISO/TC 22/SC 32: ISO 26262-1:2011 (2011).

[59] Bernsteiner, S. et al.: Radarsensormodell für den virtuellen Entwicklungsprozess (2015).

is required.

A sensor modeling method with these characteristics is named “generic grey-box modeling” in this dissertation. The first requirement is explained in Section 3.1. How to insure the generic of model is discussed in Section 3.2. The requirement on efficiency is always taken into consideration when developing the model and verified after modeling.

3.1 Identification of Important Dynamic Sensor Performances

Before the development of the framework for generic grey-box modeling, it is necessary to define the dynamic sensor performances or, in other words, to identify the important dynamic sensor performances to be modeled.

The limitation on the dynamic sensor performance representation in black-box models is primarily due to the model parameterization based on the performance indicators in sensor specification. The sensor can meet these indicators only under a handful of test conditions defined in the specifications. However, various influence factors can influence the actual sensing performance. For example, on the one hand, external physical phenomenon in wave propagation, such as atmospheric attenuation and multi-path interference, can affect the instantaneous wave power received by antenna that is essential for the performance of detection and measurement; on the other hand, sensor internal factors, such as antenna pattern and receiver noise, play also roles in instantaneous sensor performance. On this account the static performance indicators in sensor specification cannot reflect dynamic sensor performances under changing conditions. Accordingly, black-box models based on these performance indicators can hardly represent the dynamic sensor performance by themselves. In order to solve this problem, it is first necessary to identify the sensor performances, whose dynamic progressions have to be, but have not been described by the performance indicators in the sensor specifications.

A significant difference between the working principles of active and passive perception sensors exists. As this dissertation focuses on modeling the active perception sensors, which transmits modulated waves actively, the following discusses only the issues on the dynamic performances of active perception sensors.

The performance indicators in the sensor specifications of active perception sensors can be classified into four categories: detection capability, measured states, separation capability and latitude measurement capability. The analysis of the influence factors that can influence these performances dynamically and their influences on the functionality of ADS are as follows:

3.1.1 Detection Capability

Active perception sensors must detect objects before providing measured quantities for these objects. Sensor specification defines normally a specified range for the sensor, but it does not mean that all objects in this specified range can always be detected. Theoretically, the object detection in active perception sensor works by comparing the received power and a power threshold. An object is detected, when the received power is higher than threshold. However, in practice, the signal/noise ratio of received wave (SNR) decides whether an object can be detected. The SNR is defined as follows[60]:

$$SNR = \frac{P_{\text{signal}}}{P_{\text{noise}}}, \tag{3-1}$$

where P_{signal} is the power of signal reflected by object, and P_{noise} is the noise power.

Principally, a low SNR of received wave can lead to two kinds of detection errors: false negative error and false positive error. False negative error stands for that the sensor does not detect an object because the signal power P_{signal} is lower than the threshold. False positive error stands for that the sensor detects a non-existent object, which is because the signal power is not much higher or even lower than the noise power, and meanwhile the threshold is set too low.

As mentioned above, the SNR can be influenced dynamically by various influence factors; therefore, detection capability is a dynamic performance.

The probabilities of the detection errors are called false positive rate and false negative rate, which can significantly influence the functionality of DAS or ADS, especially for object-tracking[61]. Their essentiality for dynamical environmental interpretation in these systems reasons the necessity of dynamic modeling.

3.1.2 Measured States

As explained in Chapter 2.1.1, an active automotive perception sensor can determine at least object states in three dimensions: the radial distance between sensor and object (range), the relative velocity and the azimuth angle of object in sensor view. Advanced lidars like 2-D laser scanners and some radar sensors can also have a resolution in elevation angle. Therefore, object states (quantities) in up to four dimensions can generally be measured. Like other measuring instruments, current sensor specifications give normally a definition of measurement accuracy and range of these quantities as performance indicators. However, the SNR of the received waves plays a decisive role not only in detection

[60] Skolnik, M. I.: Radar Handbook (2008), p. 1.11.

[61] Reuter, S.: Diss., Multi-object tracking (2014).

but also in measurement accuracy and range[62]. The relationship between measurement range and SNR has already been explained by radar equation (see Chapter 2.2.1). In practice, the measurement accuracy deviates from indicator defined in specification easily, even when signal strength is high enough for a significant detection. Beside external physical phenomenon and sensor internal factors as mentioned above, object characteristics like varying reflectivity-distributions over objects at different aspect angles can also lead to the difficulty in measuring the position of an object represented by a peak in time or frequency domain.

Some functions of DAS and ADS are sensitive to the range and measurement accuracy of their perception sensors. For example, inaccurate velocity measurements can lead to incorrect object classification, or uncomfortable vehicle acceleration variation under adaptive cruise control (ACC)[63].

3.1.3 Separation Capability

With the development of DAS and ADS, the requirement on interpretation of complex traffic scenarios is increasing. A capability of multi-target detection that enables such an interpretation has growing importance for modern perception sensors. In order to detect multiple targets, a sensor must have the capability to separate one object from another firstly, or so-called separation capability. Although measuring principle and data quantization process of a sensor limit the separation capability, the separation capability is in practice also dynamic. It is influenced by the amplitudes of the signals reflected from the objects to be separated.

The signal received by a sensor has always an uncertainty (with a width in a certain measureable quantity domain). On the one hand, according to Heisenberg's uncertainty principle, it is impossible for the sensors to receive an ideal Dirac impulse from object in any measurable quantity domain. Even when scanning rays for azimuth or elevation angles, or gating pulses for range, uncertainty has to be considered as well, because the beam or the pulse have a finite width. On the other hand, uncertainty can also be caused by some data processing functions in sensors. For example, the anti-leakage processing in discrete Fourier transformation applied in various domains can produce uncertainty[64].

The uncertainty is the reason why the separation capability of a sensor is limited. Accordingly, the different uncertainties of the signals from different objects are the reason why

[62] Ludloff, A.: Praxiswissen Radar und Radarsignalverarbeitung (2008), p. 10-1.

[63] Winner, H.; Schopper, M.: Adaptive Cruise Control (2016).

[64] Andres, M.: Diss., Charakterisierung komplexer Ziele (2015).

the separation capability is dynamic. The influence of different uncertainties on separation capability can be summarized into four cases (see Figure 3.1).

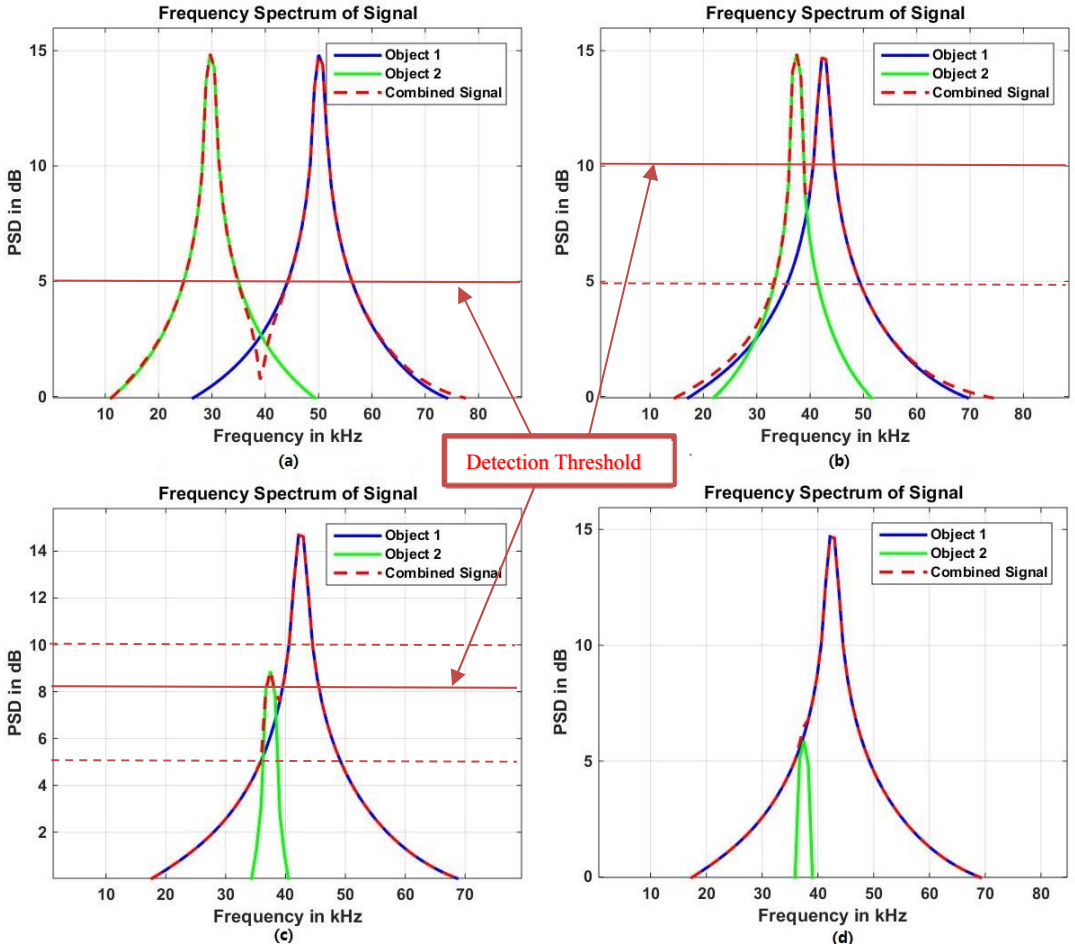

Figure 3.1 Sensor separation capability in four cases

In Figure 3.1, three curves are shown. They represent respectively the signals reflected by two different objects, and the signal superimposed by them phase-dependently (combined signal). Case (a) shows that two neighboring objects, Object 1 and Object 2 that can be separated by a detection threshold of 5 dB. By comparing the threshold with the combined signal received by sensor for detection, two objects can be detected obviously. However, when the distance between these objects in frequency domain is reduced (case (b)), only one object can be detected by using a threshold of 5 dB. In this case, some advanced sensors with dynamic threshold can estimate and set an appropriate threshold, for example, raise the threshold to 10 dB, so that Object 1 and 2 can still be separated. Case (c) shows a more complicated situation. In this case, the wave reflected by Object 2 provides a much lower power than the one by Object 1. Thus, neither the threshold of 5 dB nor the threshold of 10 dB can separate the two objects. Even the sensors with dynamic threshold have to face a hard challenge in the threshold estimation. Only when sensor settles the threshold in the same way as shown in Figure 3.1 (c), a separation can succeed.

In Case (d), the peak from Object 2 is so small that it is almost totally covered by the peak from Object 1. In this case, the separation of these two object in the frequency domain is hardly possible.

As discussed above, the separation capability of a sensor can be influenced by the (abstract) distance between two objects in a corresponding dimension, their amplitudes, their phases and the detection threshold. Unseparated objects will lead to errors of two kinds: detection error (false negative error of at least one object) and/or state measurement error due to the mixing of the states of unseparated objects.

3.1.4 Latitude Measurement Capability

Modern perception sensors must also be able to measure object latitude besides separating object, as information about object latitude, especially the object width, is essential for some ADS or DAS to interpret traffic scenarios and plan their next moves. Object widths indicate the positions of the object edges, which are, for example, useful for object tracking[65], object classification[66] and drivable region detection in traffic scenarios[67]. In principle, the object width measurement stands under the influence of both object detection and separation. As mentioned above, the detected reflecting points that cannot be separated will be recognized as one raw object. After that, a clustering algorithm[68] will be used upon the raw objects to get "real" objects (clusters). Based on clusters, a width measurement can be executed. Thus, obviously, the accuracy of width measurement is decided by how well clustering can be performed. However, the execution of the most clustering algorithms relies on the dissimilarity between raw objects. The dissimilarity calculation is decided by the size and position of the raw objects, which are dependent on their components, in other words, the existence and separation of the reflecting points. On this account the width measurement accuracy is dynamic in reality, as the performances on detection and separation are dynamic.

In summary, the major performance parameters of active perception sensors consist of the detection capability, the range and accuracy of measured states, the separation capability, and the latitude measurement capability. These performances can all change dynamically. Building a consistent relationship between these performances parameters and their influence factors should be a concrete explanation of the first requirement on active sensor modeling summarized at the beginning of this chapter.

---

[65] Darms, M. et al.: Classification and tracking (2008).

[66] Bartsch, A. et al.: Pedestrian recognition (2012).

[67] Li, Q. et al.: A Sensor-Fusion Drivable-Region (2014).

[68] Xu, R.; Wunsch, D. C.: Clustering (2009).

3.2 Determination of Generic Inputs and Outputs

In order to fulfil the second requirement on the generic, it is necessary to find out if every part in active perception sensors can be represented generically, and determine what the inputs and outputs of the model to be developed are. The analysis presented in this section and the basic idea of the framework in Section 3.3 were published in Cao et al.[69].

In order to find out the generic describable parts of active perception sensors, it is necessary to analyze their working principles at first. The working principles of a simple radar is as follows (see Figure 3.2). The analysis here is performed based on it as example.

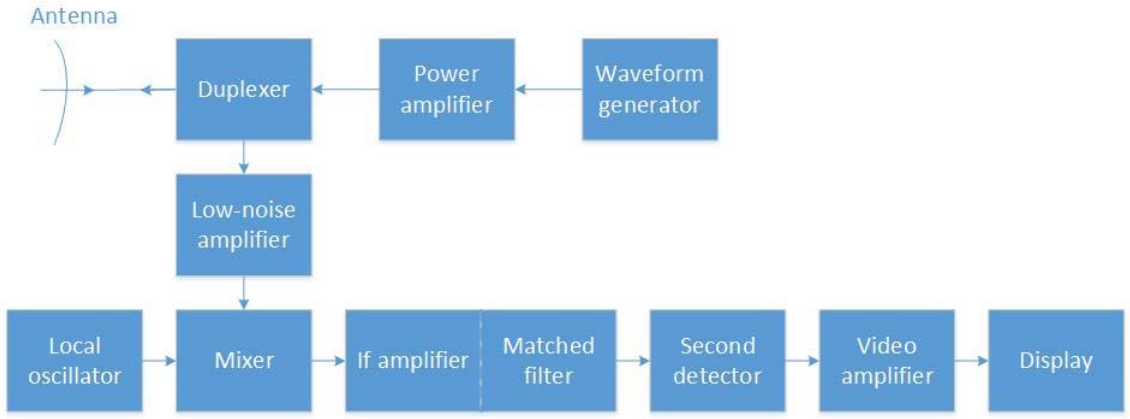

Figure 3.2 Working principle of a simple radar (with a power amplifier as the transmitter in the upper portion of the figure and a superheterodyne receiver in the lower portion of the figure) [70]

At first, the transmitter sends electromagnetic waves with modulated waveform into atmosphere through antenna. The modulation type of the waves depends on the sensor type (e.g. pulse-radar, FMCW-radar etc.). The transmitters of some radars share the antenna with the receivers. If an object exists in the way of the wave propagation, the surfaces of this object will reflect some parts of the wave. The sensor antenna will capture the reflected wave together with some noise in the atmosphere. The noise of this type is called external noise. After that, the receiver will receive the reflected waves with noise as signals. In this process, the thermal noise and semiconductor noise from the antenna circuits, pre-amplifier and demodulator (like the low-noise amplifier and mixer in Figure 3.2) make up another type of noise, internal noise. In the subsequent processing, the filter in the signal processor will try to raise the SNR of the signals, so that the signals are ready for the application in object detection and states measurement. Almost every type of sensors has its own specified filter algorithm; nevertheless, raising SNR as their objective is generic. In the detector, the required inputs depend strongly on the sensor type or the

[69] Cao, P. et al.: Perception Sensor Modeling (2015).

[70] Skolnik, M. I.: Radar Handbook (2008), p. 1.3.

modulation type. For example, simple pulse radar detects objects detecting through a threshold over signals in time domain, FMCW radar detects in frequency domain. The inputs required by the detector can be either a time sequence of the measurements or a frequency spectrum of a short wave period. After detection, the raw objects that are important for driving tasks can be identified. Unimportant objects like buildings on the roadsides will be neglected by the sensor. Their states such as range r, relative velocity v_{rel}, azimuth angle ϕ, elevation angle ϑ (if possible) will be obtained through data processing. However, as explained in Section 3.1.3 and Section 3.1.4, the "objects" in the raw object list indicate only inseparable reflecting points in atmosphere. The raw object list may deviate significantly from reality. There are two kinds of deviations. On the one hand, a real object may occupy many separable reflecting points (raw objects). The states of these "objects" can fluctuate significantly under varying aspect angles during driving, although they are from the same real object. This can cause problems for the next data processing steps like object tracking. As mentioned in Section 3.1.4, clustering algorithms are a possible solution for this problem. A clustering algorithm will provide a classification of the raw objects based on their separation and similarity, in order to achieve "real" objects. Of course, due to the performance of clustering algorithm and measurement errors, the "real" object list still can deviate from the reality. The deviation is considered normally as clustering error. On the other hand, as mentioned in Section 3.1.3, due to the limited separation capability of the sensor, more than one object in reality can be recognized as one raw object; meanwhile, as mentioned in Section 3.1.1, the detection errors, like false negative and false positive errors, exist. For reducing the occurrence probability of these errors, time based algorithms like association algorithms or tracking algorithms should be used[71] [72]. In practice, according to use cases, every sensor manufacturer selects, implements and parameterizes the algorithms above in its own way. A combination of very different solutions can be developed und used. After this part of data processing, a track for each object can be obtained. These information can be used by different applications (e. g. ADAS or ADS) or displayed to an operator as shown in Figure 3.2.

Obviously, according to the analysis above, not every part of active perception sensors can be modeled in a generic way.

On the wave propagation side, due to the different modulation types of different sensors, a modeling of the changes of electromagnetic field, as the FDTD method reveals, can hardly be a generic description. However, it is still possible to describe the major wave characteristics like wave power, phase shift, frequency shift, incidence angle or time of

[71] Blackman, S. S.: Multiple-target tracking (1986).

[72] Stewart, C. et al.: A neural clustering approach (1994).

flight generically. By using these characteristics, the physical phenomenon of wave propagation in different driving scenarios (e.g. with different vehicle constellations or under different weather conditions) can be represented.

On the sensor side, as introduced in Section 2.2.1, by modeling each sensor component separately (white-box modeling), a generic description cannot be achieved, as every sensor can have its own specific components. Therefore, it is much more meaningful for a generic description to consider an active perception sensor as a collection of the generic functional components (as shown in Figure 3.2) and their performances. It is assumed that the functional and nonfunctional safety of these components can always be insured in simulation, as finding design errors or quality problems of the sensor to be modeled is not the focus of system validation. Under the circumstances, the performances of these functional components should be modeled, as they reveal the difference between different sensors. Performance means how well a person, machine, etc. does a piece of work or an activity[73]. This means, a performance can be evaluated based on the "activity" to be done without considering which machine is used. The generic functional components are generic, as they describe the same activities for different sensors. Therefore, their performance can also be evaluated in the same way. Some generic performance criteria can be used for this evaluation, and for the modeling of these performances as well.

The functional components, "amplifier", "receiver" and "antenna" are aimed at an activity of sending/receiving/amplifying signals in different directions. How well the signals are sent, received or amplified can be described easily by an antenna performance criterion called "radiation pattern" or a certain direction-selective amplification coefficient. Therefore, the performance of amplifier, receiver and antenna can be modeled generically. The functional component, "filter", is aimed at an activity of raising SNR of signals. Its performance can be described generically by the difference between SNRs before and after the component. The activities in "detector" are the detection of raw objects and the measurement of their states. As the last cascades of sensor data processing, their performance criteria are the same as the ones for sensor (see Section 3.1). Therefore, they can be modeled generically as well. The functional components, "modulator" and "demodulator", depend strongly on the sensor type. As mentioned above, different sensors can utilize different modulation methods. In principle, they cannot be modeled in a generic way. However, regarding the object detection and states measurement, the modulation and demodulation decide the theoretically attainable limit of some sensor performances (e. g. separation capability). Since the sensor performances criteria are generic, this kind of influence can be modeled generically as well.

[73] Cambridge Dictionary: Performance (2017).

However, as mentioned above, the data processing algorithms after the detection and state measurement (clustering/association/tracking) are strongly depending on the use cases and the hypothesis of sensor manufacturers on results (e.g. how is dissimilarity defined in clustering; how are object states or measurement errors estimated etc.). Obviously, a generic modeling of these components is impossible, as neither their algorithms nor their concrete activities are present.

In summary, as a generic description, the grey box model to be developed should limit its scope to the detection and measurement of raw objects. For describing wave propagation, a model for calculating the power, phase shift, frequency shift, incidence angle or time of flight of the received waves is required. For modeling sensor generically, radiation pattern, the SNR-gain after filter and dynamic performance descriptions of sensor are necessary.

3.3 Framework for Generic Grey-Box Modeling

The discussion in Section 3.2 has divided the sensor modeling into two parts: wave propagation modeling and sensor performance modeling. The boundary lies between a broad definition and a narrow definition of sensor model. The narrow definition defines a sensor model as a model that represents a certain sensor and its activities. The broad definition extends the model to the representation of a certain sensor, its activities and the influence factors on it. When constructing a framework for generic grey-box modeling, the definition of wave propagation is also extended in the same way. An environment model that describes some influence factors on wave propagation is taken into discussion, so that the framework can have a good compatibility with the current simulation software like IPG CarMaker® (see Section 2.2.2). In this way, the framework for generic grey-box modeling of active perception sensors can be decomposed into three parts: the environment model, the sensor model, and the wave propagation model. The structure of this framework is as Figure 3.3 shows.

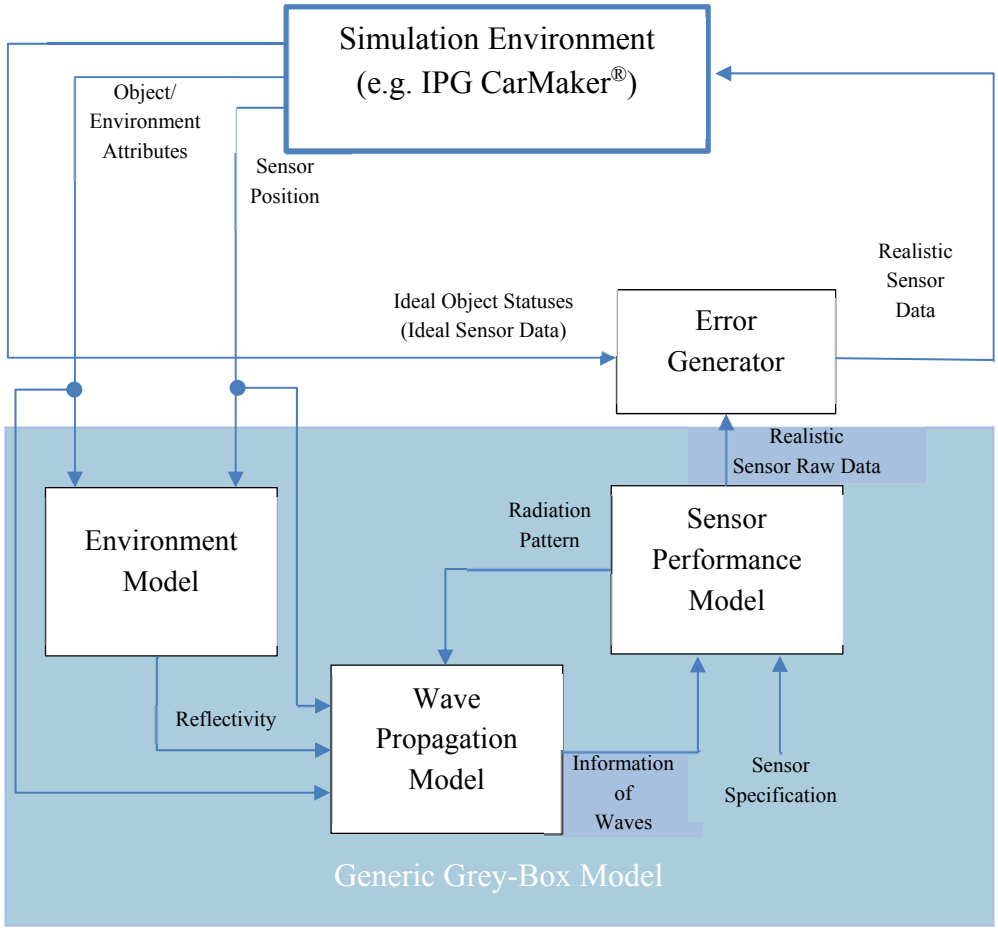

Figure 3.3 Framework for generic grey-box modeling

The sensor model to be developed is a part of a driving simulation environment, such as IPG CarMaker®. Such a simulation environment can offer ideal object statuses easily. The grey-box sensor model is designed for simulating the realistic sensor behaviors, in other words, representing the detection and measurement errors that a real sensor can make. Therefore, as Figure 3.3 shows, the grey-box sensor model simulates realistic sensor raw data at first. According to these data, an error generator will generate detection and measurement errors and add them to ideal object statuses, in order to generate realistic sensing data and send them back to the simulation environment.

According to the requirements on sensor modeling, the entire sensor model should represent the dynamic performances of the sensor. As the last cascade of the entire sensor model, the sensor performance model should describe the dynamic response behaviors of an active perception sensor on changing influence factors. As analyzed in Section 3.1, the influence factors affects the sensor performances mainly through the waves received by sensor. Therefore, as inputs, on the one hand, the sensor performance model requires information of waves from the wave propagation model. On the one hand, some static performance indicators (e.g. cell dimensions (explained in Chapter 4)) and some sensor characteristics (e.g. transmission power) in sensor specification are still useful for dynamic

performance modeling. The sensor performance model requires also this information as inputs for basic construction and calibration. As discussed in Section 3.2, the sensor model, in order to fulfil the requirement on the generic, should consist of functional components instead of physical components. Therefore, the sub-models in sensor performance model use the performance criteria of functional components as variables. When modeling a real sensor, users can parameterize these variables for simulating different performances of different sensors. On the output side, the sensor performance model provides the error generator with realistic sensor raw data, so that the error generator can generate realistic errors made by sensor based on them.

The wave propagation model describes the wave propagation in atmosphere. As discussed in Section 3.2, a generic wave propagation model can provide the sensor performance model with the major wave characteristics like wave power, phase shift or time of flight, frequency shift and receiving angle. These characteristics change, if different physical phenomenon occur on the way of propagation. According to optics, the major physical phenomenon on wave propagation are atmospheric attenuation, reflection, diffraction, refraction, interference[74]. The effect of reflection depends on the reflectivity of objects in environment. The environment model can provide this information. The effects of atmospheric attenuation and interference depend on the relative positions between sensor and reflecting points. The simulation environment can offer this kind of information. For modeling wave power of received waves, the transmission power is necessary. Therefore, the angle-selective transmission power, or so-called radiation pattern of sensor is also one of the important inputs for the wave propagation model.

The environment model calculates the reflectivity of reflectors in the driving situations. The reflectors include not only the sensor objects but also some important reflecting surfaces that influence wave propagation significantly in atmosphere. For example, some large flat surfaces, which are the main causes of interference, (e. g. road surfaces) are included. The reflectivity of a surface depends principally on the its material, surface finishing, geometry, frequency of wave, angle of incidence, angle of reflection, and so on. The model should get the surface-dependent influence factors, like material and surface finishing, from some attribute definitions in simulation environment. The geometry of a surface is important, because it decides the normal direction of the surface at the point of reflection. This information belongs also to object attributes. With this information, the environment model can calculate the angle of incidence and reflection based on the positions of sensor and reflecting points.

In summary, the discussion above leads to the framework of generic grey-box modeling in Figure 3.3 as conclusion

[74] Schneider, R.: Diss., Modellierung der Wellenausbreitung (1998).

4 Sensor Performance Model

According to the requirements set in Chapter 3, the sensor model should be able to simulate the dynamic performances of an active perception sensor under changing condition. Therefore, as the last cascade of the sensor model, the sensor performance model should,

1) offer an realistic description of sensor performances, and
2) parameterize this description by influence factors.

For this reason, this chapter starts from a method for describing sensor performances, called "Cell-Volume-Concept" (CVC), and introduces a sensor performance model developed based on this method. After that, this chapter introduces three different ways to parameterize the model of sensor performances with the influence factors on them (characteristics of waves received). The three ways lead to three different variants of the modeling method, which have different requirements on wave propagation modeling. What one of them requires is principally a generic description of ray-tracing method, which is the current state-of-the-art in grey-box wave propagation modeling (see Section 2.2.2). However, this dissertation will implement a sensor performance model by another way, which is more suitable for modeling current automotive radars.

4.1 Cell-Volume-Concept for Sensor Performance Representation

The SNR model is a way to represent the active perception sensor performances, as the SNR can influence all the performances discussed in Section 3.1. However, only the SNR alone cannot describe the separation capability. Winner[75] introduces the Cell-Volume-Concept (CVC) as an abstract representation of the radar sensor performances besides the SNR model.

CVC introduces a concept of a "cell" to solve the problem of representing separation capability. In principle, a sensor with multi-target capability can separate objects in at least one of the following dimensions of measurement quantities: radial velocity, range, azimuth angle or elevation angle. As explained in Section 3.1.3, the existence of the measurement uncertainty in the dimensions of measurement quantities limits the separation capability of sensor in these dimensions. Before the introduction of the "cell" concept, the "bin" should be introduced as first. A bin is defined as a small length in a certain measurement quantity dimension. The physical minimum discretization steps in measurement caused by the physical limitation decides its dimension. For example, the minimum bin width of range is the reciprocal of the frequency bandwidth used for modulation.

The effective measurement time and the carrier frequency determines the minimum bin width of radial velocity measured by the Doppler Effect[75].

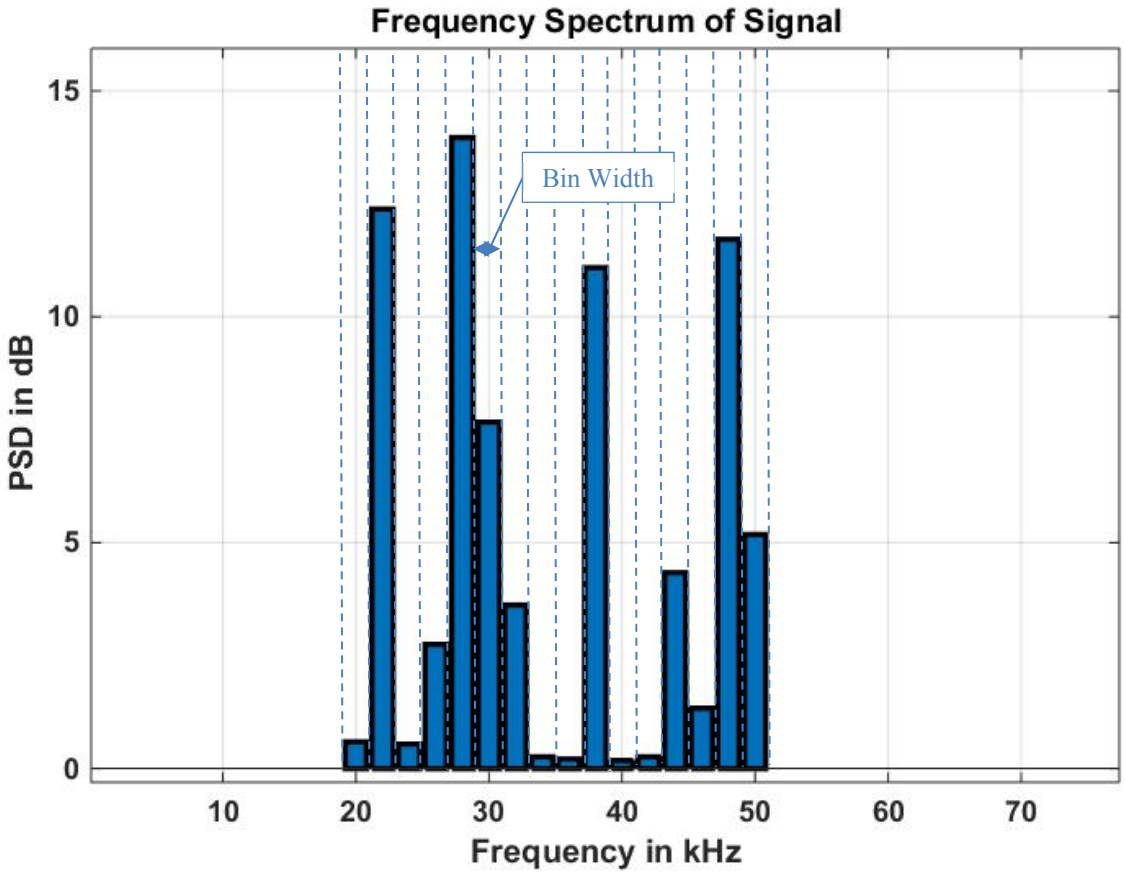

Figure 4.1 Bin description of separation capability

Figure 4.1 shows how to represent separation capability by bins. A sensor modeled in Figure 4.1 as example has a separation capability in radial velocity measured by Doppler Effect. Because of the linear relationship between radial velocity and Doppler frequency, the bins generated in the frequency dimension in Figure 4.1 can represent the bins in the velocity. Normally, in every bin, the sensor can receive signal power because of reflected wave or noise. As described in Section 3.1.3, object detection can be performed by using a detection threshold. Thus, if between two detected objects, one or more bins, which show lower power, exist, it means principally the sensor is capable of separating these two objects (It is assumed that the objects have no dimensions (point-object)). Otherwise, the sensor is not capable of separating these two objects. Theoretically, the minimum distance between two separable objects is a distance of two bins. In practice, as explained in Section 3.1.3, anti-leakage windows (the distributed curves in Figure 3.1) make the effective separation distance larger. Under these circumstances, the sensor needs a relative distance of at least three bins to separate objects. However, this depends on the signal power as well. The power-dependent dynamic representation of separation capability will be introduced in Section 4.2.

As an automotive radar measure at least states in three dimensions: range, radial velocity and azimuth angle, the bins in three dimensions compose a volume in measurement quantity space. Figure 4.2 shows a representation of such a space with bins in a 3D coordinate system.

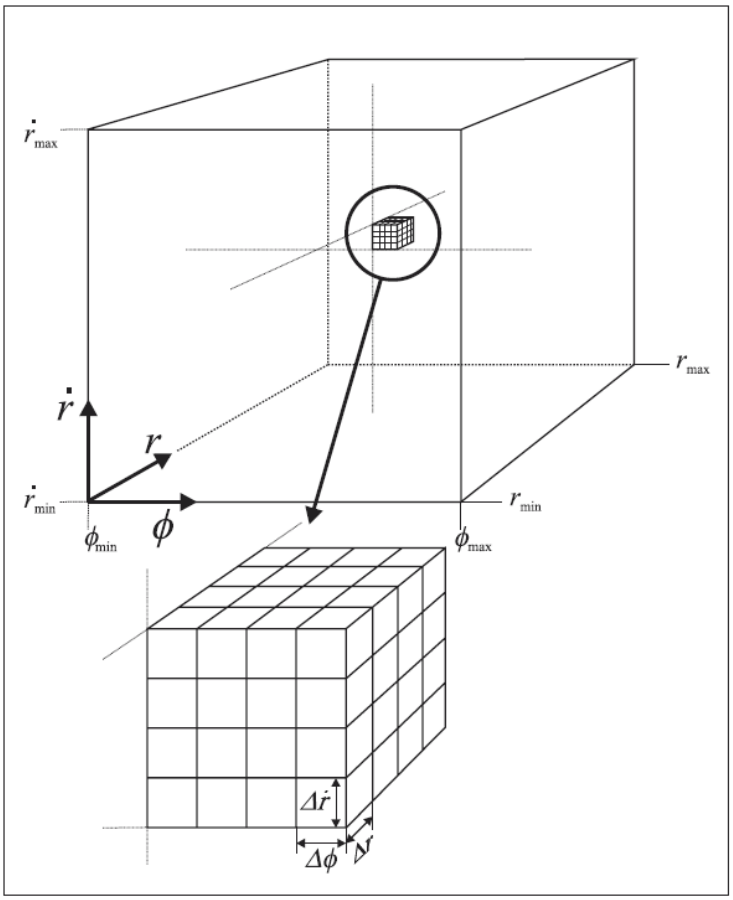

Figure 4.2 3D cell volume for radar[75]

The volume, which is defined by the bins in measurement quantity dimensions, is called "cell". Obviously, the separation capability of a sensor is better than others, if its cell dimension is smaller. All the cells together represent the entire measurable space, which is limited by the minimum and the maximum of the measurable quantities. The measurable space divided in cells is called "cell-volume". According to the 3D description, a sensor can separate two objects, only when at least one cell exists between them.

As some modern perception sensors have the possibility to separate objects in elevation angle, the cell can be generally extended to a four-dimensional space.

[75] Winner, H.: Radarsensorik (2009).

However, the CVC has to be changed for modeling some particular sensors. For example, lidar measures the relative velocity by the derivative of range. It does not have a separation capability in velocity; therefore, the relative velocity dimension does not exist in CVC for lidar. However, lidar has normally a separation capability in elevation angle because of its narrow beam, so a cell of lidar consists of the following three dimensions: range, azimuth angle and elevation angle.

Another example is FMCW radar. The cell-volume has to be deformed for modeling FMCW radar. As described in Section 2.1.1, the range and velocity measurement of FMCW radar are coupled. The FMCW radar can principally only use the separation capability in the frequency dimension to separate objects with different ranges and velocities. According to Equation 2-6, the boundaries of the n-th bin in range and velocity can be described as follows:

$$v_{\mathrm{rel}} = \frac{c}{2}\frac{n\Delta f}{f_0} - \frac{m}{f_0}\cdot r \tag{4-1}$$

where c is the light speed; m is the slope of linear frequency change; f_0 is carrier frequency; Δf is the bin width in frequency.

Thus, the bins of FMCW for positive and negative frequency slope m is as Figure 4.3 shows.

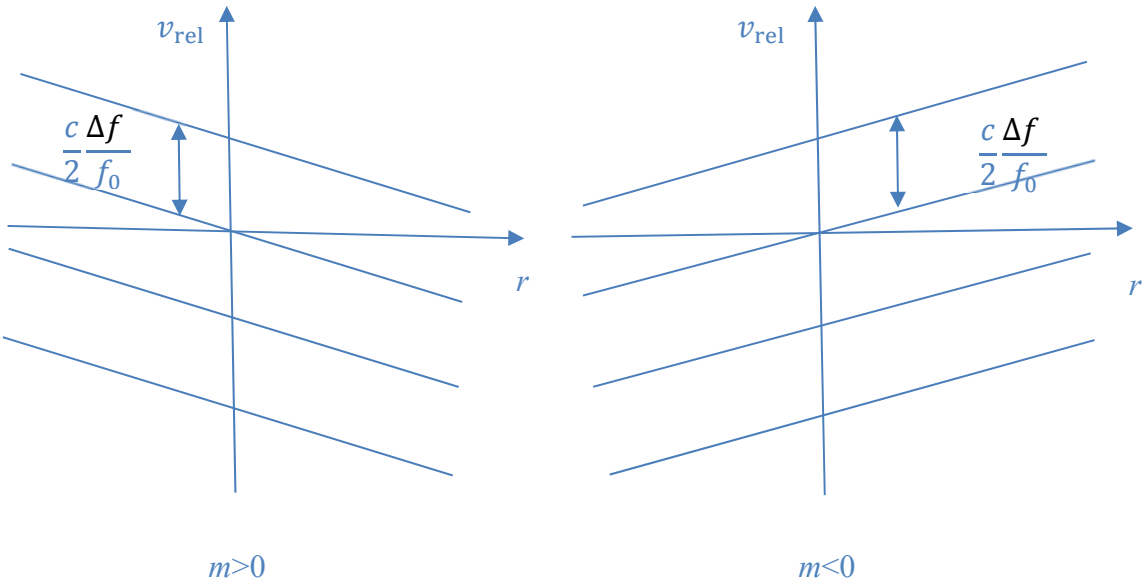

Figure 4.3 Cells for positive and negative frequency slope in FMCW

As FMCW radar uses the both frequency slopes to achieve range and velocity measurement, the cell for FMCW is, as Figure 4.4 shows, in a diamond-shape.

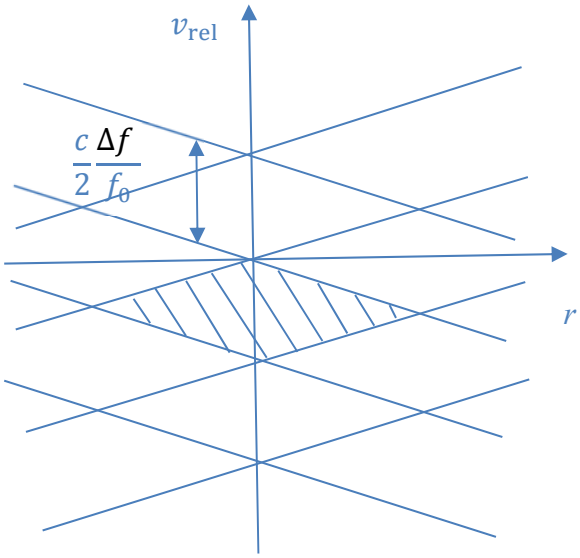

Figure 4.4 Cell-volume for FMCW radar

For the convenience of peak or width detector modeling, it is also possible to represent these cells as rectangles in an orthogonal coordinate system. For this purpose, an orthogonalization can be performed. Two new dimensions can be generated as follows:

$$\alpha = \frac{2}{c} f_0 v_{rel} + \frac{2}{c} mr \tag{4-2}$$

$$\beta = \frac{2}{c} f_0 v_{rel} - \frac{2}{c} mr \tag{4-3}$$

These dimensions are orthogonal to each other. The bins in both dimensions have a bin width of Δf, as Figure 4.5 shows.

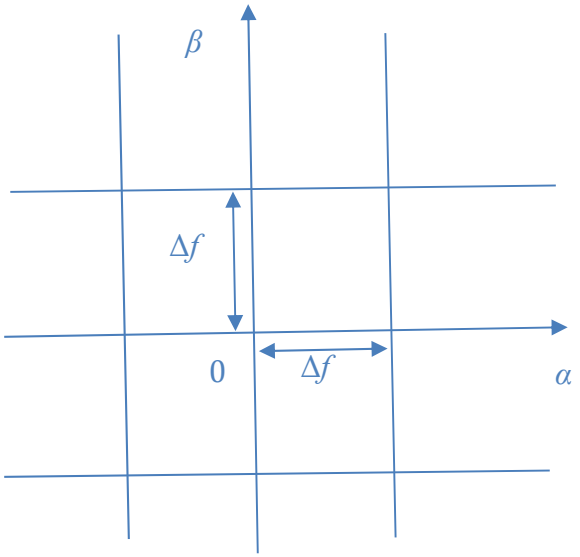

Figure 4.5 Orthogonalized cell-volume for FMCW radar

As introduced in Section 2.1.1, sensors based on Chirp Sequence Modulation, such as the sensor to be modeled in this work, are using the same method as FMCW for range measurement. However, their velocity measurement is based on two times Fourier transformation of the signal, and therefore decoupled from the range measurement. For this reason, the boundaries of cells in velocity are always parallel to the axis of the range. However, the boundaries of cells in range are not parallel to the axis of the velocity. A cell of Chirp Sequence radar is in a parallelogram shape, as Figure 4.6 shows.

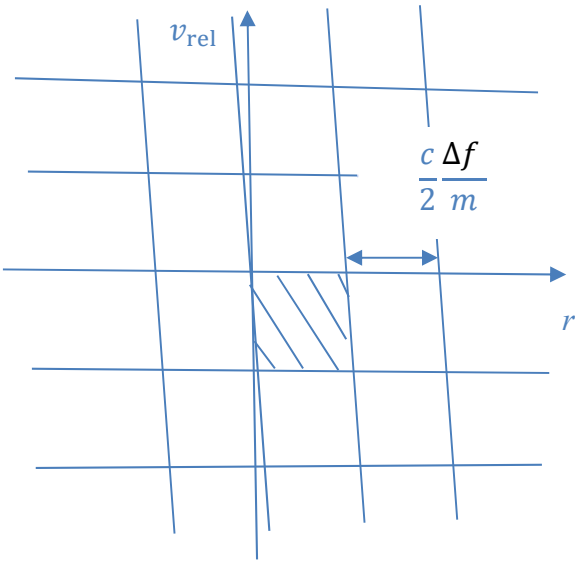

Figure 4.6 Cell-volume for Chirp Sequence Modulation

Because the slope m in Chirp Sequence Modulation is much larger than the one in FMCW, the boundaries of the range bins are almost parallel to the axis of the velocity. The effect can be seen as a shift of time-to-collision by 0.1 s or less. In case of negative slope it is an "in-build" range prediction in the same order of the needed processing time after the measurement (see Annex A).

Therefore, the subsequent discussion and modeling will use still a rectangle for representing the cell in the radar to be modeled as a simplification.

Besides separation capability, as Figure 4.2 shows, the CVC is able to represent some other performance of an active perception sensor theoretically (without considering the influences from SNR). The cell number indicates principally the number of the raw data after measurement. Anti-aliasing measures will reduce the number of useful raw data and can be a cut of cells by setting an (useful) maximum number. Depending on the way the cells are calculated, they could contain real or complex values (with phase information) that double the amount of data. The CVC is almost a lossless representation of the working principle of an ideal sensor, whose performances are only limited by the fundamental physical boundaries.

However, the CVC is originally used to describe how physical constraints can determine performances. This initial CVC cannot describe the imperfections of a real sensor, such as non-linearity in modulation, phase noise etc.. The following sections will show some potential ways of using the CVC as basis for active perception sensor modeling, which extend the usage of CVC. Table 4.1 shows some examples to help to develop intuition how diverse cells can be. The notation corresponds to the bin width (and the number of bins per dimension). An asterisk (∗) marks whether the cell dimension is complex-valued.

Table 4.1 Cell dimensions of representative active perception sensors. An asterisk marks whether the cell dimension is complex-valued. The notation corresponds to the bin size (and the number of bins per dimension).

Sensor type	Range	Radial velocity	Azimuth	Elevation	Total Cell Number
Radar 1	1 m* (256)	0.5 m/s* (256)	4°* (4)	-	262144
Radar 2	250 m* (1)	0.05 m/s* (2048)	10°* (2)	-	4096
Radar 3	1 m* (256)	1 m/s* (128)	1° (16)	-	524288
Radar 4	1 m* (256)	0.1 m/s* (256)	2°* (8)	4°* (2)	1048576
Lidar 1	3 m (128)	-	0.25° (256)	1° (4)	131072
Lidar 2	2 m (128)	-	1° (16)	-	16
Lidar 3	2 m (192)	-	0.5° (32)	1° (4)	128

4.2 Cell-Volume-Concept for Dynamic Sensor Performance Modeling

As previously explained in Section 3.1, the dynamic instantaneous strength of the received signals is a decisive influence factor on the performances of active perception sensors to be modeled. However, the instantaneous signal strength can be influenced in various way (e. g. angle-dependent object reflectivity, multi-path propagation, noise etc.). Under these circumstances, a novel method for modeling dynamic performances with the idea of integrating dynamic instantaneous strength of the received signals into CVC is developed. Two ways to implement this idea are developed in this work. One way is to discretize the measurement quantity space by cell-volumes (as Figure 4.2 shows for example) at first. After that, an algorithm should search through the space to find if a reflecting point, whose measured states are located in one of the cell-volumes (theoretically, without considering the uncertainty), exist in the environment. If so, the major information of the waves reflected from this point should be assigned to the corresponding cell, meanwhile noise is generated. The dynamic object detection, object separation, state measurement and latitude measurement can be represented based on the cell-volumes filled with wave and noise information (for the representation of the SNR influences). This approach is named CVC with Grid-based-View (GbV) of the environment. When

considering only the discretization in azimuth and elevation, the model built by this approach is directly compatible with the well-known wave propagation model, raytracing algorithm (introduced in Section 2.2.1). The other way is named Vector-Projection CVC (VeP). Unlike GbV, the objects in the environment is identified at first in this method. After that, the major information of the waves reflected by them will be projected into the space of measurement quantities. A discretization of the whole space is not necessary (if the space is not fully occupied by objects). In addition, the algorithm of VeP does not have to traverse the space for objects, which is computationally efficient, especially when not many objects exist. Both approaches will be introduced as follows, along with a hybrid approach that combines them.

4.2.1 Cell-Volume-Concept with Grid-based-View (GbV)

As mentioned above, theoretically, the GbV meshes the space of measurement quantities in to cells and searches through the entire space for finding out reflecting points, whose measured states are located in one of the cells. However, due to the physical uncertainty, the reflecting points in one bin can also influence the neighboring bins. (This is the basic reason for dynamic separation capability and states measurement.) Therefore, the search range for each cell should be extended. The physical uncertainty is represented in GbV by a convolution function in the order of magnitude of the bin dimension, and can be extended by an anti-leakage windowing or imperfections of the sensor electronics. This convolution function defines a space around the center of each cell for the searching of reflecting objects. If a reflecting point exists in the uncertainty space, the received signal strength of the waves reflected from this point could be weighted by the uncertainty representing convolution function and allocated to the cell center. Figure 4.7 shows a GbV for a radar with only separation capability in range and velocity as example. For modeling the signal in the crossed cell, an uncertainty (the square marked by thick lines) is built under the assumption that the uncertainty has a width of three bins in both dimensions. When modeling, not only the signal from the reflecting point A, but also the signals from the reflecting points B and C should be taken into consideration. The receiving signal strength of the waves reflected from these objects should be weighed by the convolution function and allocated to the cell center according to its position relative to the cell center and the phase difference between them and the cell center.

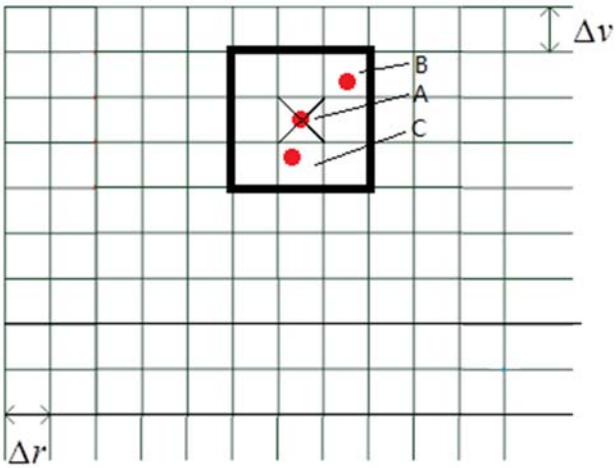

Figure 4.7 Working principle of 2D GbV

In addition, even from the same reflecting point, multiple waves could exist due to the multipath wave propagation; the signal strength of the waves reflected in different ways from different reflecting points should be superimposed in a bin with respect to the phase of each wave. For the implementation of the GbV, a reflecting surface in the reality, which has a width in range, azimuth, or elevation angle dimension, must be discretized into several reflecting points according to the cell dimension at first.

The GbV models the noise by Gaussian white noise. If the receiving signal in the cell of the sensor to be modeled is complex-valued, as mentioned in Section 4.1, a noise signal with a Gaussian distributed amplitude has to be added to the both real and imaginary components for representing the noise sources. If the receiving signal is real-valued, a noise signal whose power is chi-squared distributed or amplitude is Rayleigh distributed can be used. The signal power depends on the reflectivity of the reflecting points, the phenomenon in wave propagation, and sensor characteristics like radiation pattern etc., which are modeled in Chapter 5 and Chapter 6.

After realistic modeling of the signal in every bin, a threshold is applied on the signal, just as a real sensor does, to find out whether a certain bin can be detected. Until this step, thanks to the uncertainty, realistic signal power and realistic noise representation, a modeling of the dynamic states measurement and detection of every raw object represented by a cell is achieved. Similar to the original CVC, GbV separates also the bins by an unoccupied bin between them. However, the identification of its occupancy is not based on the theoretical existence of reflecting points in the bin, but whether the bin has a sufficient lower power for the detection than the neighbors on the both sides. In the inverse case, if some parts of a reflecting surface have low reflectivity, the reflecting surface could be separated and detected (as a kind of false-positive-errors). These behaviors represent exactly the dynamic separation capability of real sensors as discussed in Section 3.1.3.

Since the dynamic detection and separation capability are present, a modeling of dynamic latitude measurement capability based on them is also possible.

It is worth noticing that the GbV allows some objects out of the measurement quantity space to shift into the space because of the uncertainty. In addition, aliasing effects lead to some special cases, e.g. the example Radar 4 in Table 4.1 has a velocity range of only 256×0.1 m/s, which has to be multiply used to cover the required range of approx. 100 m/s. In this case at least four detection spaces must be implemented assuming a perfect de-aliasing.

Until this step, the GbV is able to represent all the major dynamic sensor performances listed in Section 4.2. However, the drawbacks of this method are as follows:

The first one is that the algorithm has to search through all cells for finding reflecting points in every simulation cycle. When modeling a perception sensor with high resolutions meaning a high number of bins, a high computing effort is required. As the total number of cells are in the most cases much higher than the number of objects to be simulated, the GbV is uneconomical. An efficient algorithm is required to minimize the computing effort caused by the "empty" cells. However, the number of occupied bins can rise independent of the number of objects as well, if the uncertainty convolution function exceeds the search range significantly.

The second one is that the identification of the reflectivity of the reflecting points is hard. Many reflecting points could exist in the range of a cell. They could lie on the same surface or different surfaces of different objects, whose states are similar. To model all the point is computing-intensive. For the decision, which point between them should be used to represent all of them, or how the total reflectivity of these points can be measured and represented by one point, an extra algorithm is required. Otherwise, quantization errors could be generated.

As inputs, principally, GbV requires the information from a specific wave propagation model, which can be considered as "generalized ray tracing method". The traditional ray tracing method discretizes the measurement quantity space only in the dimensions of azimuth and elevation. As discussed in Section 4.1, an active perception sensor can generally have separation capability in four dimensions: range, relative velocity, azimuth and elevation. Therefore, for the generation of the information required by GbV, the ray tracing method should be extended to a four-dimensional searching for reflecting points. Of course, when modeling a perception sensor, which has only separation capability in azimuth and elevation, like camera, the ray, tracing method can be utilized directly without modification.

4.2.2 Vector-Projection Cell-Volume-Concept (VeP)

Unlike the GbV, the Vector-Projection Cell-Volume-Concept (VeP) does not mesh the space of measurable quantities at first. According to the measured states, the objects in the driving environment are firstly projected into the measurable quantities space. All objects are modeled as points with the major information (ToF, radial velocity, azimuth, elevation and signal amplitude (complex for radar or real for lidar)) of waves reflected from them. The VeP uses Dirac impulse with different (complex or real) amplitudes to model the different signal amplitudes of the waves at these points. Until this step, the description has neither any losses of information nor any realistic representation of sensor performances.

However, in order to model the realistic sensor performances, a representation of physical uncertainty, as the GbV does, has to be performed as well. The uncertainty function in VeP is represented by an impulse response to Fourier-transformed convolution function in GbV. The uncertainty function is convolved with Dirac impulses, which represent the (complex or real) amplitudes of the waves (vectors). As discussed in 4.2.1, various reasons can cause the uncertainty to be modeled. Therefore, the distribution of this uncertainty can be considered unknown, and represented by Gaussian distribution. In order to execute the convolution calculation in a computer, the algorithm of VeP has to discretize the space covered by the uncertainty to cells. The type of convolution function depends on the type of anti-leakage filter, or more precisely the Fourier transform of the anti-leakage filter. For the modeling in this work, the Hanning window with linear phase shifting for complex bin dimensions, which can be considered as an finite approximation of the impulse response amplitude of Fourier transform of Gaussian distribution, is chosen as a simple instantiation. As convolution function, the Hanning window has the advantage, that it has finite short length, so that the algorithm does not have to discretize the whole space of measurement quantities.

To avoid the large discretization errors when modelling the uncertainty of a certain object, which just stays near the boundary between two cells, the width of the convolution function is identified as four bins. The Hanning window can be expressed as follows:

$$F(u) = \begin{cases} e^{j2\pi u}\cos^2\left(\frac{\pi u}{4}\right); & -2 < u < 2 \\ 0 \quad ; & \text{else} \end{cases} \tag{4-4}$$

where u is the displacement between cell center and vector position for a given dimension. Its unit is in terms of bin-width. The phase rotation function $e^{j2\pi u}$ indicates the linear phase shifting for complex bin dimensions in case that $t = 0$ is at the beginning of the measurement window. It vanishes completely (just to 1) in case when $t = 0$ is defined for the center of the measurement window. The phase shifting rate in each dimension depends also on the way the corresponding quantity is measured. For example, the azimuth angle

measurement based on planar antenna beam forming principle and the velocity measurement based on Doppler effect are both using Fourier transformation to get the value to be measured. As a simplification for the modeling in this work, it is assumed, that $t = 0$ is defined for the center of the measurement window, so that the phase rotation function can vanish to 1. The initial phase of each object vector is given by the fraction of the ratio of range over wave length $2\pi(2r/\lambda)$, which rotates more than 100 times within one bin width.

Figure 4.8 shows the VeP of a sensor with separation capabilities in two dimensions: range and relative velocity. The Hanning window is marked by thick lines in Figure 4.8 as example. After convolution, the signal amplitude on every bin center (the crosses in Figure 4.8) around an object (the circles in Figure 4.8) can be calculated based on their phase shifts.

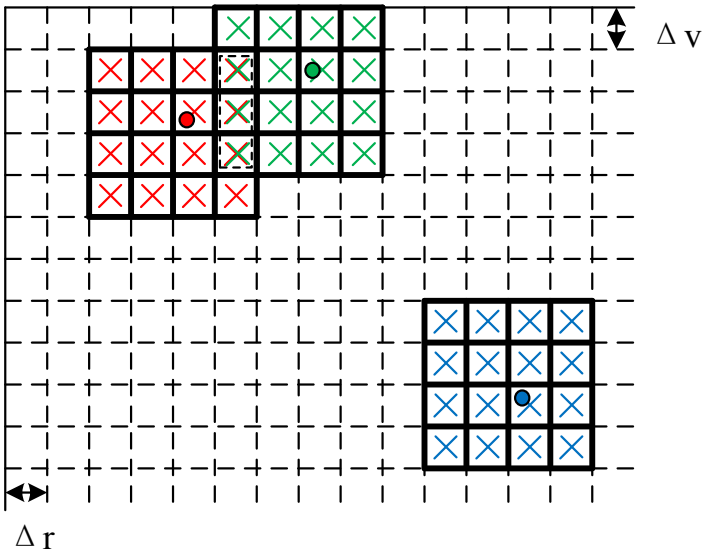

Figure 4.8 Working principle of 2D VeP

The crosses marked by the dashed rectangle in Figure 4.8 represents cells that are influenced by more than one convolution functions. In such a case, the signal amplitudes in these cells can be calculated as a superposition of all intersecting convolution functions. By this representation, the modeling of the dynamic sensor performances is possible. The subsequent process is similar to the GbV: the generation of noise and the detection based on a threshold. Unlike GbV, noise signals have only to be generated in the parts of space where the convolution was calculated. As a simplification, another stochastic process can help to generate some false positive errors out of discretized space.

In summary, the VeP can also represent all the important performances of active perception sensors listed in Section 3.1 dynamically. In comparison with the GbV, the advantage of the VeP is that the method is its high efficiency, as the algorithm does not have to search through the whole space for reflecting points. However, the drawback of this method is

that, it is unrealistic to model all the objects by a point reflector in the space of measurement quantities. In reality, as mentioned in Section 3.1.4, an object in short range can cover more than one bin in azimuth and elevation; a long object can cover more range bins; and a rotating object can cover more velocity bin because of the relative movement. Therefore, when using this method, the object representation has to be extended. A discretization of reflecting objects may be helpful, but this increases the required computing effort again. A method will be introduced in Chapter 5 for solving this dilemma. Based on it, this dissertation will model a radar by the VeP with performance parameters derived from the specification of the radar.

4.2.3 Hybrid Cell-Volume-Concept (HCVC)

For mitigating the disadvantages of both of the GbV and the VeP, the Hybrid Cell-Volume-Concept (HCVC) is developed in this work. The HCVC discretizes the azimuth and elevation dimensions and searches for reflecting points, like the GbV, at first. After that, the HCVC algorithm identifies the range and relative velocity of these points and projects them into the space of range and relative velocity, like the VeP. In the GbV part, thanks to the technologically mature ray tracing methods and the powerful modern GPUs, an efficient execution of objects searching in the azimuth and elevation dimensions can be ensured. This solves a computing effort problem of the GbV. However, the known ray tracing methods can only discretize the azimuth and elevation dimensions. If using azimuth and elevation bins to describe the range bin directly, the range bin expands its dimension with the growth of range, which is not realistic for the most active perception sensors. For this reason, the ray tracing methods can hardly be used for simulating the object separation in the range or relative velocity dimension without any modifications or specific program structure. Therefore, in HCVC, the representation of measurements in the range and relative velocity dimensions is taken over by the VeP part. As the objects have been already discretized in the azimuth and elevation dimensions at first, unlike the original VeP, the HCVC can represent objects in short range as well.

Thus, the HCVC can solve the problem of inefficient reflecting points searching in GbV and the problem of object representation in short range in VeP. However, the quantization error in the azimuth and elevation dimensions still exist. Since the ray tracing algorithm searches only for the nearest reflecting points, the other possible reflecting points in the same cell will be neglected, although a real sensor may still be able to separate them in the range and relative velocity dimensions. Thus, information loss could occur after a representation by the HCVC.

4.2.4 Conclusion and Implementation

In summary, it is possible for all the three methods: GbV, VeP and HCVC, to represent the important performances of active perception sensors dynamically. However, due to their advantages and disadvantages, they are compatible with different types of active perception sensors. For the most automotive radars that have no or poor separation capability in azimuth and elevation, the object searching in azimuth and elevation dimensions is unnecessarily complicated. Due to the poor separation capability in azimuth and elevation, the hybrid method is nothing much more than the VeP. In this case, the VeP is used here.

A radar from an industry partner is modeled in this dissertation as an example. For modeling this radar, the VeP is considered as an efficient method and selected. This sensor can measure quantities in three dimensions: range, relative velocity and azimuth angle. Therefore, the space of its measurement quantities is three-dimensional. As introduced, after object projection, the space around the objects will be discretized in cells. The cell dimension is identified according to the separation capability defined in the sensor specification. An ergodic method will be introduced in Chapter 5 for solving the problem in object representation in a short range. The signal amplitude and phase of all the cell centers is calculated based on the uncertainty convolution function. It is assumed that the sensor has a minimum uncertainty width of four bins in all dimensions. At last, the noise is generated and added on the signal, so that a realistic detection can be performed based on a threshold.

In addition, the following three points are worth noticing:

1) The sensor measures the range and relative velocity by using Chirp Sequence Modulation. As introduced in Section 4.1, the relative velocity of objects can influence the boundary of range bin. However, the influence is relatively low. The subsequent modeling will use a rectangle for representing the cell in the radar to be modeled as a simplification.
2) The sensor uses Planar Antenna Array with digital beamforming for the measurement of azimuth angle ϕ. As introduced in Section 2.1.1, it measures principally $\sin(\phi)$ to obtain the angle ϕ. Therefore, there are two ways to define the third dimension for azimuth angle measurement in the space of measurement quantities.
   a) When defining the dimension by azimuth angle ϕ, the bins after discretization are not equidistant.
   b) When defining the dimension by sine value of azimuth angle $\sin(\phi)$, the bins after discretization are equidistant.

   In this dissertation, for programming convienience, the second way is selected.
3) The sensor has two groups of transmitters and receivers, which are used for object sensing in short range and long range respectively. Therefore, the VeP should be

performed for two times for modeling the performances of this sensor. The cells in the models built for short range and long range have different dimensions, as the separation capabilities of this sensor in short range and long range are different.

5 Wave Propagation Model

The wave propagation model describes the wave propagation in atmosphere. As discussed in Section 4.2, for the radar modeling in this work, the sensor performance model VeP is selected. In this chapter, a wave propagation model that is compatible with the VeP is developed and introduced. As discussed in Section 3.2, as a generic wave propagation description, this model is able to provide the sensor performance model with the major wave characteristics like wave power, phase shift or time of flight, frequency shift and receiving angle. Since these characteristics can be influenced by various influence factors during wave propagation, the relationship between the wave characteristics and their influence factors is analyzed in this Chapter at first, and built in the wave propagation model at last. In addition, beside the influence factors during wave propagation, the transmission power decides the power of received waves as well. The most automotive radars do not transmit waves isotropically. They use reflector antenna, lens antenna or phased array antenna to bundle the waves into a certain aperture angle in order to obtain a longer detection range. However, due to the bundling, the waves in different directions cannot have the same power. The send (or receive) direction-selective power density distribution is called radiation pattern. This is modeled as a part of wave propagation model in this section as well.

5.1 Influence Factors in Wave Propagation

The active perception sensors work by transmitting modulated electromagnetic waves and analyzing the echo. In principle, the modulated waves can be influenced differently by different physical phenomena during the wave propagation. As described in the sensor performance model, they could lead to errors in detection and measurement. Since visible light can be considered as electromagnetic waves with some specific frequencies, the theories of physical optics can be directly applied to identify the disturbing physical phenomena during wave propagation. According to physical optics, the following physical phenomena may occur during wave propagation: attenuation, diffraction, physical interference, refraction, reflection[76].

[76] Schneider, R.: Diss., Modellierung der Wellenausbreitung (1998).

5.1.1 Atmospheric Attenuation:

The atmospheric attenuation reduces the signal strength of the waves after their propagation in the atmosphere. Since the signal strength is an important criterion for the object detection of the active environmental sensors, meanwhile the attenuation can affect signal strength significantly in some cases (e.g. in rain), the attenuation can be identified as one of the important physical phenomena for wave propagation modeling. The attenuation effect depends mainly on the distance the waves travel in atmosphere and the weather condition during the propagation. A 77 GHz radar can suffer a maximum total attenuation of approx. 3 dB in a worst-case scenario (e.g. object distance = 200 m, heavy rain (30 mm/h))[77]. Its influence on the signal power can be calculated and estimated with an empirical formula as follows[78]:

$$\frac{1}{L_{\mathrm{atm}}} = 10^{-2\kappa r/1000} \tag{5-1}$$

where r is the range of object in meter. L_{atm} is the losses in atmosphere. κ is the attenuation coefficient in dB/km.

Obviously, with a constant attenuation coefficient, the influence of attenuation on signal power can be calculated. However, the attenuation coefficient depends on the weather condition and the wave frequency. The weather dependence of the attenuation of the waves with different frequencies must be identified by numerous experiments and calibrations. Such experiments were not performed in the scope of this dissertation for two reasons: On the one hand, the physical investigation of the absorption spectrum is not one of the focuses in this dissertation. On the other hand, due to the water drops in different forms on different surfaces and the water splash effects, the wave propagation in rain is difficult to investigate without precise physical experiments. Because of the high costs and the low transferability, such experiments are not feasible in this dissertation. For this reason, the weather conditions are constantly defined as "clear" in the following investigation and modeling. In such a weather condition, the attenuation effects are so insignificant (according to the calculations within the operating range of the automotive perception sensors (object range < 250 m)) that the attenuation coefficient in this dissertation can always be defined as "1". Although lidar can be even more strongly influenced, especially in the case of spray or mist, it is also difficult to determine a valid model for the representation, because the sensitivity of the influence can be reduced by scattering, and the retro reflectivity of the objects can be significantly affected in bad weather.

[77] Köhler, M. et al.: Feasibility of automotive radar (2013).

[78] Winner, H.: Radarsensorik (2009).

5.1.2 Diffraction

The refraction and the diffraction of the waves in driving environments have not been described as important in practice up to now. The research carried out so far shows that the diffraction is only useful for the detection and measurement of traffic objects that are to be detected behind a crest[79]. In this case, the sensor thanks to the diffraction effect can detect an object, although the crest shades it. However, the strength of this effect strongly depends on the contour of the object, namely whether the diffracted waves reach a surface with a normal orientation, which leads to a backscattering, or not. In order to ensure the universality and the efficiency of the simulation, such special cases were not taken into account in sensor modeling.

5.1.3 Refraction

In real driving environments, the refraction can occur when, for example, the waves transmitted by sensors pass through the glass plates of the vehicles. Whether such refractions should be modeled depends strongly on the representation method of the vehicle models. If the reflectivity of the vehicles in different aspect angles is only identified by measurements, the refractive effects as a part of the reflectivity of the vehicles are automatically taken into account in the measurements and the representation. This means, in this case, the refraction need not to be modeled in addition. Otherwise, the refractive effects cannot be neglected theoretically. For example, the refraction should be modeled in the ray tracing method, in which the reflected power of each beam is calculated based on the reflectivity of the surfaces illuminated by the beam, because the refractions change the propagation directions of the beams, and furthermore, lead to errors in the identification of the surfaces illuminated by the beams.

5.1.4 Reflection

As the result of the theoretical analysis, the reflection and the physical interference are identified as the focuses of the wave propagation modeling. In principle, the detection and measurement of the active perception sensors are based on the analysis of the reflected waves. As discussed in Section 3.1, the quality of the reflection determines the detectability of the objects, the measurement accuracy and the quality of the clustering of the reflection points, the object tracking and furthermore the classification of the objects. The reflected power of a beam at a certain point on the reflecting surface depends on the material, the surface finishing, the wave frequency, the angle of incidence, the angle of

[79] Schneider, R.: Diss., Modellierung der Wellenausbreitung (1998).

incidence, and the polarization of the beam. In principle, all these factors should be considered as influencing factors during wave propagation.

5.1.5 Interference

Beside the investigation of each individual reflection, the investigation of the interactions of the waves reflected on different surfaces, or the so-called physical interference, is of importance. Since the frequency shifts caused by the Doppler Effect is relative small in comparison with the carrier frequency, the superposition of the waves reflected on different surfaces can lead to significant destructive and constructive interference. Critical influences are caused in particular by the destructive interference, as the destructive interference leads to the extinguishing of the waves. This results in false-negative errors. Since the interference is dependent on the phases of the superimposed waves and the phase shift of a wave is determined by the distance traveled by the wave, the distance traveled by a received wave should be represented with a high resolution in order to address this influence factor during the wave propagation modeling. In order to calculate these distances, the relative positions between the sensor and the reflection points should be obtained during the simulation.

In summary, the reflection and physical interference are the major influence factors to be modeled as focuses.

5.2 Wave Propagation Modeling

5.2.1 Modeling of Physical Phenomenon

As previously analyzed, the model is focused on the reflection and the physical interference only.

As mentioned above, the reflectivity of objects is modeled in the object model, which is a part of environment model. Therefore, it will be introduced in Chapter 6.

The physical interference in driving environment is normally caused by the multipath propagation of the waves. For the modeling of physical interference, the following three points are worth noticing:

1) The multipath propagation here means that the waves reflected by the same objects reach the receiving antenna by different paths (with at least a second reflection on other surfaces). Thanks to the separation capabilities of active automotive perception sensors in multiple dimensions, the waves reflected by different objects locate normally in different cells, and therefore are normally not superimposed.

2) Among the surfaces, which can lead to the second reflection, only the large one, such as roadway and crash barrier on highway, are prior to be taken into consideration. Because the interference condition will be occurred for a driving vehicle in a short time, if the surface is small. In this case, the effect of interference like false-negative errors can be compensated by object tracker, and is therefore not prior for modeling.
3) For the same reason as given in 2), only the second reflection is taken into consideration. The cases, when a wave finds the receiving antenna through more than two reflections, seldom occur and normally cannot held for a long time. An exception happens when the relative position between two large surfaces, which can fulfill the reflection condition, is relative constant (e.g. roadway and crash barrier). Such complicated cases are not modeled in this dissertation at first. They will be implemented in the further development of this model.

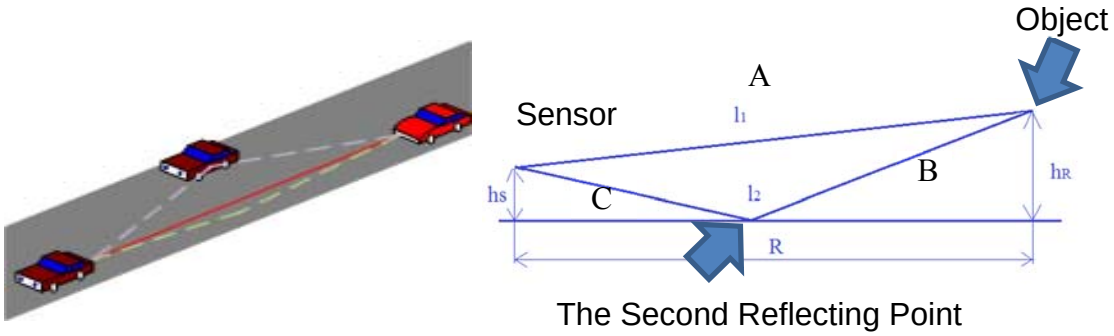

Figure 5.1 Multipath propagation in driving environment

Figure 5.1 shows the multipath propagation of the waves from active perception sensors with considering the three points above. According to Skolnik[80], when the second reflection happens on the road surface, the ratio between the power of the waves that reach the object P_{obj} and the transmitted power P_{trans} can be calculated as follows:

$$\frac{P_{\mathrm{obj}}}{P_{\mathrm{trans}}} = 4\sin^2\left(\frac{2\pi \cdot h_{\mathrm{s}} \cdot h_{\mathrm{R}}}{\lambda \cdot R}\right) \tag{5-2}$$

With considering the interference of the reflected waves, the ratio between the received power P_{rec} and the transmitted power P_{trans} can be calculated as follows:

$$\frac{P_{\mathrm{rec}}}{P_{\mathrm{trans}}} = 16\sin^4\left(\frac{2\pi \cdot h_{\mathrm{s}} \cdot h_{\mathrm{R}}}{\lambda \cdot R}\right) \tag{5-3}$$

Where h_{s} is the height of sensor, h_{R} is the height of reflecting point on object, R is the distance between sensor and reflecting point, λ is the wavelength.

[80] Skolnik, M. I.: Radar Handbook (2008).

However, these equations are valid, only when the road surface is flat and the reflection point is exactly the same for both transmit pathes. In principle, the interference is dependent on the distances traveled by the waves (l_1 and l_2 in Figure 5.1). In order to calculate the distances, the relative positions among the first reflecting point, the second reflecting point and the sensor (A, B and C in Figure 5.1) should be obtained at first. The sensor position and the object position (due to the VeP, the object here is considered as a point. A more realistic representation will be introduced in Section 5.3) can be provided by the simulation environment (e.g. IPG CarMaker®) easily. However, due the unevenness of road surface, the position of the second reflecting point cannot be calculated by simple geometric approaches. The normal direction of the reflecting surface influences the position. For this reason, an algorithm is required for identifying the position of the second reflection point.

In this dissertation, a searching algorithm is developed for this purpose; meanwhile the second reflection on the road surface is simulated as example. The searching algorithm works based on the physical reflection conditions and searches through the road area between the sensor and the object for reflecting points. The procedure can be described as follows:

1) Integration of the road unevenness
   Road unevenness is important, because it can changes the positions of the reflecting points on the road surface, and furthermore influence the interference conditions.

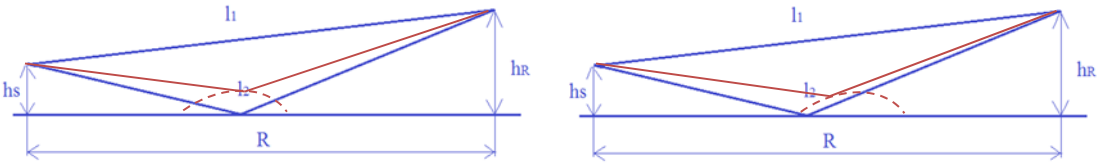

Figure 5.2 Influences of road unevenness on interference

As Figure 5.2 shows the road unevenness can changes both the height and the position of a reflecting point, which lead to a different path length of l_2 and furthermore different interference effect. As the interference effect is one of the essential influence factors for dynamic sensor performance modeling, the road unevenness should be modeled.
In the scope of a master thesis advised by author[81], different modeling methods for road unevenness are investigated, implemented and compared. The 2D inverse Fourier Transformtation is selected as an efficient method. This dissertation will

[81] Li, Y.: Master's Thesis, Modellierung der Unebenheit (2015).

not go further on the issue of road unevenness modeling, but provide an efficient way of integration.

There are principally two ways to integrate a road model.

- Generation and integration of the entire model when initializing the simulation
- Integration of the necessary part of the road when executing the simulation

The first method has an obvious drawback that it takes up a lot of computer memory, when the simulation scenario is large. The disadvantage of the second method is that the integration has to be done in every simulation cycle. As a simulation environment like IPG CarMaker® has normally a very high simulation frequency (e.g. 1000 Hz in IPG CarMaker®), the second method can be computing-intensive, which can influence the real-time capability of the simulation.

However, the road unevenness, as a physical characteristic of road, does not need to be refreshed in every simulation cycle, meanwhile only the road surface between the sensor and the objects is important for the modeling of interference. Therefore, in this dissertation, the road model integration works based on an updating of the data.

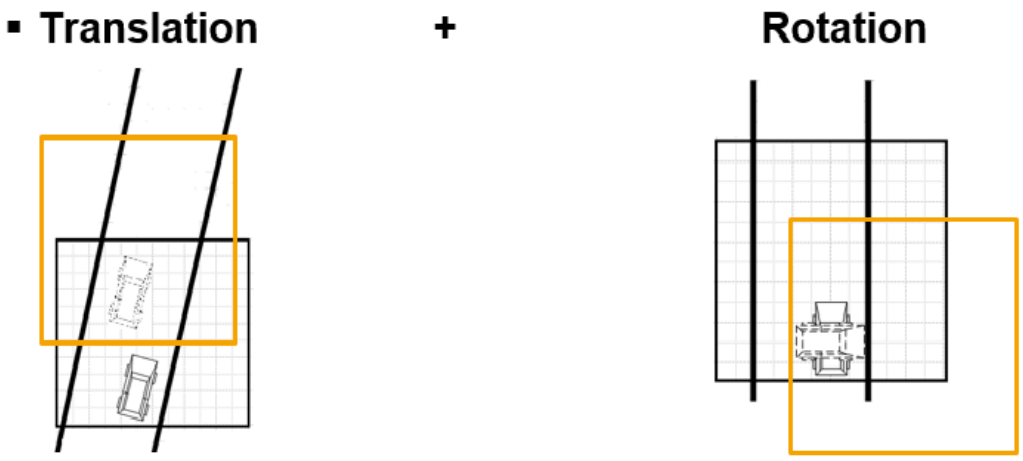

Figure 5.3 Road matrix update

As Figure 5.3 shows, the entire road surface model is not integrated. Instead of that, only a part of the road surface (interesting area) in front of the sensor is integrated (for modeling the sensor that is oriented forwards). Thus, the modeled interesting area of road surface has to move with the ego-vehicle in each simulation step. However the road surface that still stays in the next step does not need to be modeled again. Only the newcomers have to be modeled, meanwhile the old parts that do not belong to the interesting area anymore should be deleted. In the updating, the movement of the ego-vehicle is separated into translation and rotation to simplified the calculation of the boundaries of the interesting area. (see Figure 5.3)

Thus, by an updating the interesting area, the road model can be efficiently integrated without large memory capacity requirement.

2) Discretization of the road surface

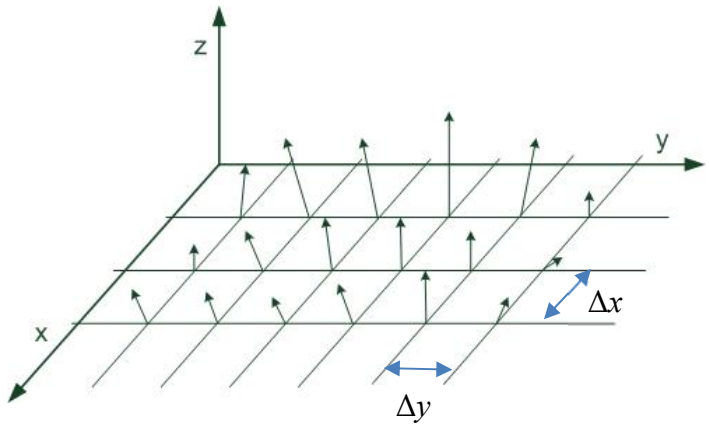

Figure 5.4 Discretization of road surface

For the processing in computer, the road surface between sensor and objects must be discretized with a grid at first, as Figure 5.4 shows. Dimension z indicates the height of the road at a certain point (x, y). The height and the normal direction at each discretized point should be obtained from a realistic road model. The road model will be introduced in Chapter 6 as a part of environment model.

A grid step of 3 m is defined in this dissertation. A finer grid is more advantageous for the localization of reflecting points and furthermore for the validity of the wave propagation model. However, the drawback lies in the simulation efficiency. A fine grid increases the number of times the searching algorithm runs. A grid step of 3 m is considered suitable, because an uncertainty of 3 m in the longitudinal direction (which means the direction from the sensor to the object) in the localization of the second reflecting point normally does not lead to a significant difference in interference effect modeling (The quantization error is small, which is proven in the following).

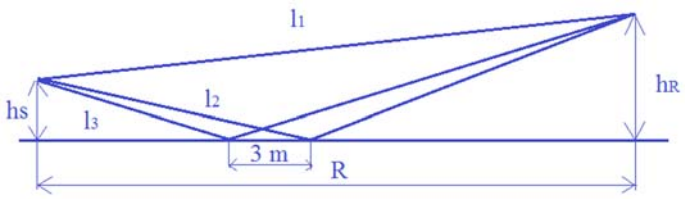

Figure 5.5 A grid step of 3 m in the longitudinal direction

Figure 5.5 shows two second reflecting points between which a distance of 3 m in longitudinal direction exists. l_2 and l_3 indicate the length of the propagation paths of the reflected waves that go through these two points. Suppose that the heights of sensor h_S and object h_R are both 0.5 m (This assumption has considered

the real heights of sensor and reflecting point of a vehicle). The longitudinal distance between sensor and object is R. The longitudinal distance between sensor and the second reflecting point of l_3 is x. The difference Δl between l_2 and l_3 is as follows:

$$\Delta l = l_3 - l_2 = \sqrt{x^2 + 0.5^2} + \sqrt{(R-x)^2 + 0.5^2} - \sqrt{(x+3)^2 + 0.5^2} - \sqrt{(R-x-3)^2 + 0.5^2} \quad (5\text{-}4)$$

The relationship are as Figure 5.6 shows:

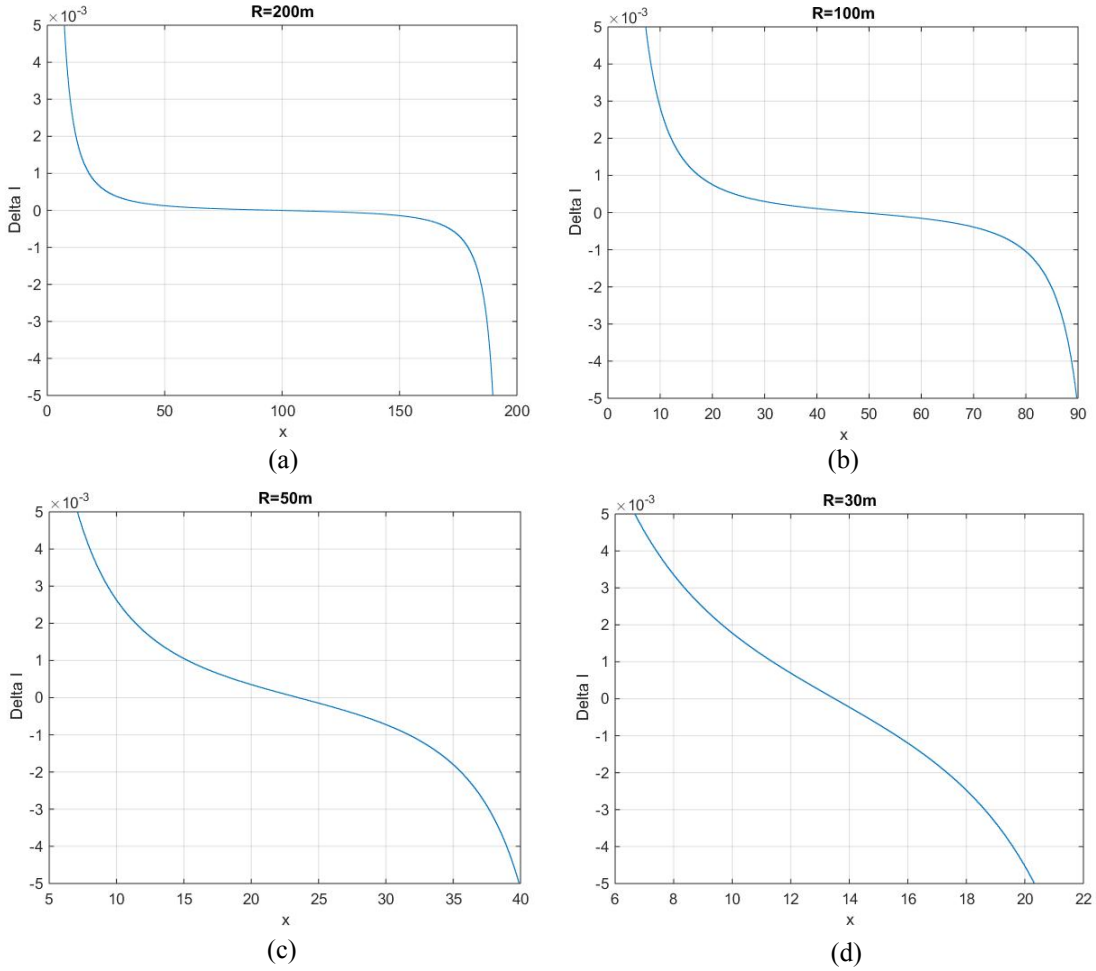

Figure 5.6 Influence of a grid step of 3 m on path length (a) R = 200 m (b) R = 100 m (c) R = 50 m (d) R = 30 m

The representation of interference is based on the phase of the waves. The wavelength of the wave transmitted by a 77 GHz radar is 3.9 mm. Figure 5.6 shows, if R > 50 m, the difference between the path length l_2 and l_3 is so small that it will not cause much phase error. Only in the cases when the second reflecting point is close to sensor or object, a large difference between the path lengths l_2 and l_3 will happen. However, these cases are seldom occurred.

However, the grid step of 3 m has two drawbacks:

a) For the short-range detection (R < 50 m, e.g. R = 30 m in Figure 5.6), the influence of a grid step of 3 m cannot be neglected. Moreover, in short range detection, more interference problems like the interference of the waves from different reflecting points on the same object could be occurred. For this reason, this dissertation will not use the wave propagation model to model the complicated short-range cases. They will be modeled as a part of the object model introduced in Chapter 6.

b) The difference between the path lengths is more sensitive to an uncertainty in the transverse direction than the one in the longitudinal direction. An uncertainty of 3 m in the transverse direction can lead to a significant difference even in long-range detection. However, on the one hand, a deviation of 3 m in the transverse direction happens also only when the road surface is very uneven or a crest exists on the roadsides. On the other hand, a linear interpolation will be made based on the normal directions of the discretized road points at last. The effect of the uncertainty can be reduced.

So, a grid step of 3 m is chosen.

3) Searching for the second reflecting points
Based on the discretized road surface, a searching algorithm is developed based on the three-dimensional reflection conditions.

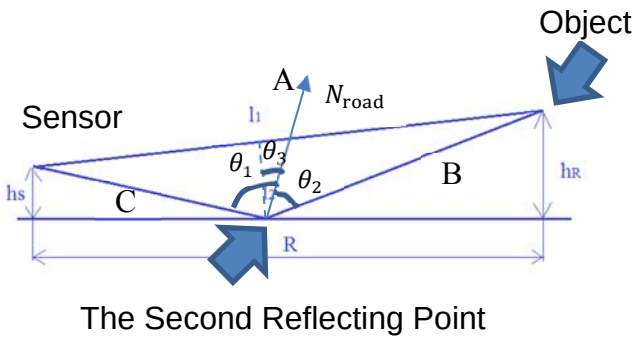

Figure 5.7 Working principle of the algorithm for second reflecting point searching

Figure 5.7 shows the working principle of the searching algorithm: N_{road} indicates the normal direction of an arbitrary point on the road, θ_1 is the angle between the normal direction and the ray C, θ_2 is the angle between the normal direction and the ray B. Obviously, the θ_1 and θ_2 are the reflection angle and the incidence angle, if the road point here is the second reflecting point. θ_3 is the angle between the normal direction and its projection on the triangle ABC.

The algorithm consists of three steps:

a) Calculation of the difference between the θ_1 and θ_2 at each point in the road point matrix with regard to the sensor position and the object position

As a necessary condition for the reflection, the incidence angle and the reflection angle at the reflecting point should be the same. In order to find the points which can satisfy this condition, the difference between the θ_1 and θ_2 is calculated at each point in the road point matrix. Due to the discretization of the road surface, $\theta_1 = \theta_2$ seldom happens. Therefore, the sign change of $\theta_1 - \theta_2$ should be observed. If such a sign change occurs between two neighboring points, the area between the points is identified as a potential reflecting area. This part of algorithm can be expressed as follows:

$$\vec{C} = \begin{pmatrix} x_{\text{sensor}} - x_{\text{road}} \\ y_{\text{sensor}} - y_{\text{road}} \\ z_{\text{sensor}} - z_{\text{road}} \end{pmatrix}, \vec{B} = \begin{pmatrix} x_{\text{obj}} - x_{\text{road}} \\ y_{\text{obj}} - y_{\text{road}} \\ z_{\text{obj}} - z_{\text{road}} \end{pmatrix} \tag{5-5}$$

$$\theta_1 = \arccos\left(\frac{\overrightarrow{N_{\text{road}}} \cdot \vec{C}}{\left|\overrightarrow{N_{\text{road}}}\right| \cdot \left|\vec{C}\right|}\right) \tag{5-6}$$

$$\theta_2 = \arccos\left(\frac{\vec{B} \cdot \overrightarrow{N_{\text{road}}}}{\left|\vec{B}\right| \cdot \left|\overrightarrow{N_{\text{road}}}\right|}\right)$$

$$\Delta\theta = \theta_1 - \theta_2 \tag{5-7}$$

where $(x_{\text{sensor}}, y_{\text{sensor}}, z_{\text{sensor}})$, $(x_{\text{obj}}, y_{\text{obj}}, z_{\text{obj}})$ and $(x_{\text{road}}, y_{\text{road}}, z_{\text{road}})$ are respectively the coordinates of the sensor, the object and the second reflecting point on the road in the global coordinate system.

b) Calculation of the angle between the normal direction at each road point and its projection on the triangle ABC (θ_3)

As the second necessary condition for the reflection, the normal direction of at the road point, incident ray and reflected ray should be on the same plane. In other words, the angle between the normal direction at the road point and the plane ABC should be equal to zero. Also due to the discretization of the road surface, the sign change of this angle should be observed. When a sign change of the angle occurs between two neighboring points, the area between the two points is identified as a potential reflecting area.

This part of algorithm can be expressed as follows:

$$\left|\vec{B}\right|\left|\vec{C}\right| \sin\alpha \, \overrightarrow{N_{\text{ABC}}} = \vec{B} \times \vec{C} \tag{5-8}$$

where α is the angle between $\vec{B}$ and $\vec{C}$,

$\overrightarrow{N_{\text{ABC}}}$ is the normal direction of the triangle ABC.

$$\theta_3 = \frac{\pi}{2} - \arccos\left(\frac{\overrightarrow{N_{\text{road}}} \cdot \overrightarrow{N_{\text{ABC}}}}{\left|\overrightarrow{N_{\text{road}}}\right| \cdot \left|\overrightarrow{N_{\text{ABC}}}\right|}\right) \tag{5-9}$$

$$= \frac{\pi}{2} - \arccos\left(\frac{\overrightarrow{N_{\text{road}}} \cdot \left(\vec{B} \times \vec{C}\right)}{\left|\overrightarrow{N_{\text{road}}}\right| \cdot \left|\vec{B} \times \vec{C}\right|}\right)$$

c) Identification of the gross positions

With the simultaneous consideration of the two necessary conditions described above, the necessary and sufficient condition for a reflection is derived. If the two conditions can be satisfied (sign of $\Delta\theta$ and θ_3 changes) simultaneously in an area on the road surface, this area can be identified as a second reflecting area, as Figure 5.8 shows. Each data group corresponds to a discretized point on road surface. The first place in data group indicates the sign of $\Delta\theta$; the second place in data group indicates the sign of θ_3.

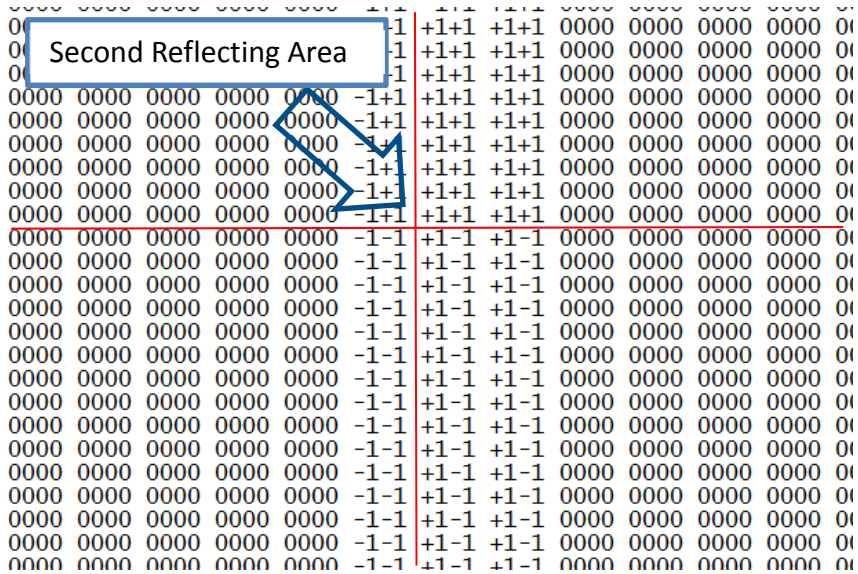

Figure 5.8 Searching for second reflecting area on road surface (The first place in data group indicates the sign of $\Delta\theta$; the second place in data group indicates the sign of θ_3)

4) Refining the localization through linear interpolation and identifying the receiving angles of the second reflecting points

Until this step, the position of the second reflecting points can be limited into a 3 x 3 m² square area. A gross representation chooses the center of the area as reflecting point. However, through a linear interpolation, a refining of the reflecting point localization can be performed. For example, if the sign of $\Delta\theta$ changes between Point P1 and Point P2, which are neighboring in Dimension x. The coordinate $x_{2\text{ref}}$ of the second reflecting point is calculated as follows:

$$x_{2\text{ref}} = \frac{|\Delta\theta_1|\cdot x_1 + |\Delta\theta_2|\cdot x_2}{|\Delta\theta_1| + |\Delta\theta_2|} \tag{5-10}$$

where $\Delta\theta_1$ is the $\Delta\theta$ at Point P1, $\Delta\theta_2$ is the $\Delta\theta$ at Point P2, x_1 is the coordinate of Point P1 in Dimension x, x_2 is the coordinate of Point P2 in dimension x.

The coordinates of the second reflecting point are defined as ($x_{2\text{ref}}$, $y_{2\text{ref}}$, $z_{2\text{ref}}$). Based on these coordinates, the receiving angles of the second reflection points in azimuth and elevation $\theta_{2\text{ref}}, \vartheta_{2\text{ref}}$ can be calculated in the sensor-fixed coordinate system.

5) Modeling of the incidence angle and material-dependent reflectivity at the second reflecting points

Beside the position of the second reflecting points, the incidence angle and material-dependent reflectivity of these points should be modeled as well. The Fresnel reflection coefficients, as a physical representation of the reflectivity, is as follows[82]:

For the horizontal polarization, Fresnel reflection coefficient V_θ^{H}:

$$V_\theta^{\mathrm{H}} = \frac{\sin\left(\frac{\pi}{2}-\theta\right) - \sqrt{\varepsilon - \cos^2\left(\frac{\pi}{2}-\theta\right)}}{\sin\left(\frac{\pi}{2}-\theta\right) + \sqrt{\varepsilon - \cos^2\left(\frac{\pi}{2}-\theta\right)}} \tag{5-11}$$

For the vertical polarization, Fresnel reflection coefficient V_θ^{V}:

$$V_\theta^{\mathrm{V}} = \frac{\varepsilon\sin\left(\frac{\pi}{2}-\theta\right) - \sqrt{\varepsilon - \cos^2\left(\frac{\pi}{2}-\theta\right)}}{\varepsilon\sin\left(\frac{\pi}{2}-\theta\right) + \sqrt{\varepsilon - \cos^2\left(\frac{\pi}{2}-\theta\right)}} \tag{5-12}$$

where θ is the incidence angle, ε is the relative permittivity, which can be complex $\varepsilon = \varepsilon' + \varepsilon'' i$, when the media is subject to power losses.

The common media on road surface and their relative permittivity under different wave frequencies are as Table 5.1 shows:

Table 5.1 Permittivity of Different Media under Different Wave Frequencies[82]

Media	Frequency	Real part ε'	Imaginary part ε''
Asphalt	18 GHz 26 GHz 94 GHz 94 GHz	4.2 3.8 6.0 3.18	-0.12 -0.3 -0.036 -0.1
Water at 20 °C (theoretic)	76 GHz	8.0	-15.0
Concrete	58 GHz	6.5	-0.4

The Fresnel reflection coefficient is a precise representation of reflection capability. However, such a white-box representation rises the complexity of the entire model. For example, by using it, the polarization of the waves after every reflection and refraction should be calculated. The representation in Figure 5.1 is just a quasi-equivalent model for wave propagation in driving environment. Some de-

[82] Schneider, R.: Diss., Modellierung der Wellenausbreitung (1998).

tailed optical phenomenon such as diffuse reflection at each point are not represented one by one in this model. Concerning these matters, it is still a question, if it is necessary for such a grey-box model to execute a precise calculation of the polarization-dependent reflection capability. In this dissertation, the Fresnel reflection coefficient is not modeled at the first step. The reflection coefficient is defined as "1". Regarding the validation results of the first version of the model, the Fresnel reflection coefficient could be added in an iterative development.

5.2.2 Calculation of the Major Wave Information

Until this step, the positions of the second reflection points can be identified. Thus, the major wave characteristics like wave power, phase shift or time of flight, frequency shift and receiving angle, which are required by the VeP, can be calculated.

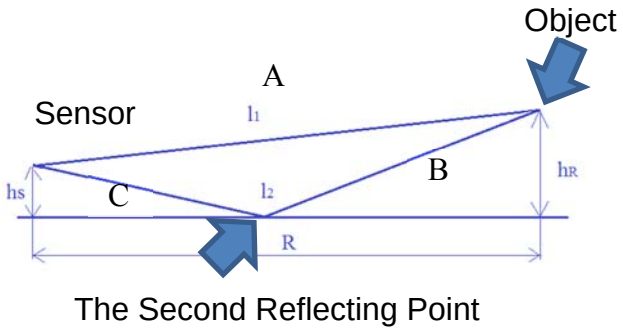

Figure 5.9 Calculations for multipath propagation

The **time of flight** of the waves received by the sensor or its phase shift, respectively, is calculated for each propagation path. According to Figure 5.9, there are four propagation paths for one object: A→A, A→B→C, C→B→A, C→B→B→C. The lengths of the paths and the time of flight of the waves on them can be calculated as follows:

$$
\begin{aligned}
l_{\mathrm{A}} &= \sqrt{(x_{\mathrm{obj}} - x_{\mathrm{sensor}})^2 + (y_{\mathrm{obj}} - y_{\mathrm{sensor}})^2 + (z_{\mathrm{obj}} - z_{\mathrm{sensor}})^2} \\
l_{\mathrm{B}} &= \sqrt{(x_{\mathrm{obj}} - x_{\mathrm{2ref}})^2 + (y_{\mathrm{obj}} - y_{\mathrm{2ref}})^2 + (z_{\mathrm{obj}} - z_{\mathrm{2ref}})^2} \\
l_{\mathrm{C}} &= \sqrt{(x_{\mathrm{2ref}} - x_{\mathrm{sensor}})^2 + (y_{\mathrm{2ref}} - y_{\mathrm{sensor}})^2 + (z_{\mathrm{2ref}} - z_{\mathrm{sensor}})^2} \\
ToF_{\mathrm{AA}} &= 2l_{\mathrm{A}} / c \\
ToF_{\mathrm{CBA}} &= ToF_{\mathrm{ABC}} = (l_{\mathrm{A}} + l_{\mathrm{B}} + l_{\mathrm{C}}) / c \\
ToF_{\mathrm{CBBC}} &= 2(l_{\mathrm{B}} + l_{\mathrm{C}}) / c
\end{aligned}
\qquad (5\text{-}13)
$$

where l is the path length, c is the velocity of the light, ToF is the time of flight.

Beside the ToF, the **transmitting and receiving directions** of different paths should be calculated as well. The transmitting direction is for the calculation of wave power meaningful, because radar does not emit the wave isotropically. The transmission power of a

wave is dependent on the direction in which it propagates. The receiving direction is important, because it decides into which cell a wave should be allocated in the VeP. In the model of some active perception sensors with a high resolution of elevation angle, the wave reflected directly and the wave reflected through multipath propagation could lie in different cells. In this case, the wave reflected through multipath propagation leads to a false-positive error or a measurement error in object height instead of interference.

Principally, the transmitting and receiving directions of different paths have the following relationship in azimuth and elevation angle.

$$\phi_{\text{rec,AA}} = \phi_{\text{rec,CBA}},\ \vartheta_{\text{rec,AA}} = \vartheta_{\text{rec,CBA}} \tag{5-14}$$

$$\phi_{\text{rec,ABC}} = \phi_{\text{rec,CBBC}},\ \vartheta_{\text{rec,ABC}} = \vartheta_{\text{rec,CBBC}} \tag{5-15}$$

$$\phi_{\text{trans,AA}} = \phi_{\text{trans,ABC}},\ \vartheta_{\text{trans,AA}} = \vartheta_{\text{trans,ABC}} \tag{5-16}$$

$$\phi_{\text{trans,CBA}} = \phi_{\text{trans,CBBC}},\ \vartheta_{\text{trans,CBA}} = \vartheta_{\text{trans,CBBC}} \tag{5-17}$$

where ϕ_{rec} is the azimuth angle of receiving direction, ϕ_{trans} is the azimuth angle of transmitting direction, ϑ_{rec} is the elevation angle of receiving direction, ϑ_{trans} is the elevation angle of transmitting direction.

The radar modeled in this dissertation does not have a separation capability in the dimension of elevation angle. Therefore, the elevation angle will be neglected in the subsequent modeling.

In addition, the **Doppler shift** of the waves reflected through different paths should be obtained as well. It decides into which bin of relative velocity the information of a wave should be allocated. The velocity of objects can be given by simulation environment. Because of the small angles between the directly and indirectly reflected wave, the Doppler shifts of the waves from the same object can hardly show a significant difference that can be separated by sensor. Therefore, as a simplification, the speed of an object is inherited by all the waves reflected on it.

In order to model the interference and furthermore the dynamic detection and measurement performance, the power of the waves reflected through different paths should be obtained. Based on the path length and the transmitting direction, a relationship between the power of the waves and the reflectivity of objects can be expressed by the equation as follows:

$$P_{\text{R}} = \frac{\sigma \cdot \lambda^2 \cdot P_{\text{total}}(\phi_i)}{4\pi(4\pi l_{\text{trans},i}^2)(4\pi l_{\text{rec},i}^2)} \tag{5-18}$$

where P_{R} is the receiving power, λ is the wavelength of the signal carrier.

$l_{\mathrm{trans},i}$ and $l_{\mathrm{rec},i}$ are respectively path lengths of a propagation path to object i in transmitting and receiving direction. ϕ_i is the azimuth angle of object i. $P_{\mathrm{total}}(\phi_i)$ is principally the transmitting direction-dependent transmission power (radiation pattern). However, since the radiation pattern in this dissertation is obtained by measurement, and the antenna gain of receiving and transmitting antenna cannot isolated from the measurement result, the total power amplification $P_{\mathrm{total}}(\phi_i)$ indicates the product of the radiation pattern and the gain of receiving antenna, which is measured in Section 5.4.

σ is the reflectivity of the object (Until here, the object is still considered as a single point reflector in VeP. The object model will be extended in Section 5.3, and its reflectivity will be modeled in Chapter 6.)

This relationship is derived from radar equation introduced in Section 2.2.1 with neglecting the atmospheric attenuation. Radar equation is a black-box sensor model. However, under the condition that the interference effect, object reflectivity, and radiation pattern are simulated in other models, it can represent the relationship between the transmitting power and the receiving power well.

Based on the information obtained until this step, the superposition of the waves in the same cell is possible.

5.3 Ergodic Stochastic Single-Point Model

As mentioned in Section 4.2.2, the drawback of the VeP is that, it is unrealistic to model all the objects by just one single point reflector in the space of measurement quantities. In reality, an object in short range can cover more than one bin in azimuth and elevation; a long object can cover more range bins; and a rotating object can cover more velocity bins because of the relative movement. Therefore, when using this method, for modeling the objects, which can occupy more than one cell, a discretization of reflecting objects is required. After a discretization, a number of reflecting points with their own relative velocities and reflectivity can describe an object. In such a way, the width, length and the rotational velocity of the object can be represented by the relative positions, relative motion and reflectivity of these reflecting points. In other words, the dynamic detection and measurement of these reflecting points can represent the width, length and rotation of the object in sensor view realistically. However, the extended object representation increases the required computing effort, because more reflecting points (subobjects) are generated for each object, and a wave propagation simulation, as introduced in Section 5.2, has to been performed for each reflecting point. For solving this problem, a so-called ergodic stochastic single-point modeling method is developed.

In principle, ergodicity refers to the consistency of the statistic results of a dynamic system in time and space. A classic example of ergodicity is as follows:

"Suppose you are concerned with determining what the most visited parks in a city are. One idea is to take a momentary snapshot: to see how many people are this moment in park A, how many are in park B and so on. Another idea is to look at one individual (or few of them) and to follow him for a certain period of time, e.g. a year. Then, you observe how often the individual is going to park A, how often he is going to park B and so on."[83]

If the two statistics show the same result, the system is ergodic.

Accordingly, the ergodicity can be used for the modeling of objects. An object in the sensor view can be modeled as a group of reflecting points (corresponds to the parks in the example above) with different reflectivity (corresponds to the people in the example above). Based on this result, an ergodic dynamic system can be created. On the one side, the model can also be considered as a momentary snapshot of the situation that unit-reflectivity "visits" different places on the object surface. When more unit-reflectivity visits the same place, the reflectivity of this place will be higher. On the other hand, it is possible to obtain the same result by "following" a unit-reflectivity, which is visiting different places, for a certain period of time and observing how often the unit reflectivity has "visited" the different places on the object surface. The probability that the unit-reflectivity "visits" a certain place on the object corresponds to the reflectivity of the object at the place. In this way, by selecting the second interpretation of the result, an efficient way of modeling the object can be obtained. The modeling process is described in the following.

The ergodic stochastic single-point modeling starts principally from the objects, as introduced in VeP. In order to simplify modeling, the objects should be represented in the simulation environment with templates that have simple geometric shapes. As a first approach, the cuboid template is used to represent an object geometrically (see Figure 5.10). Based on the cuboid template, an additional model for the representation of the reflectivity is created and integrated into the template as well. Since the reflectivity of the objects depends on the angles of incidence, the angles of reflection at every point on the object surface and the detailed geometrical forms of the objects, a calculation of reflectivity distribution based on the cuboid template is meaningless. However, the cuboid template identifies the boundaries of the space where reflectivity should be defined. The reflectivity distribution of the objects here should be identified by real measurements and calibrations, and generically modeled with a stochastic process in order to take into account the realistic influences of the geometric shape of an object. This object model will be introduced in Chapter 6 in detail.

[83] Tarko, V.: What Is Ergodicity? (2017).

Figure 5.10 Cuboid template of object in simulation environment[84]

As introduced above, the ergodic concept is used based on the reflectivity distribution of object. This means, only a single point with unit-reflectivity represents an object at one moment. The probability of its appearance on the object surface is as stochastically distributed as the distribution of the reflectivity on the surface. Thus, a realistic reflectivity distribution can be generated in several cycles of the simulation by accumulating the unit-reflectivity in all the cycles according to their positions.

It is worth noticing that enough times of the simulation should be performed, so that the reflectivity distribution can be represented realistically. Furthermore, the real measurement cycle time of the sensor to be modeled should be taken into consideration as well. The simulation environment used in this dissertation is IPG CarMaker®, which offers a simulation cycle time of 1 ms. The measurement cycle time of the sensor to be modeled is 60 ms. In order to represent the measurement cycle time of this sensor, the simulation can be repeated at most 60 times for each reflection distribution. (see the implementation in Annex B)

It is also worth noticing that excessive times of simulation should be avoided. Otherwise, the position and the orientation of the object could have significant changes, which can change the reflectivity distribution again.

5.4 Radiation Pattern

As mentioned above, the radiation pattern is one of the most important components in wave power calculation. Every sensor has its individual radiation pattern, which is decided by the geometric form of antenna and wave sending/receiving method. Therefore,

[84] IPG: CarMaker (2015).

a generic modeling of this characteristic is hardly feasible. The radiation pattern of a certain active perception sensor can be identified by measurement and calibration. In the measurement and calibration, corner (cube) reflectors (see Figure 5.11), whose reflectivity can be calculated based on their geometric dimensions, are normally used.

Figure 5.11 Corner reflector

The reflectivity of a corner reflector σ can be calculated as follows[85]:

$$\sigma = \pi \frac{L^4}{3\lambda^2} \tag{5-19}$$

where L is the diagonal dimension if the corner reflector (see Figure 5.12), λ is the wavelength of the wave reflected by the corner reflector.

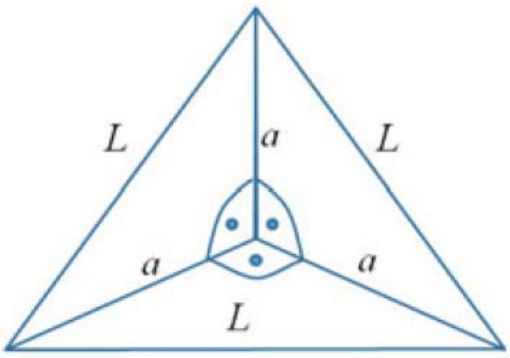

Figure 5.12 Geometry of a corner reflector[85]

[85] Winner, H.: Radarsensorik (2009).

The corner reflector used for the measurement of the radiation pattern has a diagonal dimension of 8 cm, and therefore a reflectivity of 2.83 m^2 (≈ 4.52 dBm^2) for a 77 GHz radar.

The experiment of the measurement of radiation pattern in this work is performed as Figure 5.13 shows. The corner reflector changes its position to reflect the waves from the sensor in different azimuth angles. A measurement step of 0.5° in azimuth angle is selected in the experiment. In order to reduce the influence of interference on the measurement results, the corner reflector is put on the ground ($h_R = 0$ m). The height of sensor is 52 cm ($h_s = 0.52$ m).

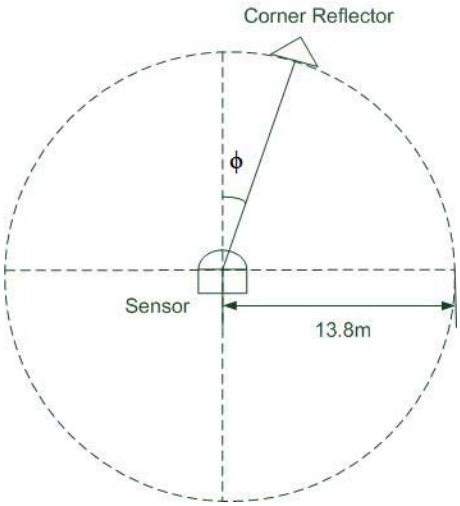

Figure 5.13 Measurement of radiation pattern by corner reflector ($h_R = 0$ m, $h_s = 0.52$ m)

With the measured receiving power P_R, the total power amplification $P_{total}(\phi_{obj})$ (including the influence of the radiation pattern, the gain of transmitting and receiving antenna) can be calculated with regard to Equation 5-18 as follows:

$$P_{total}(\phi_{obj}) = \frac{4\pi(4\pi \cdot r^2)^2 P_R}{\sigma \cdot \lambda^2} = \frac{4\pi(4\pi \cdot (13.8\text{ m})^2)^2 P_R}{\sigma \cdot (3.9\text{ mm})^2} = \frac{47.5 \times 10^{11}}{\sigma} P_R \tag{5-20}$$

which is expressed in dBmW for a 77 GHz radar as follows:

$$P_{total}(\phi_{obj}) = 126.8\text{ dB} + P_R\text{ / dB-}\sigma\text{ / dBm}^2 \tag{5-21}$$

In the experiment described above, the power of the waved reflected by the corner reflector and received by the long-range antenna of the radar to be modeled in different azimuth angles is measured (see Annex C).

According to the Equation 5-21, the total power amplification $P_{\text{total}}(\phi_{\text{obj}})$ is calculated and presented as

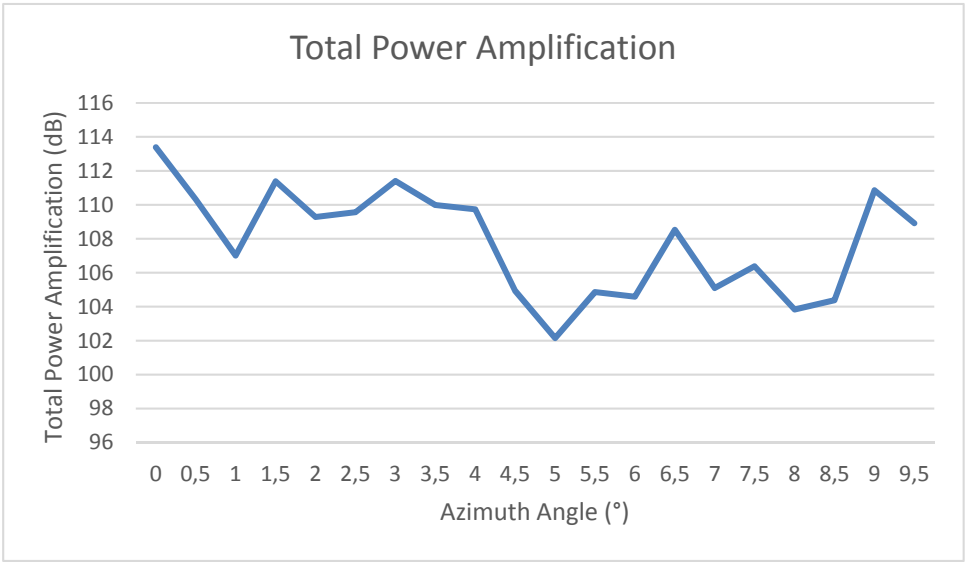

Figure 5.14 shows:

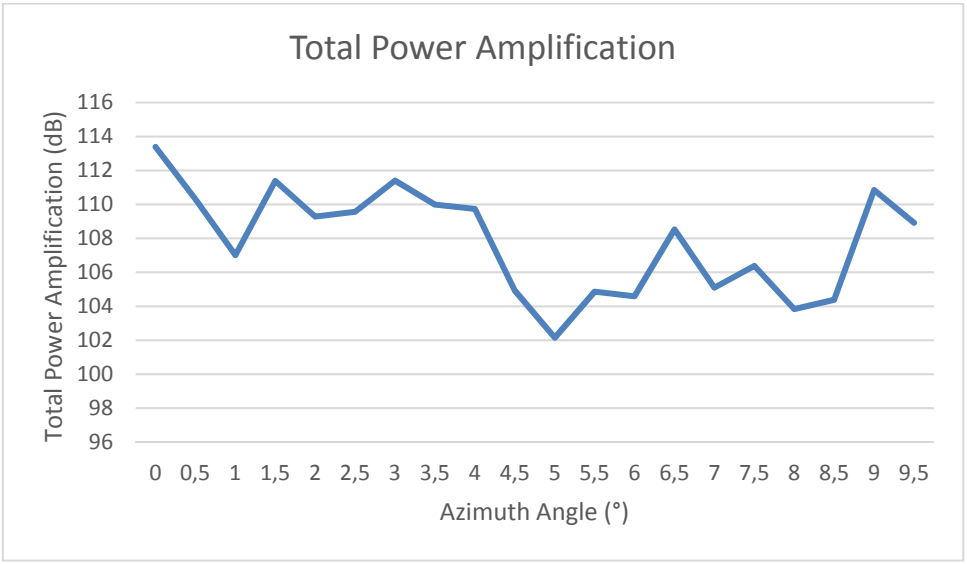

Figure 5.14 Total power amplification

As the angular aperture of the long-range antenna of the radar to be modeled is ±9°, also considering the measurement uncertainty and the symmetry of the radiation pattern (according to the symmetric detection range defined in the sensor specification), the receiving power with azimuth angles between 0° and 9.5° are measured.

In this dissertation, only the azimuth angle dependent power amplification $P_{\text{total}}(\phi_{\text{obj}})$ of the long-range antenna of the radar to be modeled is measured. The one of the short-range antenna is not measured, because the influence of the azimuth angle dependent radiation pattern, gain of transmitting and receiving antenna is already taken into consideration,

when modeling the reflectivity distribution of object in short range in Chapter 6. Therefore, the modeling of the azimuth angle dependent power amplification of short-range antenna is not necessary.

6 Environment Model

As mentioned above, in order to enable the wave propagation model and the VeP, the power of the waves should be present. According to the radar equation, the wave power must be calculated based on the reflectivity of objects. Unlike the corner reflector, due to their various geometric forms, the common objects have normally an incidence angle dependent reflectivity, which cannot be calculated by a certain equation easily. Therefore, object models for the representation of their reflectivity are required. Fortunately, some statistical similarities can be addressed between the objects of the same type, which indicates a possibility for the generic modeling, e.g. of pedestrians or of vehicles.

In this chapter, as one of the most important parts of the environment model, a generic object model for the vehicles is developed as example based on the measurement results. It consists of two parts, the vehicle model for the long-range detection and measurement and the vehicle model for the short-range detection and measurement. The long-range model is a model based on RCS (Radar Cross Section) as the most reflectivity models do. It has taken the influences of aspect angle (in other words, incidence angle) into consideration. The short-range model is a model for representing the reflectivity distribution on the different vehicles under different aspect angles, which is necessary for the dynamic modeling of sensor performances in short range, especially for the ergodic method in wave propagation model introduced in Chapter 5. It enables the calculating the power of waves reflected on different points of vehicle surfaces in driving environment. Unlike the most current methods (e.g. Andres[86], Marx[87]), this model is not built for any specified vehicles, but a generic description, which can be parameterized for modeling different vehicles. Furthermore, compared to the other current methods with similar fidelity, the modeling method in this dissertation is based on macroscopic vehicle characteristics and therefore has advantages regarding calibration and representation efforts.

The unevenness of the road surface is relevant for the distribution of the second reflecting points on the road surface due to the reflection conditions. With the different distributions of the reflections, the interference is influenced differently. Therefore, the road model is required with regard to a realistic unevenness. The current methods for the modeling of the roads such as the inverse Fourier transformation or the generation of the white noise have typically been designed for vehicle dynamics studies, and are therefore only suitable for one-dimensional modeling. In the scope of a master thesis advised by author[88], the

[86] Andres, M.: Diss., Charakterisierung komplexer Ziele (2015).

[87] Marx, B. J.: Diss., Bewertungsverfahren für die Radareigenschaften (2014).

[88] Li, Y.: Master's Thesis, Modellierung der Unebenheit (2015).

inverse Fourier transform is considered as a more efficient method, and have been extended and implemented in the two-dimensional domain. In this dissertation, a method for integrating road model and improving the simulation efficiency is developed and implemented. It has already been introduced in Section 5.2.1. This chapter will not go further on this issue.

6.1 Vehicle Reflectivity Model

In order to obtain the wave power for modeling the interference and finally simulating the dynamic sensor performance, the reflectivity of vehicle is necessary. As discussed in Section 5.3, a model for the aspect angle dependent reflectivity on a single point is not sufficient for the object modeling in short range (see Figure 6.1) for four reasons:

1) The object dimensions can be normally measured by an active perception sensor, which cannot be modeled by a point.
2) Due to the radiation pattern, the power of the waves that arrive different places of an object is different. Since an object can cover a large range of azimuth angles in sensor view in short range, the influence of azimuth angle dependent transmitting power on the receiving power cannot be neglected like in long range.
3) For the same reason as for Point 2, the waves reach an object in short range cannot considered as quasi-parallel rays. The incidence angles in different places of an object are different.
4) The waves reflected in different places of an object can superimpose on each other as well.

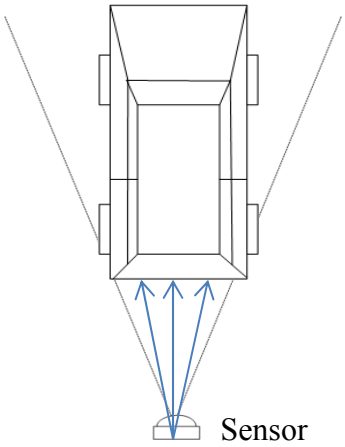

Figure 6.1 Object in short range

Therefore, a discretized description of object reflectivity, in other words, a modeling of reflectivity distribution is necessary. Furthermore, unlike in long range, the incidence angle of waves reflected by an object in short range is decided not only by the aspect angle

(heading angle) but also by the azimuth angle of the object, due to the unneglectable object dimensions. This means, the reflectivity distribution model for vehicle in short range should take the influences of azimuth angle and heading angle into consideration. Moreover, obviously, the distance between the object and the sensor influences also the incidence angles at each reflecting point, and therefore should be considered as influence factor in modeling. In principle, not only the azimuth angle but also the elevation angle can influence the reflectivity and the transmitting power, but the influence of elevation angle is as a simplification not discussed in this dissertation. In reality, both the elevation angle of object in sensor view and the object-heading angle can change, for example, when the object is climbing a ramp. However, considering the modeling and test effort, the influence of elevation angle is neglected at first. It will be measured and modeled in further investigations.

In summary, the reflectivity distribution model should describe the influences of azimuth angle, heading angle and distance. After modeling, as mentioned in Section 5.3, this distribution can be used as probability density function in the ergodic stochastic single point model to rise the simulation efficiency.

However, such a discretized description is not always required. For simulating the long range detection and measurement, the discretized description, which due to the numerous reflecting points to be modeled takes up much memory space and reduces the simulation efficiency, cannot bring much increasing in the validity of simulation (for the same four reasons above). Therefore, in this dissertation, the reflectivity of an object in short range is modeled as a distribution; meanwhile an object in long range is still modeled as a single point. The boundary between vehicle model for long range and short range is not corresponding to the boundary between the short-range antenna and the long-range antenna of the radar to be modeled. It depends on the separation capability of the radar in azimuth angle. The long-range antenna of the radar has a cell size of 1.6° in azimuth angle. Since a vehicle has normally a width W of 2 m, as Figure 6.2 shows, a vehicle cannot be separated in a range of at least approximately $R = \frac{W}{\sin(\phi_{\text{cell}})} = 2/\sin(1.6) \approx 70$ m.

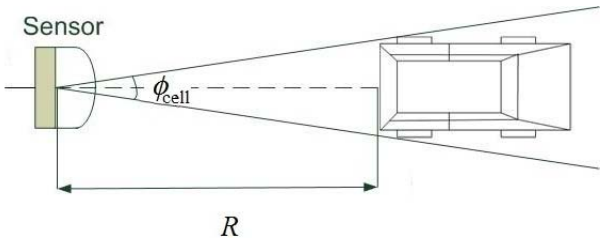

Figure 6.2 Minimum appropriate range of single point model

Therefore, for modeling of vehicles with a range of more than 70 m, the single point model is used as vehicle model in this dissertation, while the reflectivity distribution model is used to model the vehicles with a range of less than 70 m.

6.2 Experiment Design

In order to model the reflectivity (distribution) of vehicles and investigate the relationship among object distance, azimuth angle, heading angle and the reflectivity, some experiment must be performed at first. The reflectivity (distribution) of vehicle under different distances, azimuth angles and heading angles should be measured.

As mentioned above, a radar sensor from industry is to be modeled in this dissertation as example. It is used in the experiments for the measurement of vehicle reflectivity as well. As a typical radar, this sensor can measure quantities and separate objects in three dimensions: range, relative velocity and azimuth angle. For short range and long-range detection, it has two groups of antennas respectively.

As introduced in Chapter 2, this sensor measures the range and the relative velocity by Chirp Sequence Modulation, and measures the azimuth angle by planar antenna array. Therefore, the range bin and relative velocity bin can be considered as equivalent, while the azimuth angle bin is not. (The larger the azimuth angle is, the larger the azimuth angle bin is.) However, this non-equivalence is only significant in the short-range antenna. The azimuth angle bins of long-range antenna can be approximately considered as equivalent because of its small aperture angle.

As outputs of the sensor, information on three levels can be obtained by using a sensor specific measurement interface: data on object level, data on cluster level and data on peak level. These three levels correspond to three steps of the data processing in sensor. The data on peak level consist of data (receiving power etc.) of peaks in each range gate (range bin), azimuth bin and relative velocity bin. The data on cluster level indicates the data of the clustered peaks (clusters). The data on object level indicates the data of the tracked and associated clusters (objects).

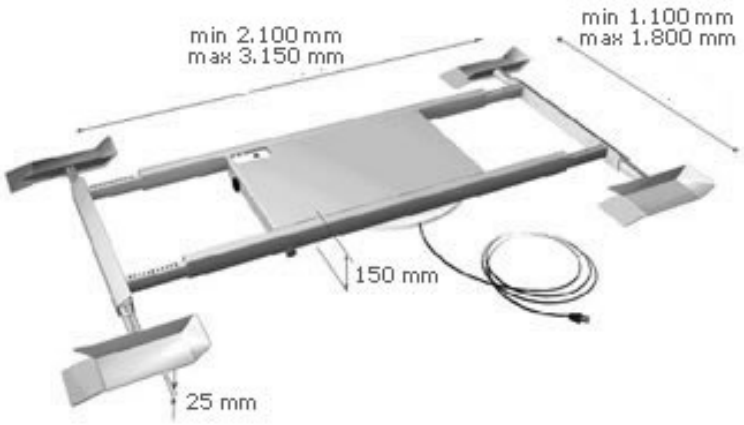

Figure 6.3 Vehicle revolving stage: BUMAT DB 2/25[89]

Figure 6.3 shows the vehicle revolving stage, which is used in the experiments in this dissertation for changing the heading angle of the object vehicle. This stage can rotate a vehicle on it at very low speed, so that a pseudo-static measurement of the reflectivity of a vehicle at different heading angles can be performed continuously. A pseudo-static measurement is here required; otherwise, the influences of measurement latency of sensor will affect the measurement accuracy.

As discussed above, besides the heading angle, the influence of the azimuth angle and the distance between sensor and object should be taken into consideration as well; therefore, the measurement of a rotated vehicle is repeated under different azimuth angles and distances. Furthermore, in order to develop a generic model for modeling the reflectivity of different vehicles, four vehicles in different geometric forms are measured: Volkswagen Caddy, Volkswagen Multivan T5, BMW i3 and Volkswagen Golf.

The experimental design is as Figure 6.4 shows:

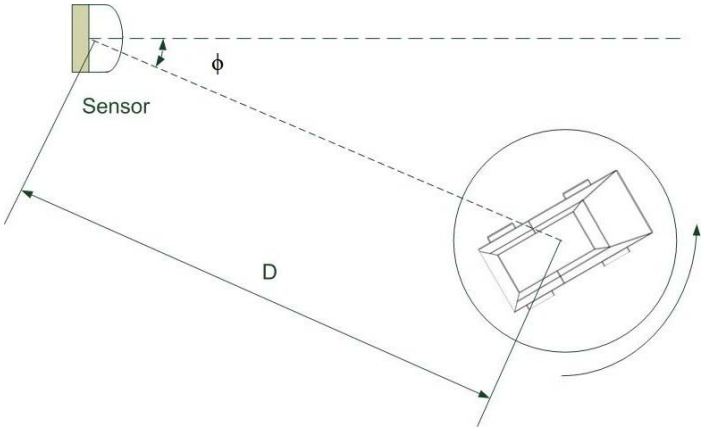

Figure 6.4 Experimental design for the identification of vehicle reflectivity

[89] Burgmeier, T.: BUMAT Drehbühnen Autodrehbühnen (2017).

As described above, in the experiment, the vehicle revolving stage changes the heading angle of the vehicle to be measured.

For modeling the vehicle in long range, the azimuth angle does not need to be changed. For single point model, the heading angle is equal to the aspect angle, therefore the measurement of aspect angle dependent reflectivity of different vehicles is achieved in the experiment by changing heading angle at a azimuth angle of 0°. For investigating the influence of interference, the reflectivity at three different distances (40 m, 70 m and 110 m) are measured.

For the reason analyzed above, for modeling the vehicle in short range, beside the changing heading angle, the azimuth angle ϕ is changed in the experiment from 0° to 20° with a step of 5° and three distances D are chosen: 5 m, 10 m, and 20 m.

The situation of the experiment is as Figure 6.5 shows. The experiment is performed at the August-Euler-airport in Darmstadt, where no much other objects that can interfere exist. In addition, in order to avoid the influence of elevation angle and atmospheric attenuation, flat road surface and bright weather are chosen as conditions for the execution of the experiment.

Figure 6.5 Experiment situation (with Volkswagen Caddy)

6.3 Vehicle Reflectivity Model for Long Range

In the scope of a master thesis advised by author[90], the RCSs of different vehicles at different aspect angles are measured and a typical RCS representation is provided as Figure 6.6 shows (see Annex D). The 0° in Figure 6.6 corresponds to the vehicle rear.

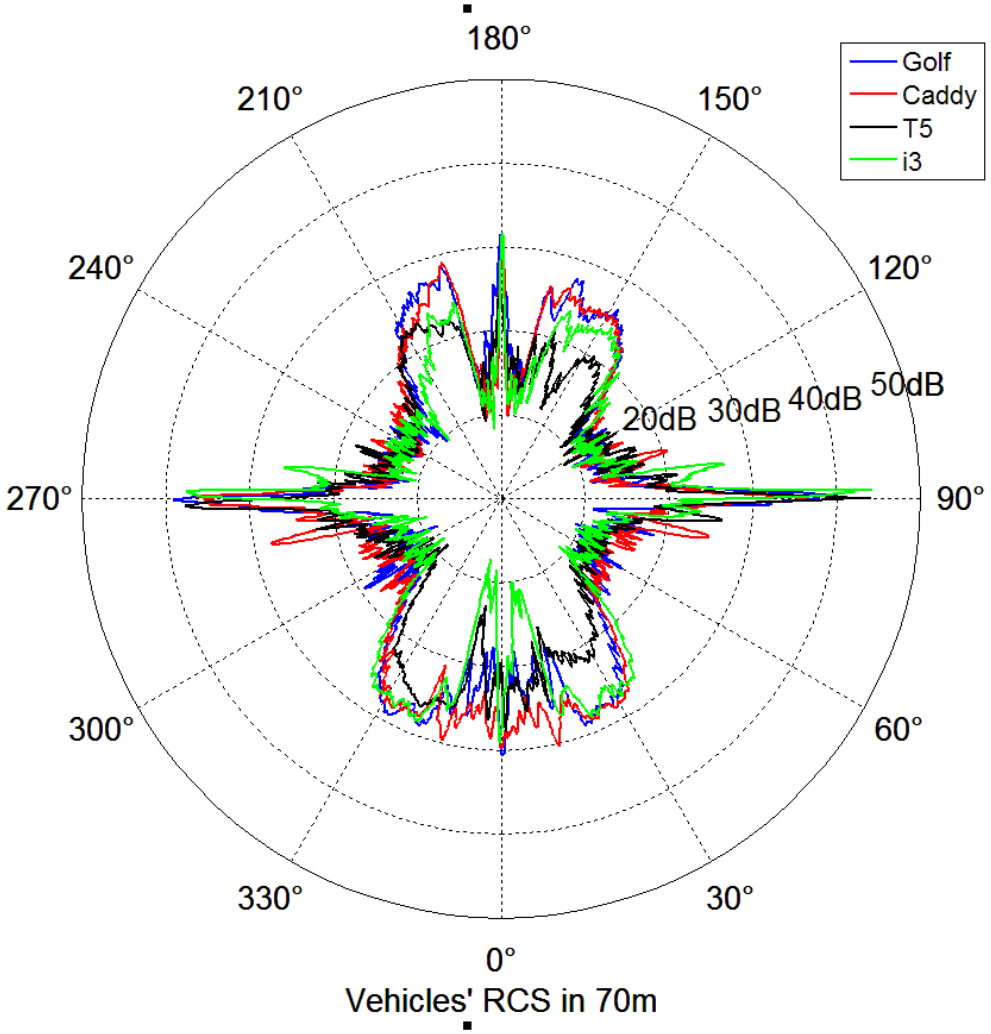

Figure 6.6 RCS of different vehicles at different aspect angles, a distance of 70 m and a sensor height of 52 cm[90]

To observe separately, this representation can be converted to Figure 6.7.

[90] Qin, L.: Master's Thesis, Untersuchung der Reflexionseigenschaften (2016).

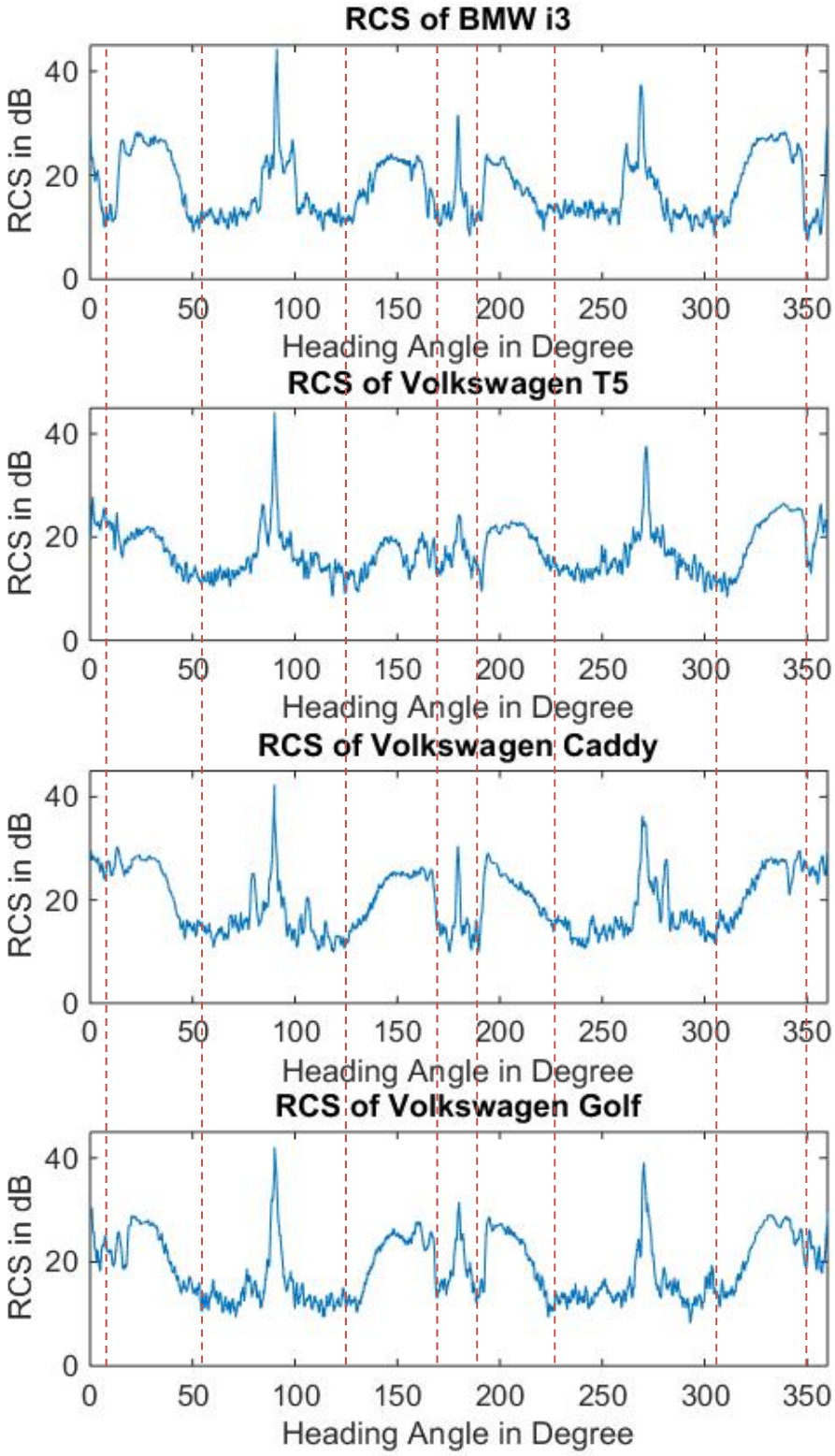

Figure 6.7 RCS of different vehicles at different aspect angles and a distance of 70 m (separated)

After comparing the RCSs of different vehicles at different aspect angles and a distance of 70 m, naturally, differences exist. However, obviously, they share some common characteristics as well. They can be described as follows:

1) Despite the significant different area of the front surfaces of different vehicles, especially between the ones of Volkswagen T5 and Volkswagen Golf at 90°, the reflectivity show no significant difference. The peaks at 90° lie on approx. 40 dB. This could happen because of the specular reflection. The diffuse reflection could play an inessential role in the wave reflection on vehicle surfaces. Based on this assumption, for example, at a heading angle of 90°, the most wave power should be reflected by a certain middle area of the vehicle side surface, and therefore is independent of how large the entire surface is.
2) Despite the different RCS of the different vehicles at different heading angles, the curve progressions in the 0° to 360° heading angle range, as Figure 6.7 shows, consist of eight peaks. The peaks at 0°, 90°, 180° and 270° are principally caused by the large reflectivity of a vehicle, when its front, side or back surface are facing the sensor. However, these peaks are reduced quickly, which can support the assumption of specular reflection in Point 1. The other peaks could be understood as caused by the corners between the front, side or back surfaces, which are mostly rounded, and therefore can provide a better angle insensitivity.
3) Because of the symmetry of the vehicles, the curve progression from 0° to 180° can be considered as equal to the one from 360° to 180°. Therefore, five peaks can represent the RCS progression.
4) Although the reflection capability of the corners of different vehicles are different, their peaks share a similar heading angle range, approx. [10°, 55°], [125°, 170°] and symmetrically [305°, 350°], [190°, 235°].

These characteristics can be observed in the measurement results at a distance of 110 m and 40 m as well.

Under these circumstances, in this dissertation, the vehicle reflectivity for long range will be phenomenologically modeled by five peaks, or in other words, five windows (see red dashed lines in Figure 6.7). Since the reflectivity at 0°, 90° and 180°, as mentioned above, are sensitive to the heading angles, Poisson window is chosen for modelling the peaks at these angles as follows:

$$RCS_{\mathrm{Poisson}}(\theta) = \sum P_{\theta_0} e^{-(|\theta-\theta_0|)^{1/2}/\tau}, \text{with } \theta \in [\theta_0 - \frac{N_{\mathrm{width}}}{2}, \theta_0 + \frac{N_{\mathrm{width}}}{2}] \quad (6\text{-}1)$$

where θ_0 is 0°, 90° or 180°, P_{θ_0} is the RCS at these angles, τ is constant, which can be identified as follows:

$$\tau = \frac{(N_{\mathrm{width}}/2)^{\frac{1}{2}}}{\ln(P_{\theta_0}/D_0)} \quad (6\text{-}2)$$

where D_0 is the RCS at the peak width N_{width}. In the dissertation, according to Figure 6.7, the peaks around 0°, 90° or 180° are limited in angle ranges [350°, 10°], [55°, 125°] and [170°, 190°]. Their widths N_{width} are 20°, 70°, and 20° respectively. The general RCS

at the boundaries of the peaks for all the measured vehicles is about 10 dB. (For the peak in angle ranges [350°, 10°], the RCS at the boundaries is about 20 dB):

$$D_0 = \begin{cases} 20\ \text{dB}, & \text{for the peak in } [350°, 10°] \\ 10\ \text{dB}, & \text{for the others} \end{cases} \tag{6-3}$$

For the heading angle-insensitive peaks, the Hanning window is chosen concerning its similar form, easy parametrization and finite length. The Hanning window can be expressed as follows:

$$RCS_{\text{Hanning}}(\theta) = (P_{\theta_0} - D_0)\cos^2\frac{\pi(\theta-\theta_0)}{N_{\text{width}}} + D_0, \text{with } \theta \in [\theta_0 - \frac{N_{\text{width}}}{2}, \theta_0 + \frac{N_{\text{width}}}{2}] \tag{6-4}$$

where θ_0 is 20° or 160°, P_{θ_0} is the RCS at these angles, N_{width} is the width of the windows and equal to 70° for the both peaks.

Thus, by measuring and parameterizing the RCS at the heading angles 0°, 20°, 90°, 160° and 180°, the heading angle dependent RCS of different vehicles can be modeled as a sum of the peaks above.

The model for BMW i3 is shown in Figure 6.8 as example (Models for the other vehicles are shown in Annex F.).

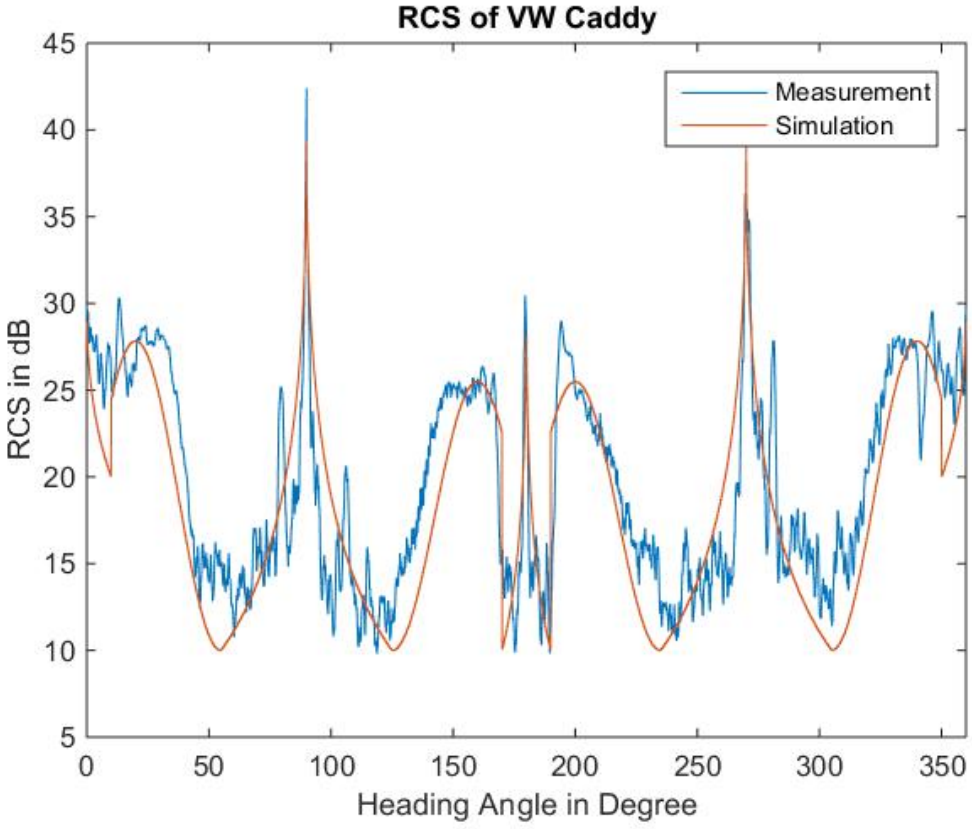

Figure 6.8 Simulated RCS of VW Caddy

Figure 6.9 shows the diagram in polar coordinate system.

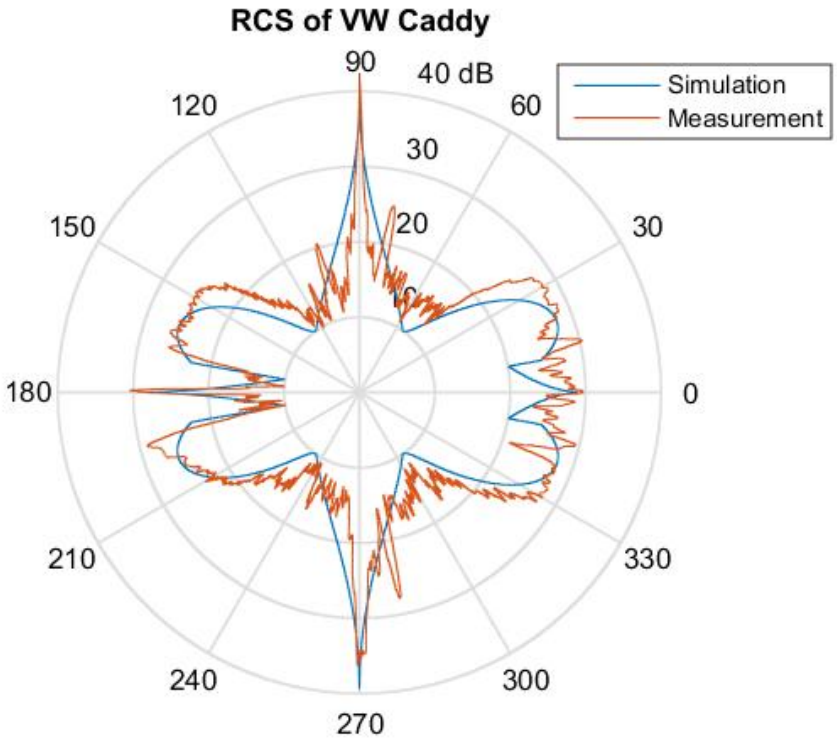

Figure 6.9 Simulated RCS of VW Caddy in polar coordinate system

The measurement results of the vehicles at a distance of 40 m and 110 m, as Figure 6.10 and Figure 6.11 show, can support the idea that the distance between sensor and object has influence on the detection and measurement. Obviously, the amplitudes of the peaks at a same angle in the diagrams change, which can be considered as the influence of interference. The detailed influence will be investigated in model verification in Chapter 7 by reducing the distance continuously but pseudo-statically.

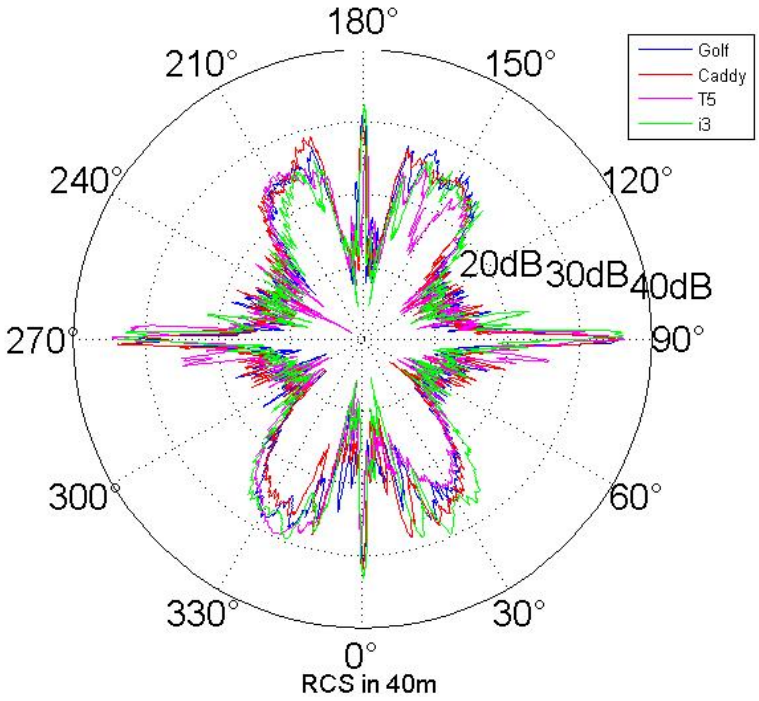

Figure 6.10 RCS of different vehicles at different aspect angles and a distance of 40 m[91]

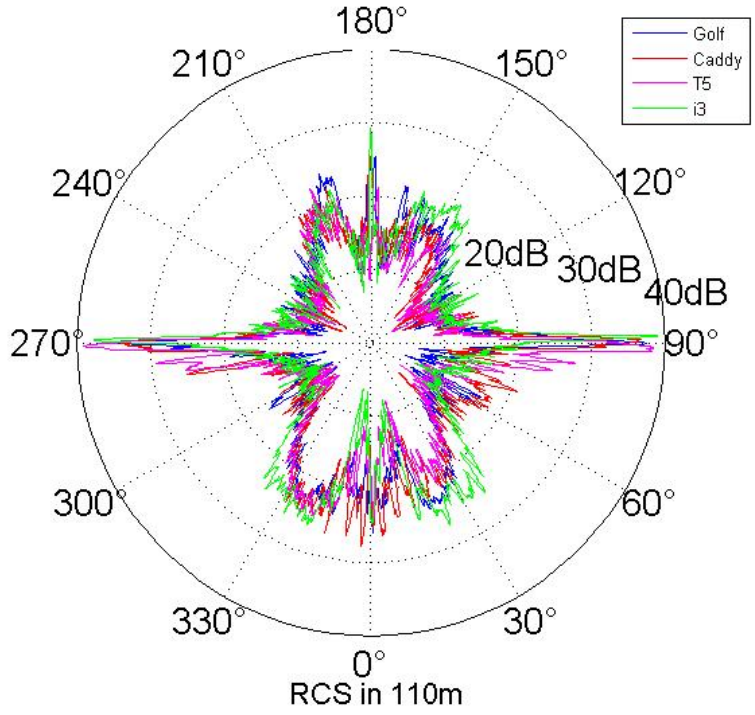

Figure 6.11 RCS of different vehicles at different aspect angles and a distance of 110 m[91]

[91] Qin, L.: Master's Thesis, Untersuchung der Reflexionseigenschaften (2016).

However, obviously, the distance changes only the amplitudes of the peaks. The common characteristics found above are not changed.

6.4 Vehicle Reflectivity Model for Short Range

As introduced in Chapter 2, the radar to be modeled uses the antenna planar array to measure the azimuth angles of objects and therefore has a non-equivalent separation bin in azimuth angles. By analyzing the data on the peak level. The receiving power in each range bin and azimuth angle bin can be obtained. Based on these raw data, a receiving power distribution over the vehicle surface in short range can be achieved (see Annex E). (Since the sensor has not separation capability in elevation angle, only a receiving power distribution over azimuth angle is possible.)

Preconditions and Data Preprocessing

Although the receiving power in each bin is accessible, unlike the object modeling for long range, the RCS of the reflecting points in each bin cannot be accurately calculated by using radiation pattern. On one hand, the incidence angles at different reflecting points in the same bin are different, a representation of the transmission power in an azimuth bin by the transmission power at bin center is not sufficient. On the other hand, unneglectable interference exists between the waves reflected from different reflecting points, even when they are in the same bin. The interference condition will change, when the azimuth angle of the object in sensor view changes. Therefore, the influences of interference and radiation pattern cannot be isolated from the measurement results. Under these circumstances, a vehicle reflectivity model for short range including the effects of interference and radiation pattern is developed. Due to the included radiation pattern, the developed model is sensor-specific, which can only be used to model the objects detected and measured by the radar to be modeled at first. If the receiving power distribution in this model can be proven independent on radiation pattern in further investigation, the model could be suitable for the modeling of other sensors as well. However, validation is required, before utilization. Due to the included interference effect, the sensor height could influence the distribution as well. In this dissertation, the sensor height is defined as 52 cm. It is the typical grille height of passenger cars, where a radar is often installed. However, despite the sensor-specific and the sensor-height-specific factors, the method for modeling the vehicle reflectivity in short range can be generically utilized. Furthermore, like in the model for long range, some macroscopic characteristics can be shared by different sensors with different heights.

Furthermore, the model here is developed under the assumption that all reflections take place on the first surface a wave reaches. Thus, the distribution of receiving power over the range can be neglected in modeling as simplification. Since the heading angle of a

vehicle in the simulation is always accessable, the receiving power distribution over the range can be derived from the distribution over azimuth angle under the assumption above and the cuboid template assumption, as Figure 6.12 shows.

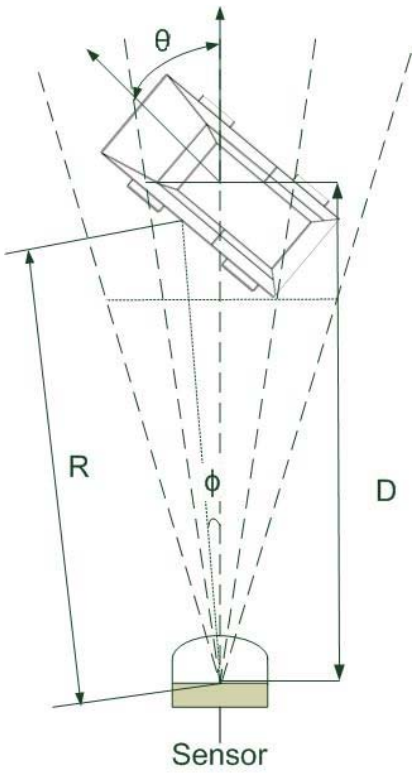

Figure 6.12 Calculation of receiving power distribution over range

Suppose the vehicle in Figure 6.12 has a length of L, a width of W and a heading angle of θ in sensor-related coordinate system. The range of the first reflecting point R on the vehicle surface at an azimuth angle of ϕ can be calculated as follows:

If $\theta < 0$;

If $\phi < \arctan\frac{W\cos\theta + L\sin\theta}{2D(\sin^2\theta - \cos^2\theta) - (W\sin\theta + L\cos\theta)}$

$$R = \sqrt{\left(\frac{D + \frac{W}{2\sin\theta}}{\cot\phi - \cot\theta}\right)^2 + \left(\frac{\frac{W\cot\phi}{2\sin\theta} + D\cot\theta}{\cot\phi - \cot\theta} - D\right)^2} \tag{6-5}$$

If $\phi > \arctan\frac{W\cos\theta + L\sin\theta}{2D(\sin^2\theta - \cos^2\theta) - (W\sin\theta + L\cos\theta)}$

$$R = \sqrt{\left(\frac{D - \frac{L}{2\cos\theta}}{\cot\phi - \tan\theta}\right)^2 + \left(\frac{-\frac{L\cot\phi}{2\cos\theta} + D\tan\theta}{\cot\phi - \tan\theta} - D\right)^2} \tag{6-6}$$

If $\theta > 0$;

If $\phi < \arctan\frac{-W\cos\theta + L\sin\theta}{2D(\sin^2\theta - \cos^2\theta) + (W\sin\theta - L\cos\theta)}$

$$R = \sqrt{\left(\frac{D-\frac{L}{2\cos\theta}}{\cot\phi-\tan\theta}\right)^2 + \left(\frac{-\frac{L\cot\phi}{2\cos\theta}+D\tan\theta}{\cot\phi-\tan\theta} - D\right)^2} \tag{6-7}$$

If $\phi > \arctan\frac{-W\cos\theta+L\sin\theta}{2D(\sin^2\theta-\cos^2\theta)+(W\sin\theta-L\cos\theta)}$

$$R = \sqrt{\left(\frac{D-\frac{W}{2\sin\theta}}{\cot\phi-\cot\theta}\right)^2 + \left(\frac{-\frac{W\cot\phi}{2\sin\theta}+D\cot\theta}{\cot\phi-\cot\theta} - D\right)^2} \tag{6-8}$$

If $\theta = 0$;

$$R = \frac{D-\frac{L}{2}}{\cos\phi} \tag{6-9}$$

where D is the distance between the sensor and the geometric center of the vehicle.

Thus, only the distribution of receiving power over the azimuth angle should be measured. After calibrating the receiving power with dB and the simple point with heading angle in degree, the data is trimmed by the ground-truth width of the vehicles at different heading angles, so that the bins out of vehicle (with noise only) are not shown. For a sensor, which is at D away from object center, the ground-truth width W_{ground} of a vehicle with a length of L, a width of W and a heading angle of ϕ in sensor-related coordinate system is calculated as follows:

$$A = \sqrt{\left(\frac{W}{2}\right)^2 + \left(\frac{L}{2}\right)^2} \tag{6-10}$$

$$\theta_{\text{cor}} = \arctan\frac{L}{W} \tag{6-11}$$

$$W_{\text{ground}} : \left[\text{Min}\begin{pmatrix}\arctan\frac{A\sin(\pi-\theta_{\text{cor}}+\theta)}{D+(A\cos(\pi-\theta_{\text{cor}}+\theta))}, \arctan\frac{A\sin(-\pi+\theta_{\text{cor}}+\theta)}{D+(A\cos(-\pi+\theta_{\text{cor}}+\theta))}, \\ \arctan\frac{A\sin(-\theta_{\text{cor}}+\theta)}{D+(A\cos(-\theta_{\text{cor}}+\theta))}, \arctan\frac{A\sin(\theta_{\text{cor}}+\theta)}{D+(A\cos(\theta_{\text{cor}}+\theta))}\end{pmatrix},\right.$$
$$\left.\text{Max}\begin{pmatrix}\arctan\frac{A\sin(\pi-\theta_{\text{cor}}+\theta)}{D+(A\cos(\pi-\theta_{\text{cor}}+\theta))}, \arctan\frac{A\sin(-\pi+\theta_{\text{cor}}+\theta)}{D+(A\cos(-\pi+\theta_{\text{cor}}+\theta))}, \\ \arctan\frac{A\sin(-\theta_{\text{cor}}+\theta)}{D+(A\cos(-\theta_{\text{cor}}+\theta))}, \arctan\frac{A\sin(\theta_{\text{cor}}+\theta)}{D+(A\cos(\theta_{\text{cor}}+\theta))}\end{pmatrix}\right] \tag{6-12}$$

Thus, the changing receiving power distribution can be observed clearly, as Figure 6.13 shows for example.

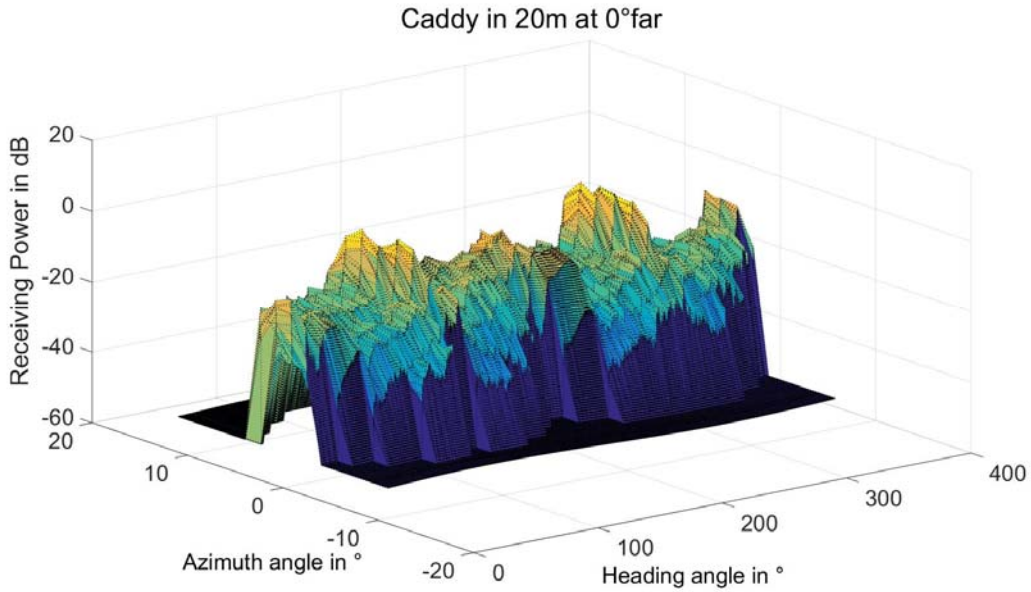

Figure 6.13 Receiving power distribution after calibration and trimming

In order to obtain a better resolution in azimuth angle, the data received by long range antenna are used as much as possible. However, in the experiments at a azimuth angle of 15° and 20°, the usage of the data from long range antenna is not possible, because the vehicle stays out of its measurement range of azimuth angle.

For modeling the receiving power distribution, the unit of receiving power should be converted from dBm to mW, so that the power can be directly added and integrated. The measuring results after converting are as Figure 6.14 shows for example.

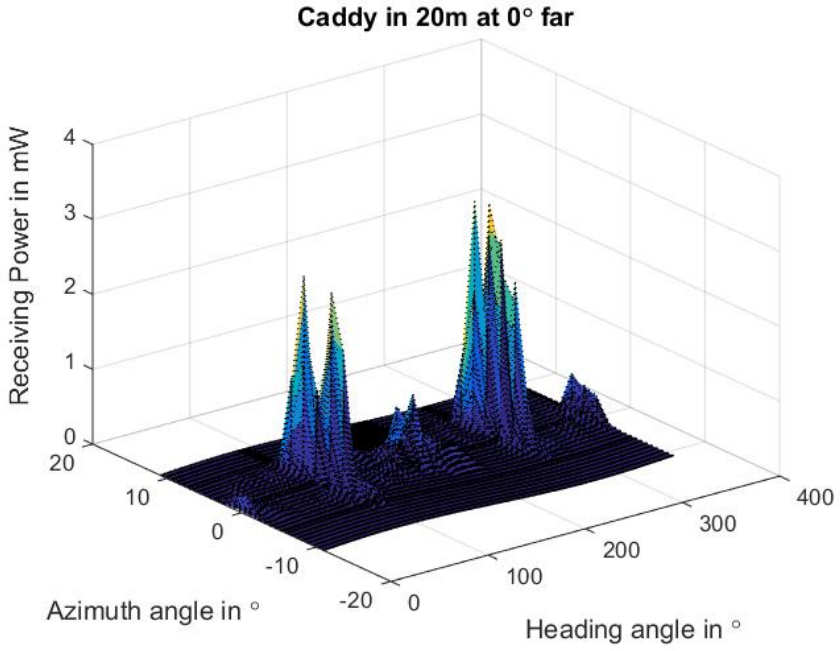

Figure 6.14 Receiving power distribution in mW

Modeling

In a microscopic view, a generic modeling of the receiving power reflected by different vehicles is because of their different geometries not feasible. However, by comparing the receiving power distributions from different vehicles, some common characteristics, which are important for the dynamic sensor performance modeling, are found.

In principle, there are four points worth noticing:

1) The most receiving power distributions over the azimuth angle have an approximate peak form. This is a basic assumption and simplification for the following modeling.
2) However, the peak amplitude $P_{\max}$ changes its value with the heading angle. This point of view is supported by the measured RCSs of the different objects in long range (see Section 6.3).
3) The position of the peak ϕ_0 in azimuth angle changes with the heading angle as well. This characteristic can directly affect the separation capability of a sensor when observing an object at different heading angles.
4) The width of the peak changes with the heading angle. On one hand, the real area of the vehicle surface facing to sensor changes with the heading angle. On the other hand, this change indicates the real distribution of reflecting points as well. When modeling, the total receiving power at each heading angle S_{P} is calculated by the integral of the receiving power distribution, and its change with heading angle is modeled for representing the changes of peak width. It is done for three reasons:
   a) The different geometric forms of the peaks with the same width can be taken into consideration in modeling.
   b) This integral indicates the reflectivity of the entire object, which as a basic characteristic of different objects should be modeled realistically.
   c) The integral decides the receiving power of each unit reflectivity in ergodic method. For example, to represent a receiving power distribution by 60 times modeling of the unit reflectivity. Each unit reflectivity should represent a receiving power of $S_{\mathrm{P}}/60$.

For modeling the common characteristics above, the Gaussian distribution is chosen as a simple solution to represent the receiving power distribution over azimuth angle (With Gaussian distribution, the stochastic unit-reflectivity for the ergodic method can be generated by Box-Muller-method.). The developments of its peak amplitude $P_{\max}$, peak position ϕ_0, and integral S_{P} with heading angle are modeled separately. Besides, the influence of the position of an object is investigated. Principally, other window functions can

be used for the modeling as well. A peak separation method[92] can model an asymmetric peak as the sum of multiple elementary peaks, in order to represent the course more accurately. However, it is worth noticing that these complex functions bring normally more parameters, which have sometimes no physic meaning. This makes the generic investigation and modeling of the relationship between these parameters and heading angle difficult.

A Gaussian distribution represents the receiving power distribution $P_{\mathrm{Gauss}}(\phi)$ over azimuth angle as follows:

$$P_{\mathrm{Gauss}}(\phi) = P_{\max} \mathrm{e}^{-\frac{1}{2}\cdot\left(\frac{(\phi-\phi_0)}{k}\right)^2} \tag{6-13}$$

where ϕ is the azimuth angle in degree, the scale factor k is decided by the integral of the distribution S_{P}, as follows:

$$k = \frac{S_{\mathrm{P}}}{\sqrt{2\pi} P_{\max}} \tag{6-14}$$

In this way, for example, the diagram in Figure 6.14 can be modeled by Gaussian distribution as Figure 6.15 shows.

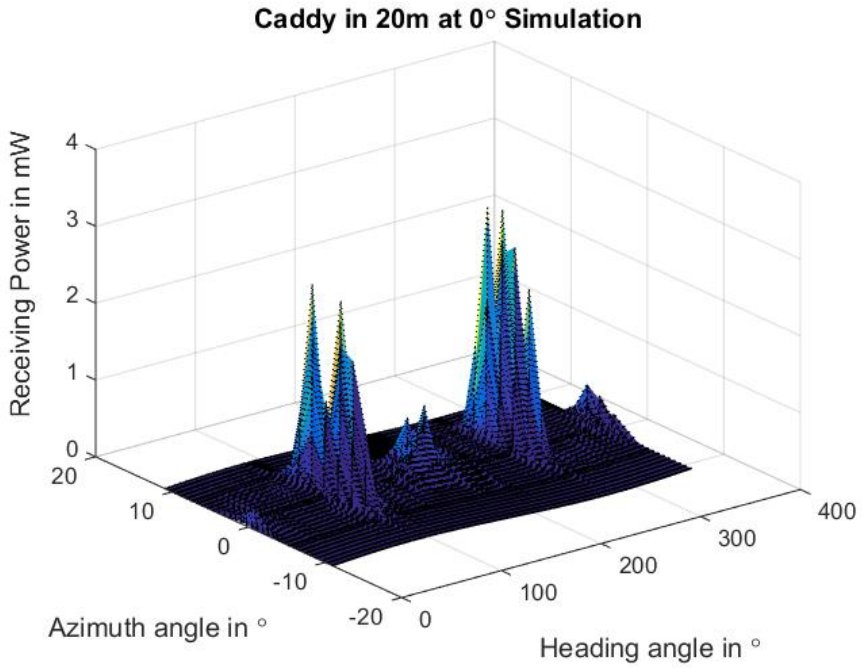

Figure 6.15 Simulated receiving power distribution by Gaussian distribution

The simulated received power at four different heading angles are as example in

Figure 6.16.

[92] NETZSCH: Peak Separation (2017).

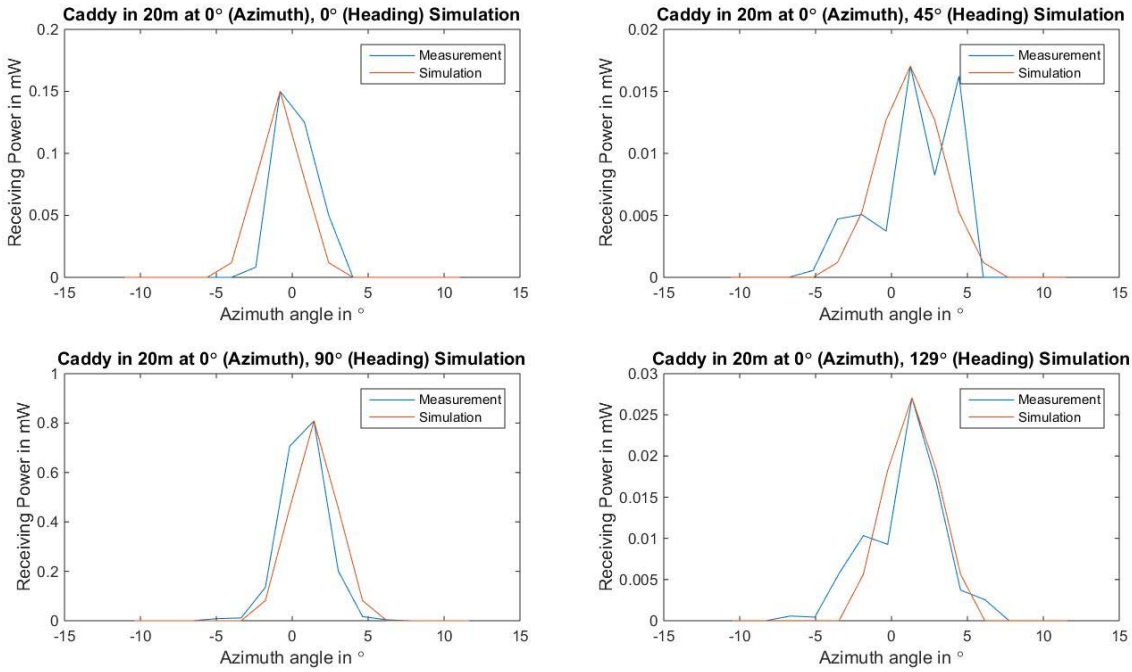

Figure 6.16 Receiving power distribution over azimuth angle for VW Caddy in 20 m at an azimuth angle of 0° and different heading angles (simulation vs. measurement)

As

Figure 6.16 shows, in most cases, the measurement result shows only one peak at each heading angle, therefore the simulated curve can be suited to the measurement (through parameterization). A relative significant difference is occurred at a heading angle of 45°, where two peaks exist. Fortunately, such a situation mostly happens when the receiving power is low. Thus, this happening can be considered as merely caused by noise. The noise modeling in the VeP can compensate the difference to a certain extent.

The peak amplitudes P_{max} of different vehicles at a azimuth angle of 0° and different heading angles are as Figure 6.17 shows:

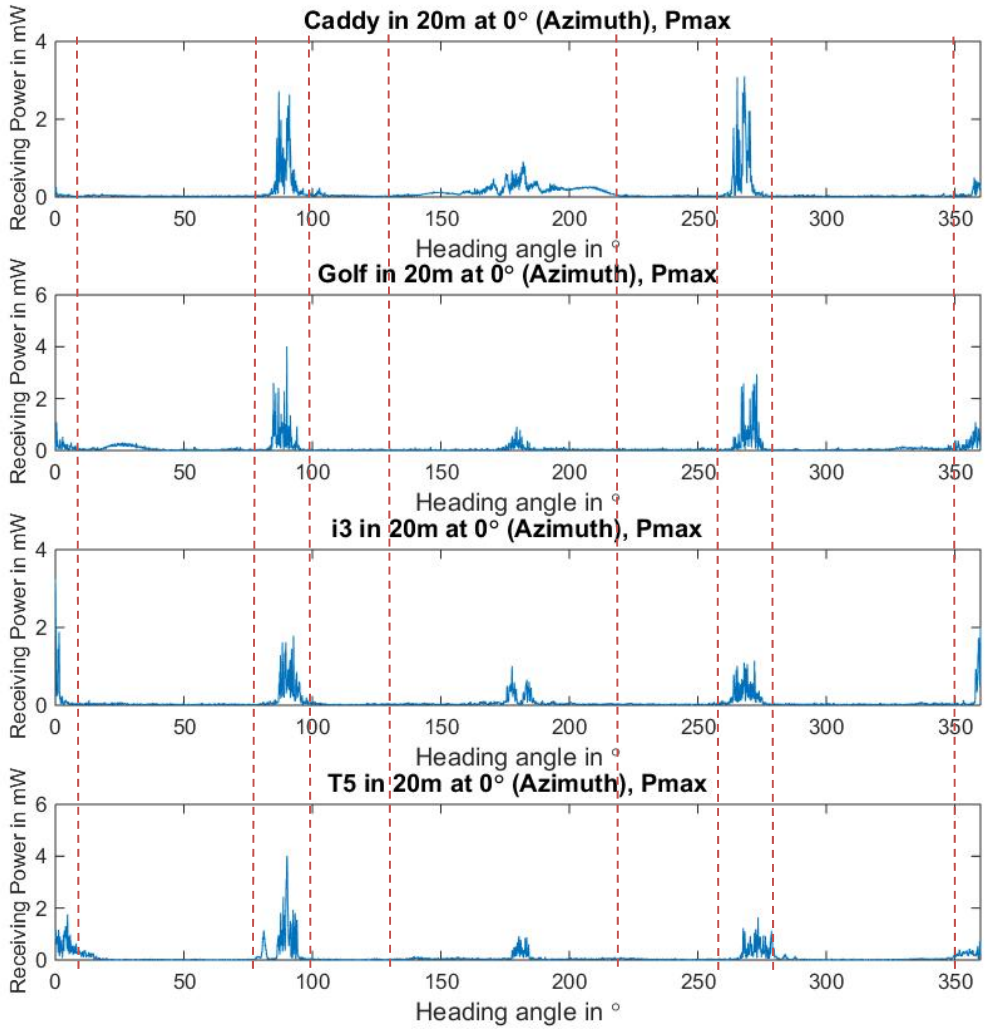

Figure 6.17 The peak amplitudes of receiving power from different objects at different heading angles

Because of the symmetry of the vehicle geometry, the asymmetrical part of the measurement results can be considered as noise. Thus, obviously, the peak amplitude curves consist of 5 peaks in the ranges of [350°, 10°], [80°, 100°], [130°, 220°] as well as [260°, 280°], and an offset of approx. 0.02 mW.

Because of the form of the peaks, the Poisson window, as Equation 6-1 shows, are used to model the peaks. For this modeling, the peak amplitudes at heading angles: 0°, 90° and 180° should be measured at first. Without considering the offset, at the boundaries of the peaks, the power values of peak is reduced to 0.01 mW. Therefore,:

$$D_0 = 0.01 \tag{6-14}$$

The comparison of the simulated peak amplitudes and the measured peak amplitudes for Caddy in 20 m is shown in Figure 6.18 as example. (Models for the other vehicles are shown in Annex G.)

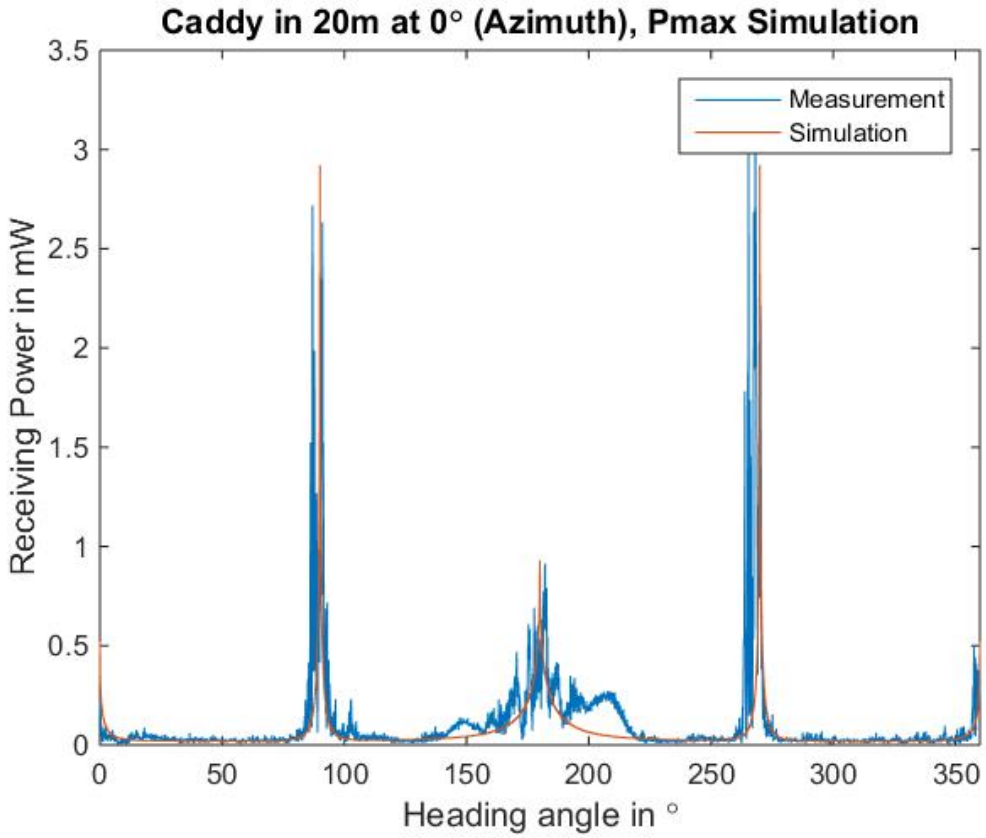

Figure 6.18 Simulated peak amplitudes of receiving power from VW Caddy at different heading angles

The integral of the receiving power distribution S_P of different vehicles at a azimuth angle of 0° and different heading angles are as Figure 6.19 shows:

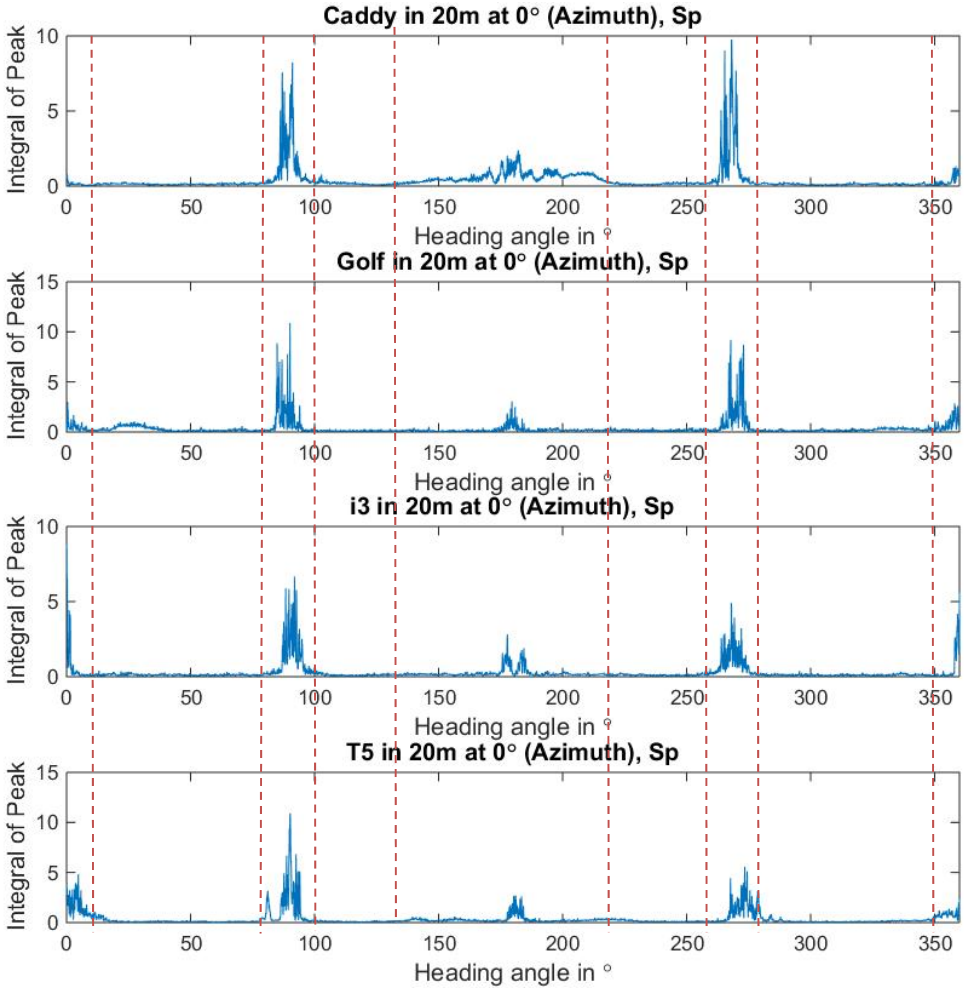

Figure 6.19 The integral of receiving power distribution from different objects at different heading angles

These curves are similar to the curves for the peak amplitudes, therefore the similar modeling method is used. (Models for different vehicles are shown in Annex G.)

The peak position ϕ_0 of different vehicles at a azimuth angle of 0° and different heading angles are as Figure 6.20 shows:

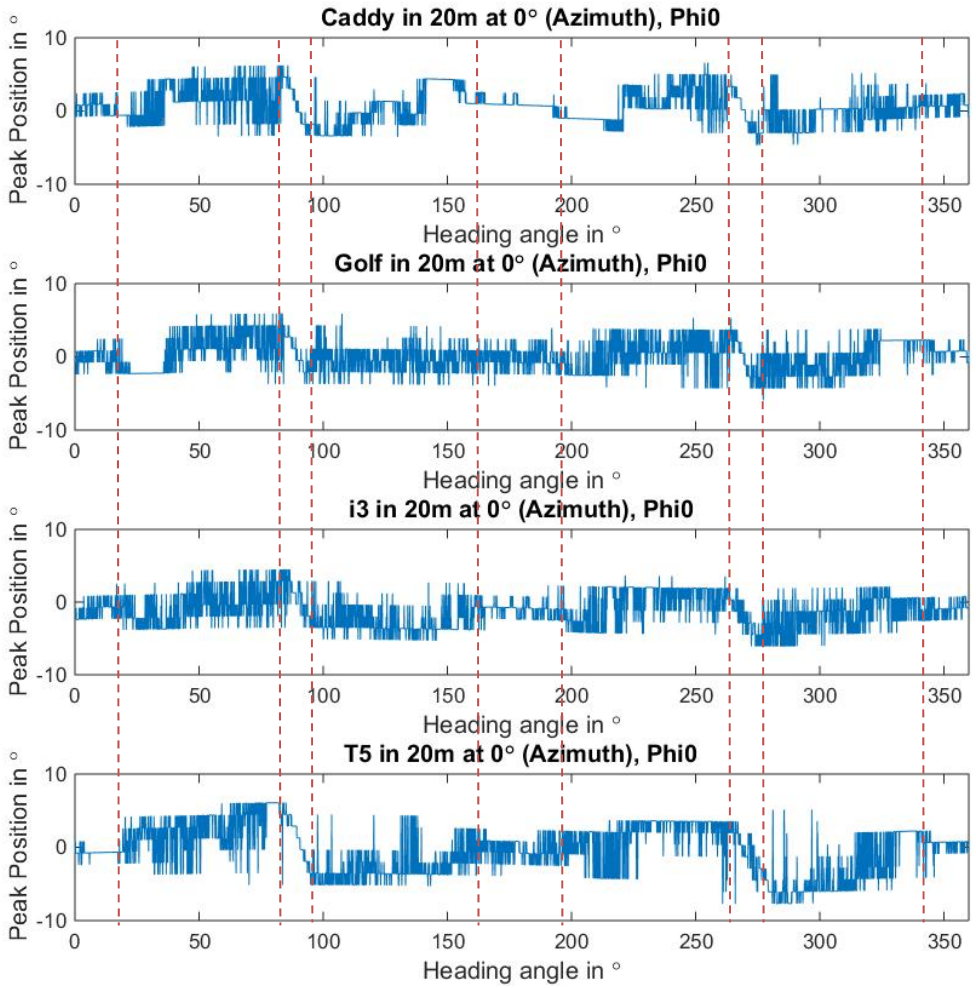

Figure 6.20 Peak position of receiving power from different objects at different heading angles

According to Figure 6.20, the following common characteristics can be observed:

1) Obvious linear movements of the peak position from right side to left side exist in heading angle ranges of [85°, 95°], [265°, 275°]. These movements can be considered as a moving of the reflecting point on a rotating ellipsoid surface, which can represent the side surface of a vehicle well.
2) The peak stays almostly in the middle in heading angle ranges of [340°, 20°] and [165°, 195°]. It could be caused by the interaction of multiple reflecting points on the front and back surfaces. Because of the symmetric geometry, the reflecting point distribution is also symmetric.
3) The curve progressions in the other ranges of heading angle cannot be easily recognized, due to noise. However, according to the measurement results in long range, in these ranges, the corners between side surface, front surface and back surface should play a essential role in reflectivity. Therefore, this dissertation tries to simulate the peak position in the other ranges of heading angle as corner position (see Figure 6.21).

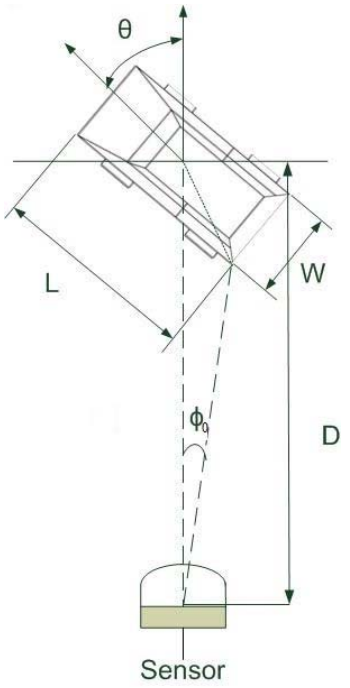

Figure 6.21 Vehicle corner position calculation

The reflecting corner position ϕ_0 of a vehicle with a length of L and a width of W at a heading angle of θ is calculated as follows:

$$\phi_0(\theta) = \begin{cases} \arctan\frac{-A\cos(\theta+\theta_{\text{cor}})}{D-A\sin(\theta+\theta_{\text{cor}})}, & 20° \le \theta < 85° \\ \arctan\frac{-A\cos(\theta-\theta_{\text{cor}})}{D-A\sin(\theta-\theta_{\text{cor}})}, & 95° \le \theta < 165° \\ \arctan\frac{A\cos(\theta+\theta_{\text{cor}})}{D+A\sin(\theta+\theta_{\text{cor}})}, & 195° \le \theta < 265° \\ \arctan\frac{A\cos(\theta-\theta_{\text{cor}})}{D+A\sin(\theta-\theta_{\text{cor}})}, & 275° \le \theta < 340° \end{cases} \tag{6-15}$$

where D is the distance between the sensor and the vehicle center,

$$A = \sqrt{\left(\frac{L}{2}\right)^2 + \left(\frac{W}{2}\right)^2} \tag{6-16}$$

$$\theta_{\text{cor}} = \arctan\frac{L}{W} \tag{6-17}$$

The comparison of the simulated peak positions and the measured peak positions for Caddy in 20 m at different heading angles is shown in Figure 6.22 as example.

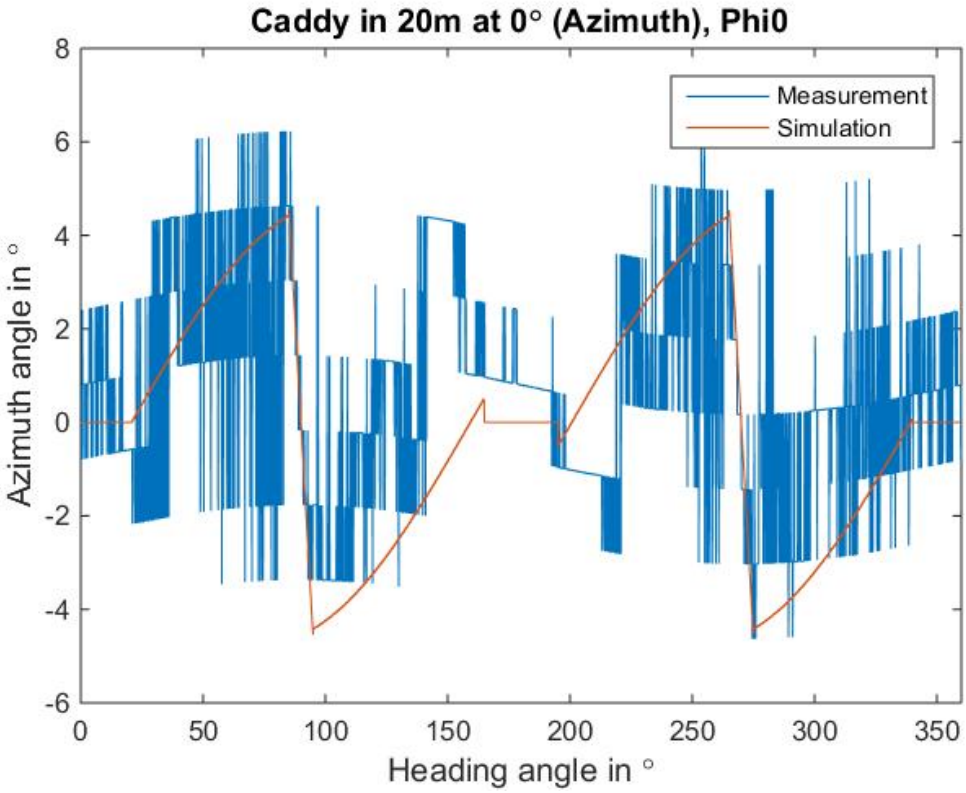

Figure 6.22 Simulated peak positions of receiving power from VW Caddy at different heading angles

In modeling, the difference between the corner positions of a real vehicle and the ones of a cuboid template is taken into consideration. As shown in Figure 6.22, the gross curve progression is simulated.

6.5 Sensitivity Analysis

Analyzing Azimuth Angle Sensitivity

Until here, a vehicle reflectivity model for short range at an azimuth angle of 0° and a distance of 20 m is developed. In the following, the influences of azimuth angle and distance on it are investigated.

Figure 6.23 shows the peak amplitudes of the receiving power from Volkswagen Caddy at different azimuth angles.

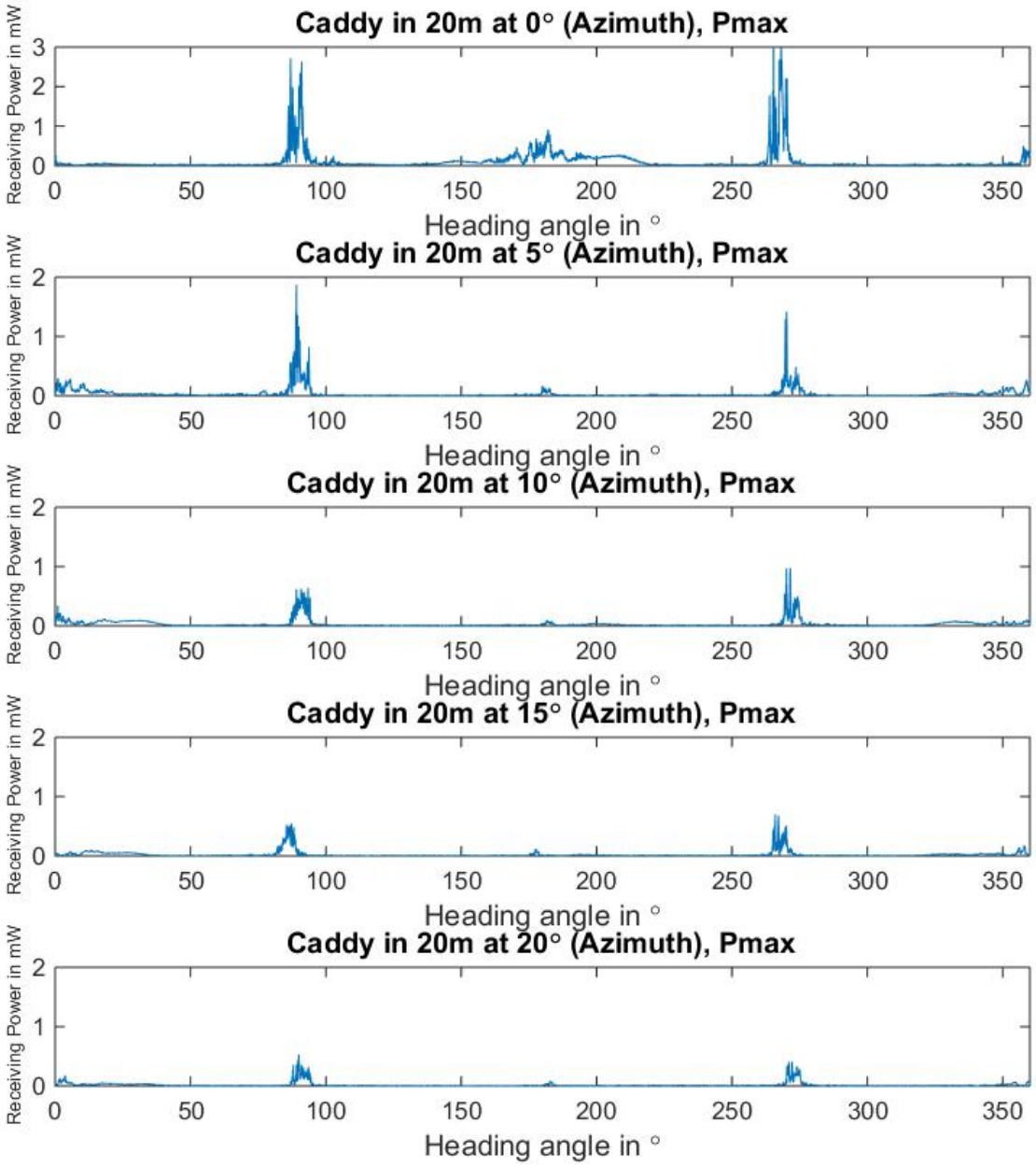

Figure 6.23 The peak amplitudes of receiving power from Volkswagen Caddy at different azimuth angles and heading angles

Obviously, the common characteristics are copied in each diagram. However, the Amplitude of the peaks in the diagrams reduces with the increasing azimuth angle. Es indicates the influences of radiation pattern. As the radiation pattern is sensor-specific, a generic modeling is not necessary. In modeling of the radar to be modeled, the peak amplitudes at the other azimuth angles will be interpolated.

Figure 6.24 shows the integral of the receiving power distribution from Volkswagen Caddy at different azimuth angles.

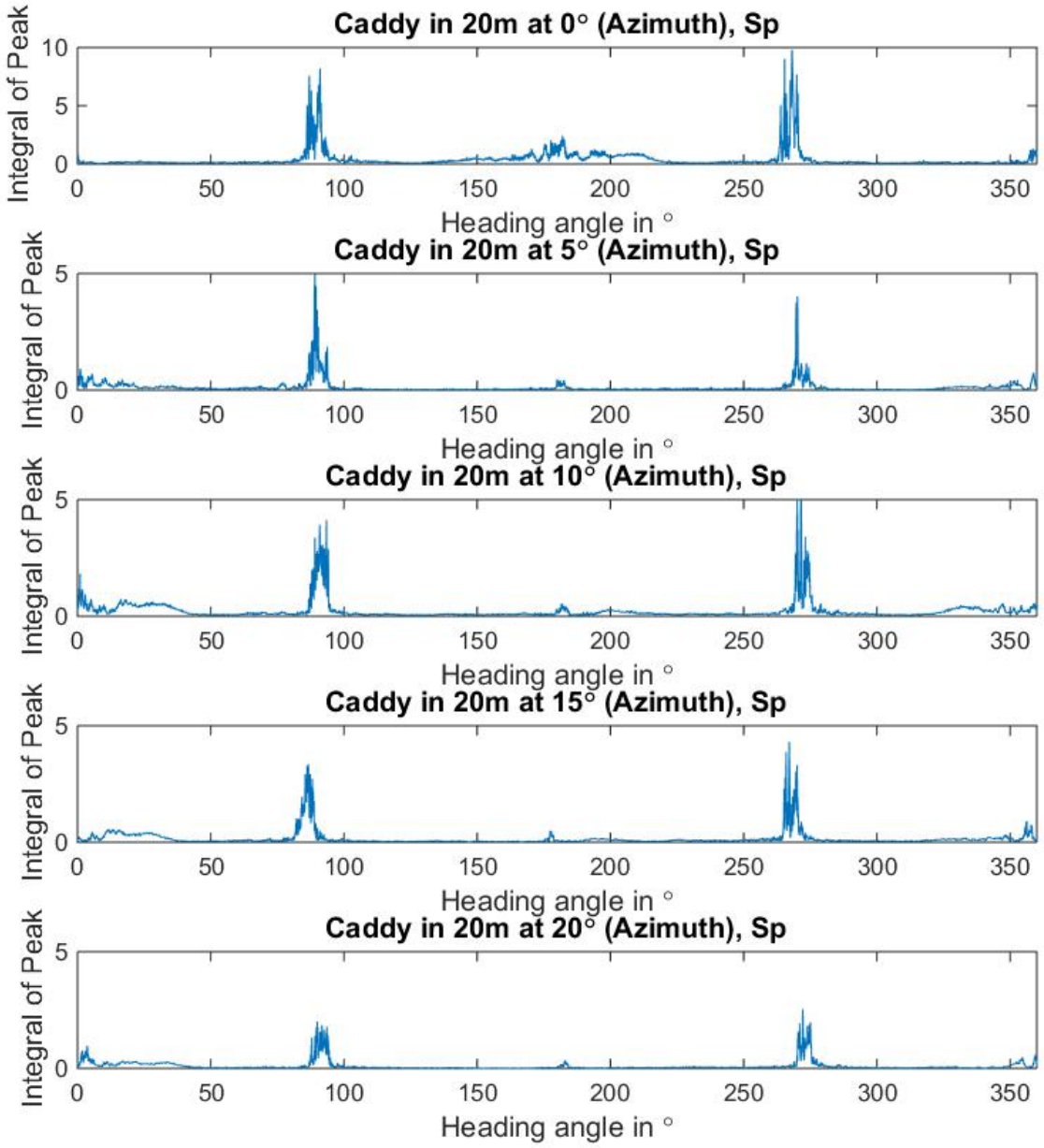

Figure 6.24 The integral of the receiving power distribution from Volkswagen Caddy at different azimuth angles and heading angles

Obviously, the common characteristics are copied in each diagram as well. As done for the peak amplitudes, in modeling of the radar to be modeled, the integral of the receiving power distribution at the other azimuth angles will be interpolated as well.

Figure 6.25 shows the peak positions of the receiving power from Volkswagen Caddy at different azimuth angles.

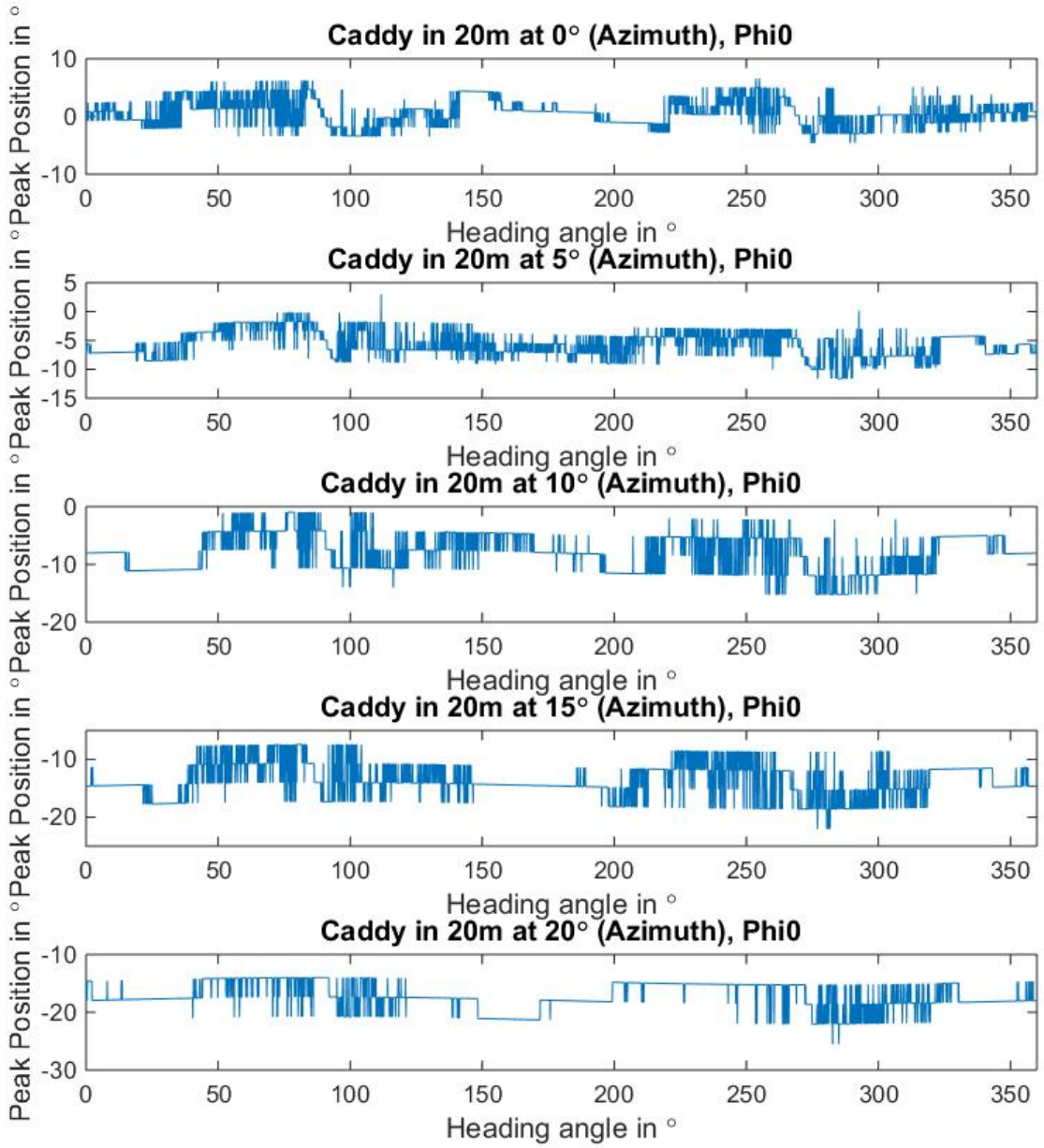

Figure 6.25 The peak positions of the receiving power from Volkswagen Caddy at different azimuth angles and heading angles

The linear movements of the peak positions from right side to left side in heading angle ranges of [85°, 95°], [265°, 275°] are copied. For modeling the other parts, the equation 6-15 should be extended as follows:

$$\phi_0(\theta) = \begin{cases} \arctan\frac{D\sin(\phi_v) - A\cos(\theta+\theta_{\text{cor}}-\phi_v)}{D\cos(\phi_v) - A\sin(\theta+\theta_{\text{cor}}-\phi_v)}, & 20° \le \theta < 85° \\ \arctan\frac{D\sin(\phi_v) - A\cos(\theta-\theta_{\text{cor}}-\phi_v)}{D\cos(\phi_v) - A\sin(\theta-\theta_{\text{cor}}-\phi_v)}, & 95° \le \theta < 165° \\ \arctan\frac{D\sin(\phi_v) + A\cos(\theta+\theta_{\text{cor}}-\phi_v)}{D\cos(\phi_v) + A\sin(\theta+\theta_{\text{cor}}-\phi_v)}, & 195° \le \theta < 265° \\ \arctan\frac{D\sin(\phi_v) + A\cos(\theta-\theta_{\text{cor}}-\phi_v)}{D\cos(\phi_v) + A\sin(\theta-\theta_{\text{cor}}-\phi_v)}, & 275° \le \theta < 340° \end{cases} \quad (6\text{-}18)$$

where ϕ_v is the azimuth angle of the vehicle center.

Thus, Figure 6.26 shows the simulation result as an example.

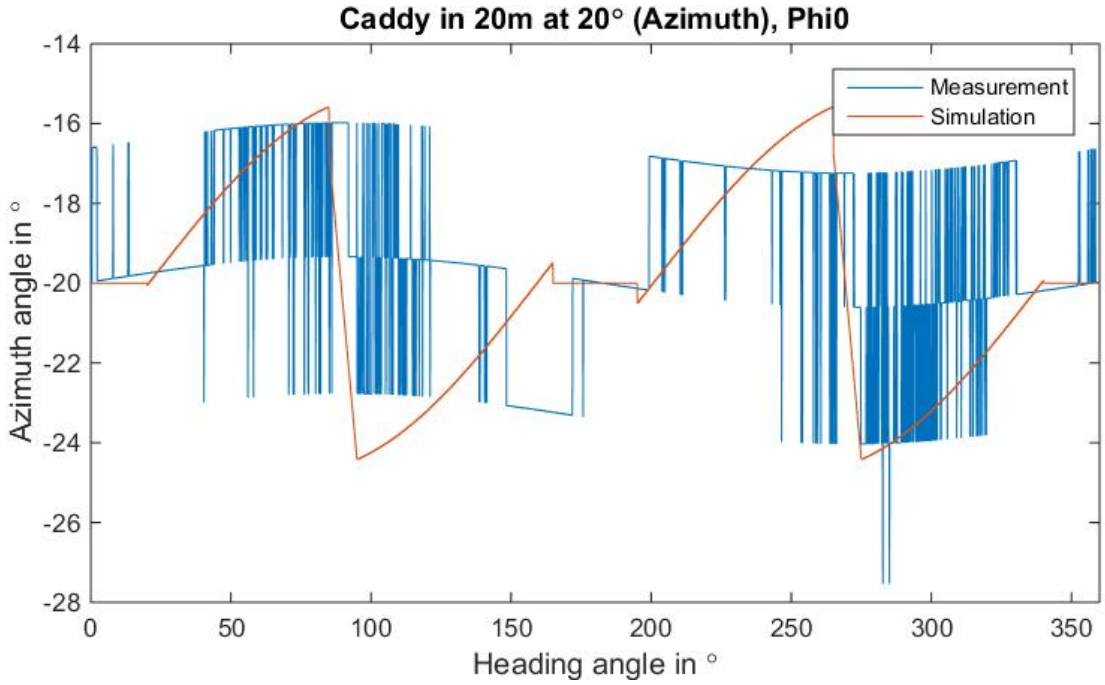

Figure 6.26 Simulated peak positions of receiving power from VW Caddy at an azimuth angle of 20°

Analyzing Distance Sensitivity

Figure 6.27, Figure 6.28 and Figure 6.29 show respectively the peak amplitudes, the integral of distributions and the peak positions of the receiving power from Volkswagen Caddy in different distances.

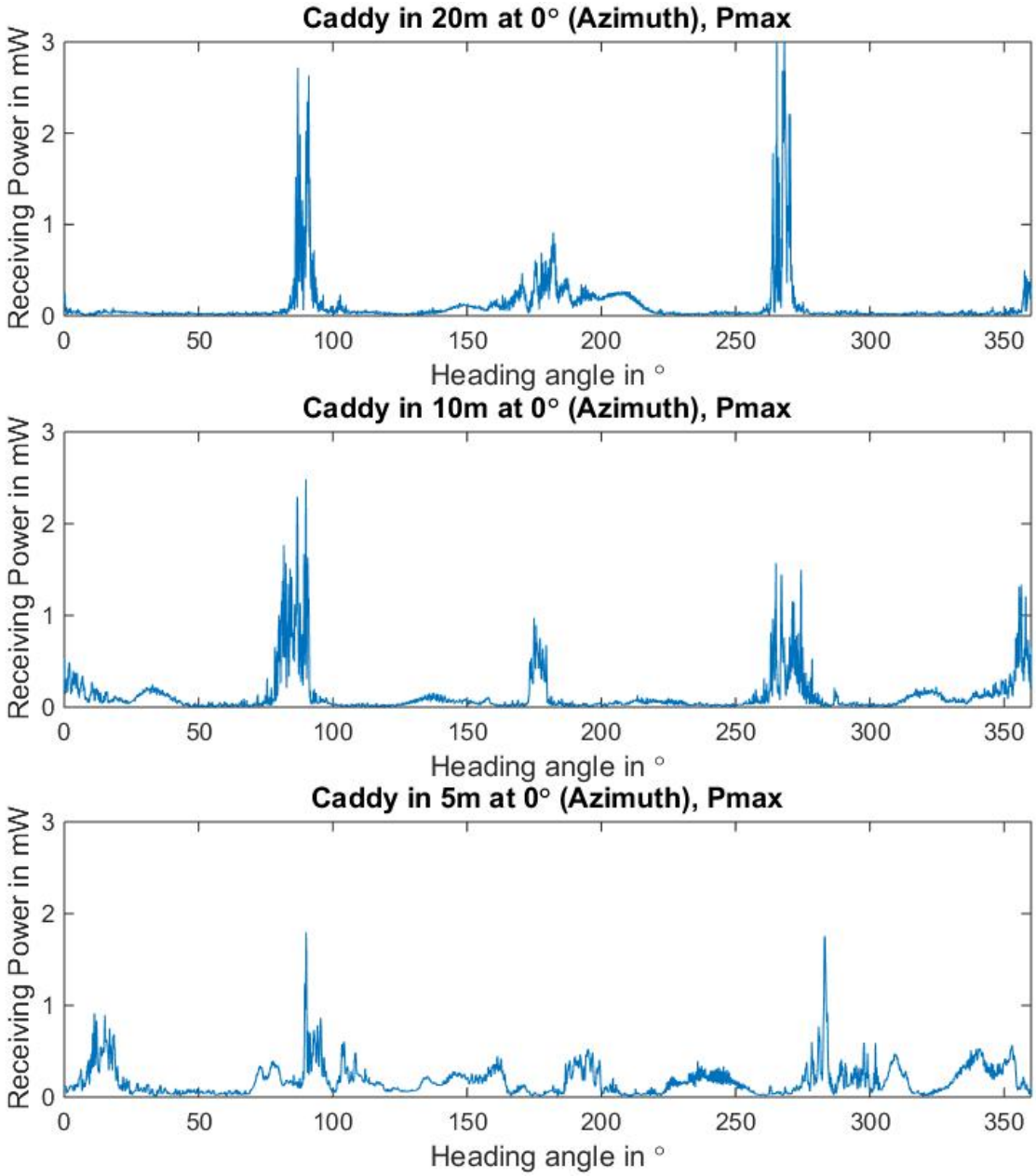

Figure 6.27 The peak amplitudes of receiving power from Volkswagen Caddy in different distance and at different heading angles

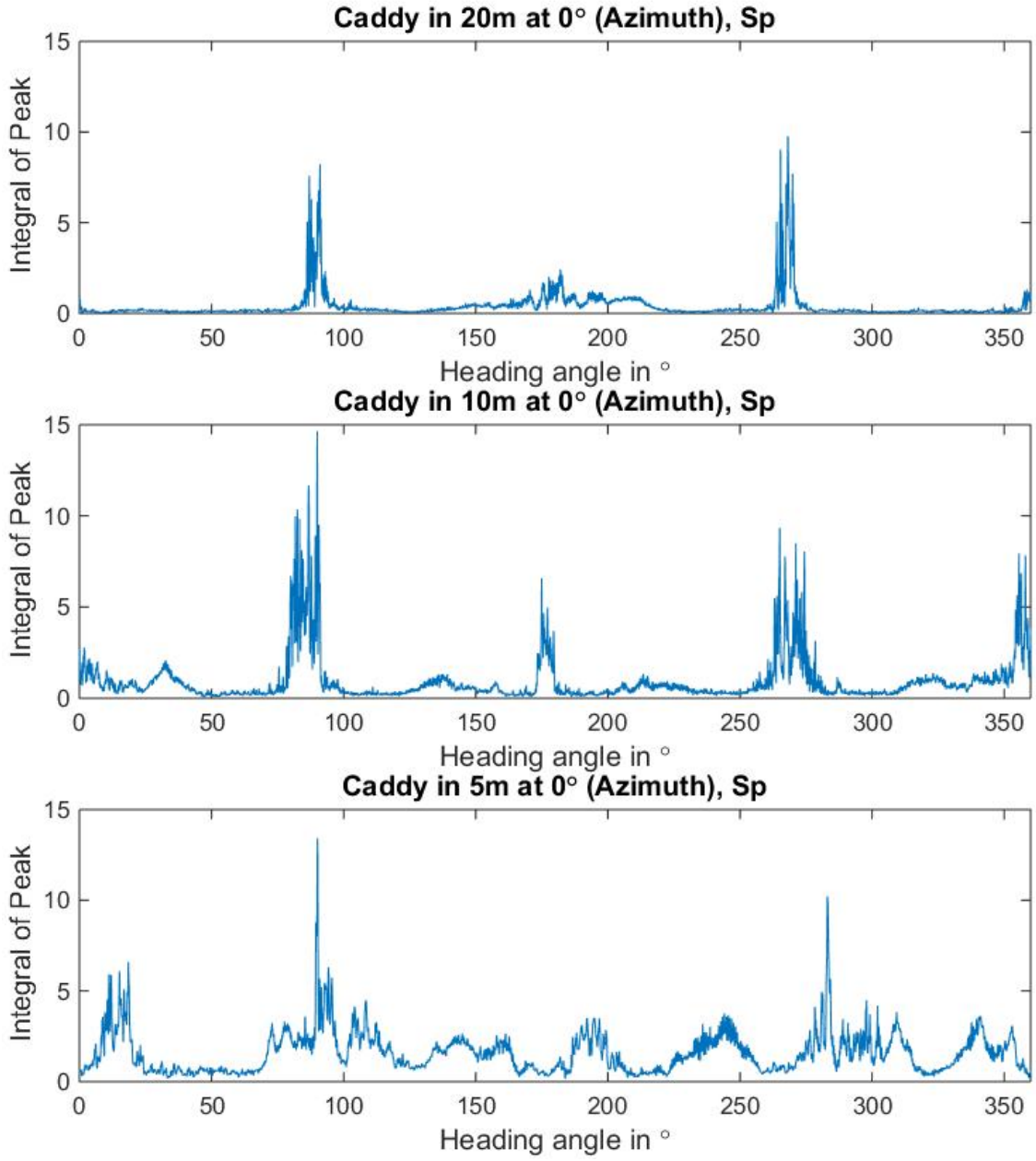

Figure 6.28 The integral of the receiving power distribution from Volkswagen Caddy in different distance and at different heading angles

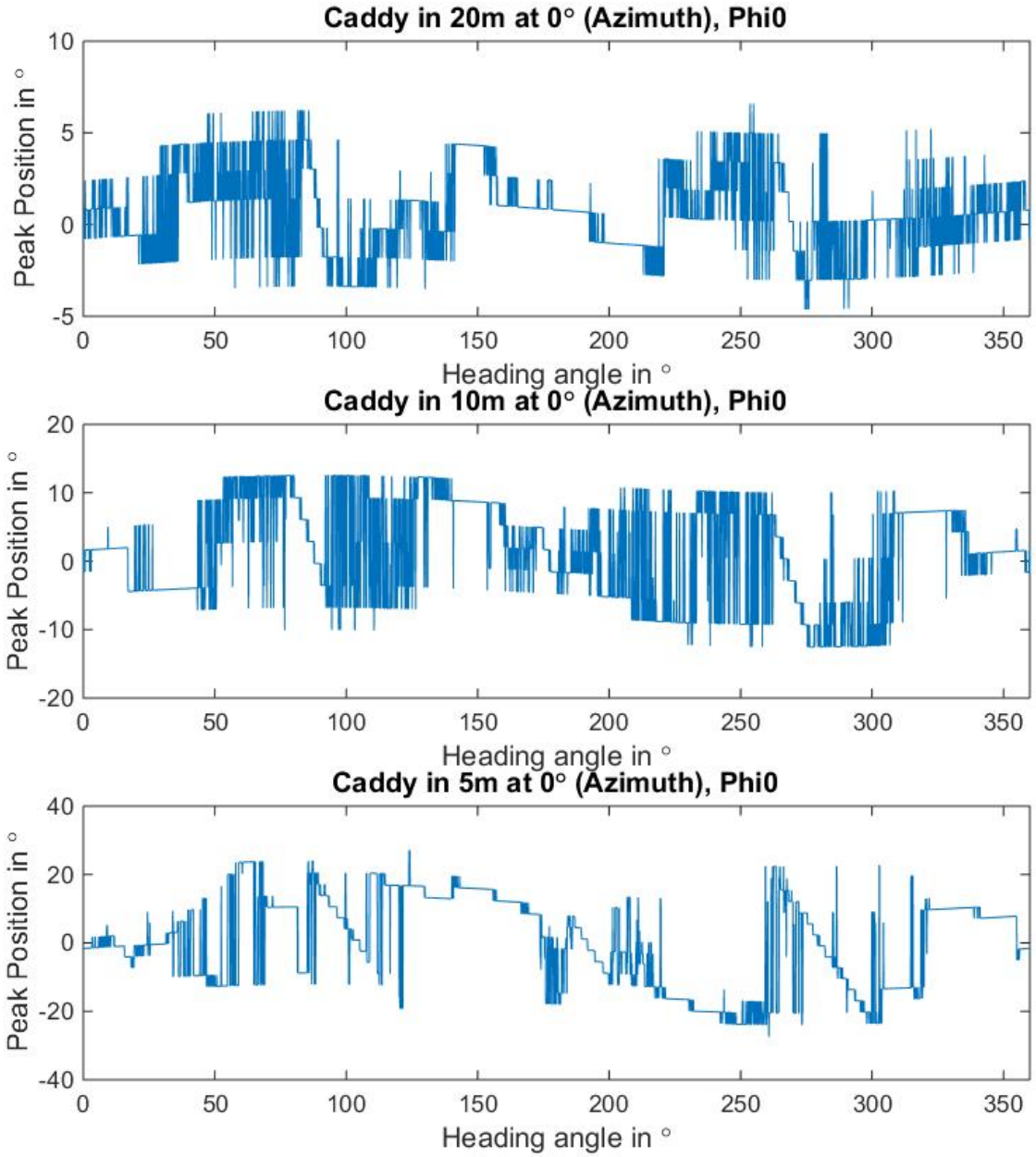

Figure 6.29 The peak positions of the receiving power from Volkswagen Caddy in different distance and at different heading angles

Obviously, the common characteristics are copied from the measurement results in 20 m to 10 m. However, the measurement results in a distance of 5 m have not totally inherited these common characteristics. It could be caused by the multiple reflections, their interference and the diffuse reflections in the extremely near range. These effects are not modeled in this dissertation anymore for two reasons:

1) In this extremely near range, because of the high receiving power and SNR, the detection and the measurement are robust. The modeling of dynamic sensor performance is less meaningful than in the other cases.

2) At such a distance, a specified azimuth angle corresponds to a width of 0.28 m - 0.4 m. A false separation of object will hardly lead to a false-positive of a drivable area.

Until here, the vehicle reflectivity model for short range with regard to the radar to be modeled is developed.

6.6 Summary

Till this step, except the distance sensitivity of the receiving power from the objects in the short range area, the object reflectivity model is completed. A generic modeling of the reflectivity of different vehicles is on the basis of a model calibration possible.

For modeling the reflectivity of an object in the long range area, calibration measurements of its RCS at the heading angles 0°, 20°, 90°, 160° and 180° are required. With these measurement results, the reflectivity of the object at other heading angles can be generated.

For representing the reflectivity of an object in the short range area, a modeling of the distribution of the signal power, which is received from the object surface at different heading angles, distributed over azimuth angles is executed. For modeling the receiving power distribution over azimuth angles at a certain heading angle, a Gaussian distribution is used. Its form is decided by the maximum receiving power at this heading angle $P_{\max}$, the integral of the reiceiving power over azimuth angle S_{p} and the position of the maximum receiving power in azimuth angle ϕ_0. The changing of these three parameters with the heading angle is modeled as well.

For modeling the $P_{\max}$ and S_{p}, their corresponding values at a heading angle of 0°, 90° and 180° should be measured for calibrating the model. For modeling the azimuth angle sensitivity of the $P_{\max}$ and S_{p}, their corresponding values at a heading angle of 0°, 90° and 180° and different azimuth angles (here as example: 0°, 5°, 10°, 15°, 20°) should be measured for calibrating the model. The smaller the measurement step in azimuth angle is, the higher the modeling fidelity could be. The modeling of the distance sensitivity of $P_{\max}$ and S_{p} will be discussed in Chapter 7.

For modeling the ϕ_0, the length and the width of the vehicle to be modeled, as well as the azimuth angle of the object and the distance between the sensor and the vehicle should be measured at first.

7 Model Verification

Till this part of the dissertation, the grey-box modeling of the radar to be modeled is implemented. All the components discussed above are created and integrated into the sensor model. To verify the functionality of this model, three different tests are executed: direct object approaching, object approaching in curve driving and the detection of neighboring objects. These test cases represent three representative use cases, where automotive perception sensors must face the problems of the dynamic performances as described in Section 3.1. Therefore, they are chosen to verify if the created model has fulfilled the requirements of dynamic performance modeling set at the beginning. Direct object approaching is aimed at verifying the modeling of the dynamic behavior of the received power with the changing distance between the sensor and the object. Object approaching in curve driving is mainly aimed at verifying the modeling of the dynamic behavior of the received power with the changing relative aimuth angle and heading angle between orientation of the sensor and the object. Finally, the detection test of neighboring objects can be used to verify if the separation capability of the sensor and its dynamic behavior related to the object heading angles are modeled realistically. To have a deterministic verification result and simple error identification, the comparison between simulation and measurement is not happened on the level of statistical performance criteria, but on the raw data level.

7.1 Direct Object Approaching

In the experiments of direct object approaching, two different reflectors are chosed as object. One of them is a corner reflector, and the other is a real vehicle, a VW Caddy. The corner reflector is used to verify, whether the signal interference discussed above can be observed, and whether its effect can be exactly described by Equation (5-3). The VW Caddy is used, on one hand, for a continuous analysis of the distance sensitivity of the received power, which was not possible in Chapter 6. On the other hand, the measurement results of the VW Caddy is used for verifying the grey-box model as well.

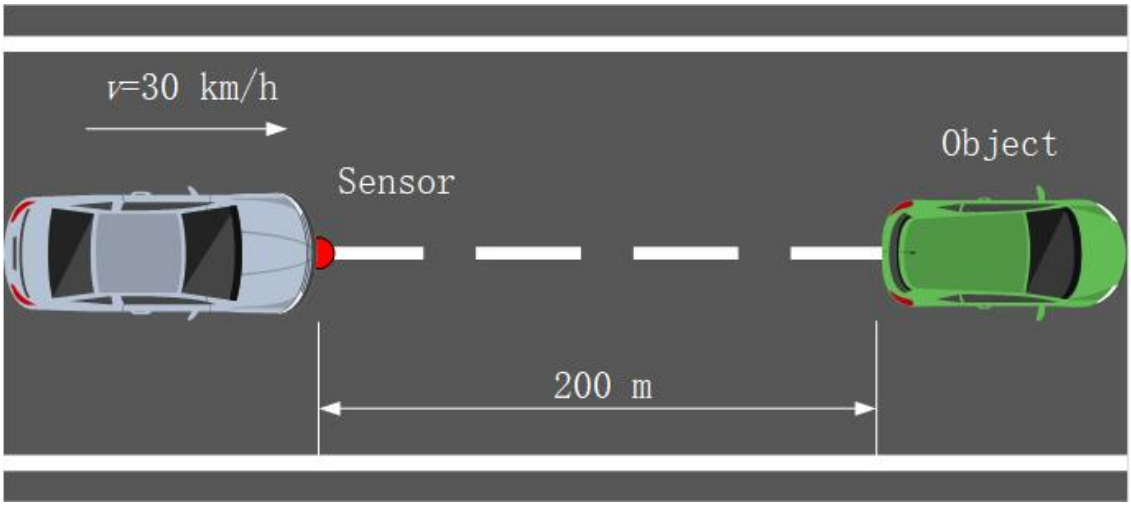

Figure 7.1 Direct object approaching

Figure 7.1 represents the execution of the experiment. The sensor to be modeled is fixed on a vehicle with a height of 52 cm (as same as the sensor height when measuring the vehicle reflectivity). The corner reflector (diagonal dimension: 24 cm) has a height of 52 cm as well. As the sensor to be modeled has a detection range of 200 m, the approaching starts from this distance. The approaching is executed at a very low velocity (about 30 km/h), so that the influence of object tracking algorithm can be reduced as much as possible. Furthermore, in this way, the more measurement data can be obtained for the same distance. Thus, the influence of noise can be reduced. For a further reduction of the influence from stochastic errors, each experiment is repeated for five times.

The first group of experiments is executed by using corner reflector as object. The five repeated measurements show good reproducibility. The measured Power of the cell with maximum receiving power P_{max} from corner reflector and r^{-4} hypothesis according to the radar equation with regard to distance and the reciprocal of distance is as Figure 7.2 shows. Due to its small dimension in latitude, the corner reflector is detected in the most cases as point object. From this point of view, P_{max} is able to represent the receiving power from the corner reflector. The r^{-4} curve is calibrated according to the P_{max} of the reflector in 20 m.

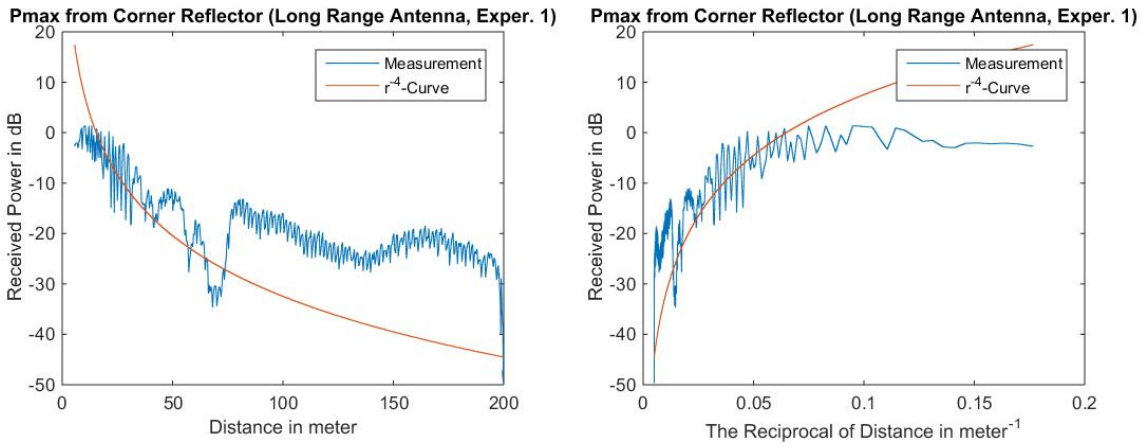

Figure 7.2 Power of the cell with maximum receiving power from the corner reflector and r^{-4} hypothesis (with regard to distance (left figure) and the reciprocal of distance (right figure))

Figure 7.2 shows that P_{max} from the corner reflector reduces over proportionally with the increasing of the distance, which conform to a large extent to the r^{-4}-hypothesis in radar equation. However, in the right figure, it is obvious, that the measured received power is lower than the hypothesis in short range. It can be caused by the cell size of the radar. In short range, the corner reflector is larger than a cell, so the receiving power from reflector is divided into more than one cell. In this way, power of the cell with maximum receiving power P_{max} indicates just a part of the receiving power (lower than real receiving power), and therefore, cannot represent the receiving power from the corner reflector any more.

Furthermore, the waves in the curves could be caused by the interference of multi-path reflections. However, according to Formula (5-3), the peak period of the wave caused by interference should be about 0.0072 m^{-1} (when $h_s = h_R = 0.52$ m). Obviously, in the long range area, the received power can still show a similar period. In the short range area, the period is reduced. In the short range area, the corner reflector cannot be considered as a point-reflector anymore and has to calculated more in detail by its field strength coverage function[93]. However, the sensor can still not separate the corner reflector as more than one object. Therefore, the received power from the corner reflector presented in Figure 7.2 is principally a result of the sum of the signal power reflected from different reflecting areas on the corner reflector. To verificate this point of view, a simple simulation experiment is executed. Without considering the r^{-4}-principle, the influence of the dimension of the corner reflector in height can be calculated by the integral of Formula (5-3) over the height of reflector:

$$\int_{h_0}^{h_1} 16\sin^4\left(\frac{2\pi \cdot h_s \cdot h_R}{\lambda \cdot R}\right) d_{h_R} \tag{7-1}$$

[93] Skolnik, M. I.: Radar Handbook (2008).

where, h_0 is the height of the lowest point of the corner reflector. h_1 is the height of the highest point of the corner reflector. In this experiment, h_0 = 0.41 m, h_1 = 0.63 m.

The result is as Figure 7.3 shows.

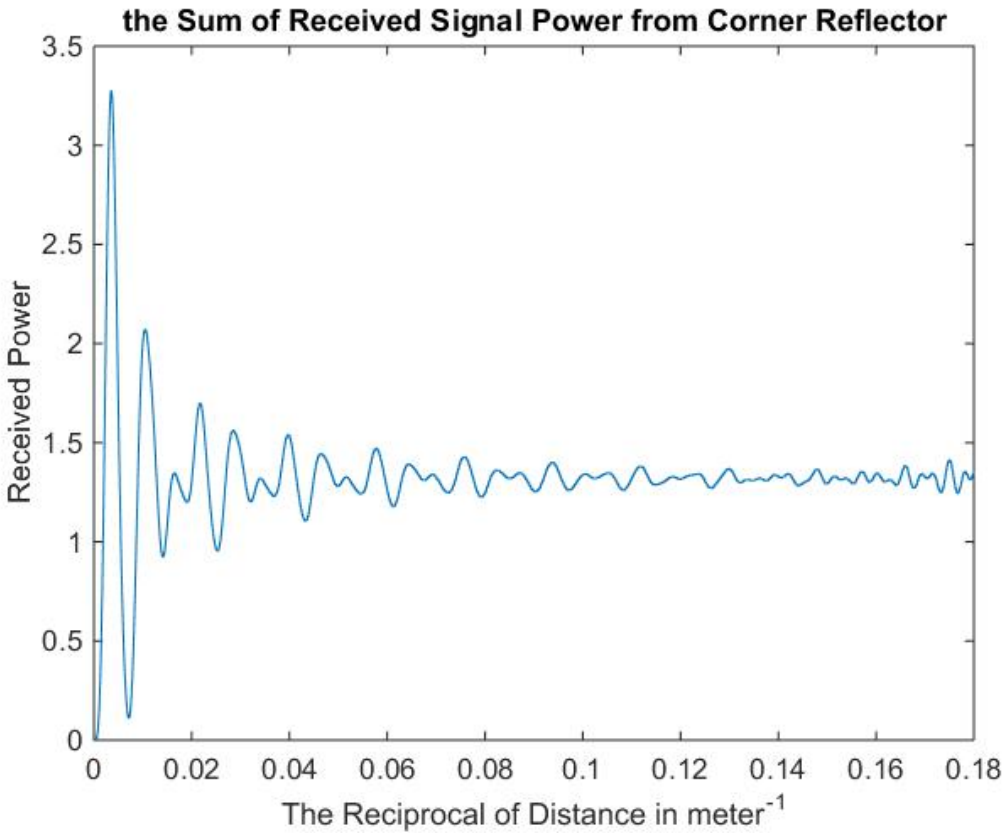

Figure 7.3 Simulation for the total power of the received signal from corner reflector

Obviously, the period of the peaks is reduced to a comparable level to the measurement.

The second group of experiments is executed by using VW Caddy as object.

Due to the dimension of a real vehicle in longitude and latitude, the total receiving power should be represented by the integral of receiving power distribution S_p (see Section 6.4). It is an accumulation of the power of the cells, which stay in a range between the minimum and the maximum range of the vehicle, and meanwhiles at an azimuth angle between the minimum and the maximum azimuth angle of the vehicle. The integral of the receiving power distribution from VW Caddy and r^{-4} hypothesis with regard to distance and the reciprocal of distance is as Figure 7.4 shows. The r^{-4} curve is calibrated according to the S_p of VW Caddy in 20 m.

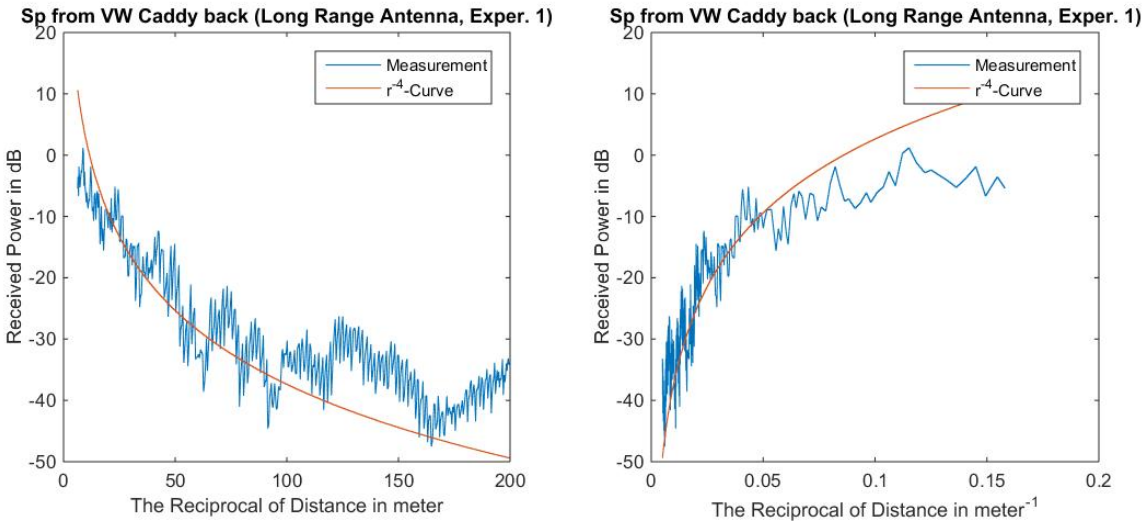

Figure 7.4 The integral of the receiving power distribution from VW Caddy and r^{-4} hypothesis (with regard to distance (left figure) and the reciprocal of distance (right figure))

Obviously, the measured receiving power is lower than the r^{-4} hypothesis in short range area. On the one hand, this can be caused by limited aperture of the long range antenna. In extrem short range, the sensor can only illuminate a part of the vehicle surface. On the other hand, the angle of incidence of the wave on most parts of vehicle surface increases with reducing range, and most waves are reflected away. Thus, the reflectivity of the vehicle is reduced, and therefore, the receiving power is lower than the hypothesis.

Just like the corner reflector, the back side of VW Caddy shows an "interference wave" in the long range area. In the short range area, the peak period is reduced as well. As discussed above, this effect can also be explained by the sum of the signal amplitudes reflected by different reflecting areas on the back side of VW Caddy. As shown in the right figure of Figure 7.4, the period of the wave between 0.028 m^{-1} and 0.076 m^{-1} is almost constant (with totally 17 peaks in this range area). Therefore, a wave with a period of about 0.003 m^{-1} ((0.076 m^{-1} - 0.028 m^{-1})/17 = 0.003 m^{-1}) and a amplitude of about 5 dB (observed from the figure) in the short range area can represent the distance sensitivity of the received power in the short range. The peak amplitudes $P_{\max}$ in Section 6.4 can be modulated by this wave to simulate this effect.

The received power simulated by the grey-box model is as Figure 7.5 shows.

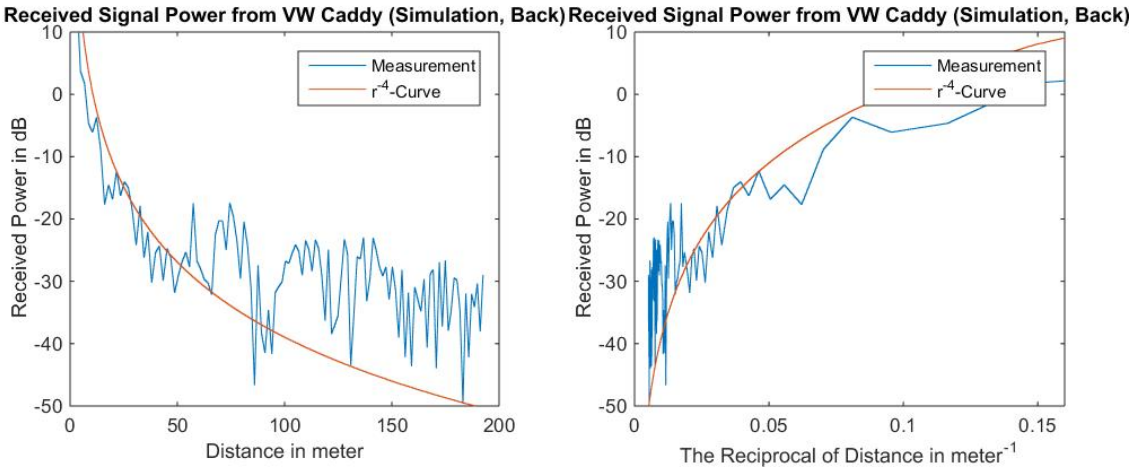

Figure 7.5 Simulation of received signal power from VW Caddy (Back Side) and r^{-4} hypothesis (with regard to distance (left figure) and the reciprocal of distance (right figure))

Comparing Figure 7.5 and Figure 7.4, the decreasing tendency of received power with increasing distance is represented. The interference effect with a peak period of about 0.0072 m^{-1} in the long range area is simulated. The wave with a peak period of about 0.003 m^{-1} in the short range area is reproduced as well. However, the simulated wave amplitude in the long range area is higher than the reality. It could be caused by the simplification in modeling the road reflectivity, which is defned as “1” here. The modeled reflectivity is higher than the reality, which leads to the more significant constructive and destructive effect of interference in the simulation.

7.2 Object Approaching in Curve Driving

In this experiment, the vehicle approaches the object vehicle (VW Caddy) in curving driving. The objective of this experiment is to verify if the model can represent the dynamic receiving power under changing heading- and azimuth angle.

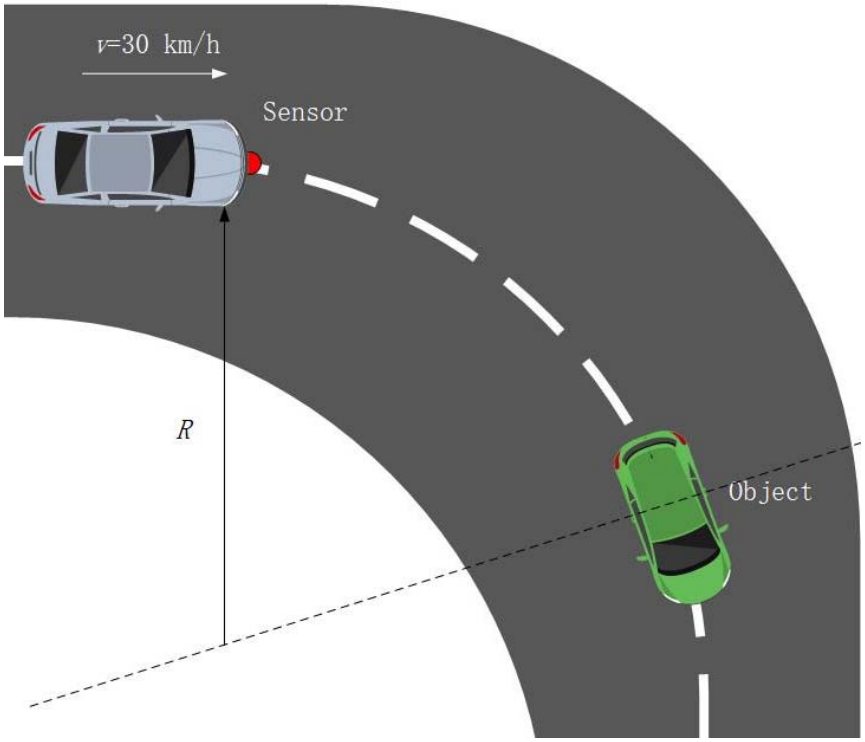

Figure 7.6 Object approaching in curve driving

Figure 7.6 represents the execution of the experiment. The sensor to be modeled is fixed on a vehicle with a height of 52 cm (as same as the sensor height when measuring the vehicle reflectivity). To verify the sensor model in realistic use cases, the standard curve radiuses for testing ACC systems are used. As defined in ISO 15622, the curve radiuses of 125 m and 250 m for testing class III and class IV ACC systems are chosen. The curve radius of 500 m for testing class II ACC systems is neglected, because the influence of heading angle under large curve radius is not as significant as under the others. Like the direct object approaching, the approaching is executed at a very low velocity (about 30 km/h. Each experiment is repeated for five times and simulated in IPG CarMaker® (see Figure 7.7).

Figure 7.7 Curve driving in real world vs. in simulation

For the representation of the experiment result, the heading angle of the object vehicle should be calculated.

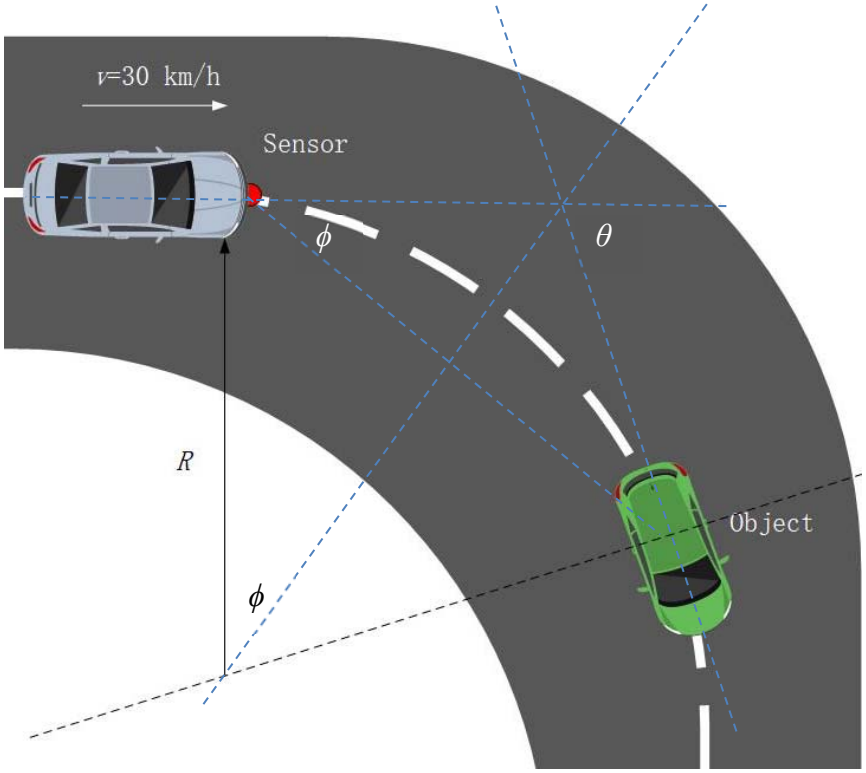

Figure 7.8 Calculation of heading angle

Figure 7.8 shows how the heading angle is calculated. The azimuth angle ϕ of the object can be measured by the sensor. According to the Figure 7.8, a static relationship between azimuth angle ϕ and heading angle θ of the object in this experiment exists, which can be described as follows:

$$\theta = 2\phi \tag{7-2}$$

Figure 7.9 shows the measured receiving power from VW Caddy under different heading angles and the r^{-4} hypothesis based on the radar equation (see Section 2.2.1). The r^{-4} curve is calibrated to the measured receiving power at the maximum heading angle. The curve radius is 125 m. For representing the influence of heading- and azimuth angle on received power better, the maximum receiving power $P_{\max}$ from the vehicle is plotted.

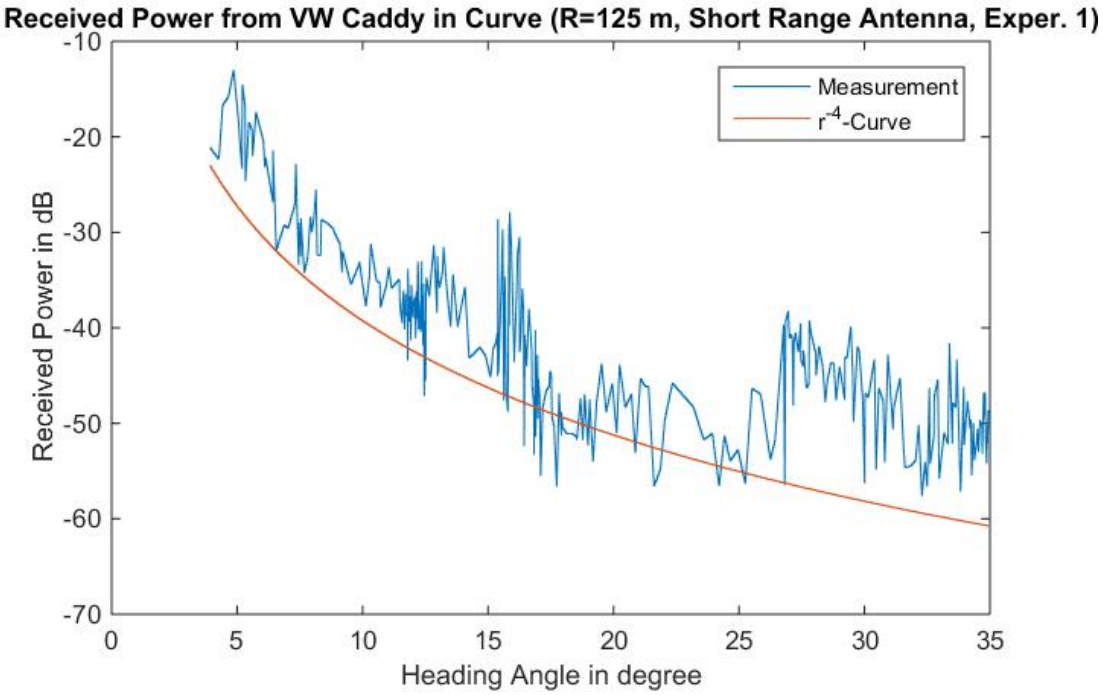

Figure 7.9 Received power from VW Caddy in curve driving and the r^{-4} hypothesis (with regard to heading angle)

Figure 7.9 shows three main characteristics.

1) The received power increases over proportionally with the decreasing of heading angle. Compared to the r^{-4} curve, its increasing rate is higher at small heading angles. This indicates the raising reflectivity of the object with the decreasing of heading angle.
2) At the start point, the sensor is about 70 m far away from the object. Compared to Figure 7.4, the received power is much lower, which can also be explained by the influence of heading and azimuth angle.

Figure 7.10 shows the simulated data. Obviously, all the main characteristics mentioned above are simulated. Difference exists at large heading angles (where the boundary between the short range model and the long range model is ($r \approx 70$ m). This can be caused by the interference effect in the transition area, which can be modeled neither by the long range model nor by the short range model. The sensor modeling for the transition area can be improved in the future research.

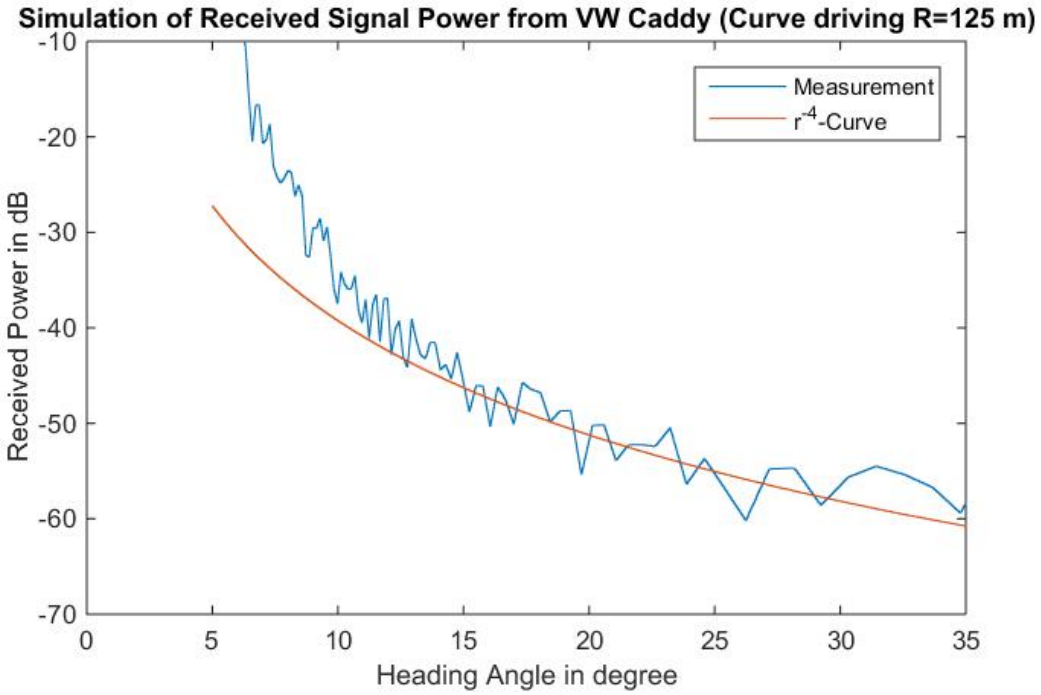

Figure 7.10 Simulation of received power from VW Caddy in curve driving and the r^{-4} hypothesis (with regard to heading angle)

7.3 Detection of Neighboring Objects

In this experiment, two neighboring objects are settled in front of the sensor for detection. The objective of this experiment is to verify the influence of heading angle on separation capability and if the model can represent the dynamic separation capability under changing heading angle.

The first step of this experiment is to identify the separation capability of the sensor for point objects (which are not sensitive to the heading angle). Two corner reflectors are 13.8 m in front of the sensor. In the experiment the azimuth angle difference between the corner reflectors is increased step by step, until a separation of the reflectors can be achieved by the sensor. Finally, as result, 4.125° is identified as the minimum separatable azimuth angle difference between the corner reflectors.

The second step is to separate real vehicles instead of point reflectors. Two vehicles are settled 13.8 m in front of the sensor. The initial azimuth angle difference between them is 4.125°. The initial heading angles of both vehicles are 90° (see Figure 7.11).

Figure 7.11 Detection of neighboring objects

However, the vehicles in initial status cannot be separated by the sensor. This phenomenon can be explained by the existence of a certain clustering algorithm in sensor data processing. After that, the heading angle of one of the vehicle is increased step by step. Till a heading angle difference of about 20°, a separation is succeeded. This proves the existence of the heading-angle-dependent movement of the reflectivity peak.

In the simulation, this experiment was reproducted. The peaks in the cell-volume, which represent the two object vehicles, are overlapped at first. With an increasing heading angle difference, they are step-by-step separated. The phenomenon in detection of neighboring objects was represented by the model well.

7.4 Simulation Efficiency

As one of the most important requirements on the sensor model, simulation efficiency should always be taken into consideration on model verification.

For the simulation of the test cases described above, a Lenovo T430 laptop[94] is used. In IPG CarMaker, the speed of the program execution can be shown on the software GUI. For all the simulations above, the speed of the program execution can reach at least 12.7 times faster than real-time.

[94] Features: CPU: Intel(R) Core(TM) i7-3520M CPU @ 2.90 GHz*2; RAM: 15.7 GB; System: Windows 7 Professional (64 Bit)

Moreover, for a further test of the simulation efficiency, the object approaching test is extended. Since the simulation efficiency depends mainly on the number of objects. The object approaching simulation is performed with different number of objects.

Table 7.1 Result of simulation efficiency test

Experiment	*Number of Objects*	*Speed of Execution*
1	1	15xRT (Real Time)
2	3	11.2xRT
3	5	9.8xRT

Obviously, with neither specific CPU nor stand alone graphic card, an accelerated simulation execution in the test cases above is possible. The requirement on the simulation efficiency of the sensor modeling is fulfilled.

8 Conclusion and Outlook

8.1 Conclusion

This work provides a novel grey-box method for modeling the active automotive perception sensors. Compared to the existing methods (white-box methods or black-box methods), this grey-box method has mainly three advantages:

1) It has the ability to simulate realistically the dynamic relationship between some external influence factors and sensor performance.
2) It is a general modelling method, which can be used for modelling most of the automotive perception sensors on the market by parameterization and calibration.
3) It ensures the simulation efficiency and makes the accelerated execution of the simulation-based ADS validation possible, without requiring high-performance computing resources.

The basis of the modelling method in this work is the Cell-Volume-Concept (CVC). By CVC, the performance of the active perception sensors can be generally represented, which makes a general modeling of the sensor performance possible. By combining CVC with dynamic signal strength in every cell, the values in the general description can be dynamically varied. Unlike the existing methods, the grey-box model is not limited by the fixed performance metrics defined in sensor specification. It uses dynamic signal strength to model the dynmic sensor performance in every specific case.

To obtain the dynamic signal strength, a wave propagation model is created. It models the relationship between the changing driving environment and the instantaneous signal strength received by the sensor. In this work, the spherical radiation, the reflection and the interference caused by multiple reflection of the electromagnetic waves are identified as essential phenomenon (influence factors) for the received signal strength and simulated. An ergodic method for increasing the simulation efficiency is provided as well.

As one of the most important simulation parts in wave propagation model, the modeling of reflection requires models for representing the object reflectivities. The reflectivity is dependent on the object heading angle, the azimuth angle in sensor view, as well as the distance between the sensor and the object when considering the multiple reflecting points on the object surface. This work provides a general description for vehicle reflectivity, which divides the detection area of a sensor into two parts: the long range area, where a general vehicle can only be detected as a point-object, and the short range area, where the multiple reflecting points on the vehicle surface should be separately treated. In this work,

a 2D modeling of object reflectivity is achieved, which means the dependence of reflectivity on the azimuth angle and the yaw angle of the objects is modeled. The influence of elevation angle, pitch angle and roll angle is not modeled yet. Furthermore, as an important part of the driving environment, the road uneveness can influence the received power as well. This work provides an efficient way to integrate road models.

According to the model verification, the simulated sensor data has shown the expected dynamic behaviors in the three test cases for the verification. In the verification test cases, the grey-box model can dynamically simulate the raw sensor data, which can make the dynamic modeling of the essential sensor performances (identified in Section 3.1) possible. Meanwhile, its simulation efficiency has reached a satisfying level.

8.2 Outlook

For the sensor performance description, GbV can be implemented beside VeP in the future research. Compared to VeP, GbV has the advantage that it can reach every surfaces and every reflecting points in the way of wave propagation without considering the affiliation or the relative position between surfaces and objects. Thus, on the one hand, the object-type-oriented reflectivity model (e. g. the vehicle reflectivity model in this work) can be generalized to general surface reflectivity model. The modelling effort can be reduced. On the other hand, the representation of multiple reflection is much easier than VeP, when the amount of the reflecting points is huge.

For the object model, on one hand, the reflectivity model can be extended to 3D. Thus, the dynamic reflectivity of the objects on the roads with changing height (e. g. mountain path) can be represented as well. On the other hand, the reflectivity model for the short range area in this work is created based on the measured data under the influence of interference. The influence is phenomenologically estimated and extrapolated according to the measurement results of verification tests. For more exact modelling, the interference effect should be isolated (e. g. by specific test facility like absorbing carpet) and separately investigated.

A Simplification of Cell-Volume for Chirp Sequence Modulation

A theoretical cell-volume of Chirp Sequence radar is in a parallelogram shape. However, because of the large slope *m* in frequency modulation, the cell-volume can be simplified as rectangle. The effect can be seen as a shift of time-to-collision by less than 0.1 s. The derivation is as follows:

$$v_{\mathrm{rel}} = \frac{c}{2}\frac{nf_{\mathrm{cell}}}{f_0} - \frac{m}{f_0}\cdot r \tag{A-1}$$

$$r = \frac{c}{2}\frac{nf_{\mathrm{cell}}}{m} - \frac{f_0}{m}v_{\mathrm{rel}} \tag{A-2}$$

$$\frac{\mathrm{d}r}{\mathrm{d}v_{\mathrm{rel}}} = -\frac{f_0}{m} \tag{A-3}$$

where $f_0 = 77\ \mathrm{GHz} \approx 10^{11}\ /\mathrm{s}$, $m = \frac{>100\ \mathrm{MHz}}{<100\ \mu\mathrm{s}} => 10^{12}\ /\mathrm{s}$

Therefore, $\frac{\mathrm{d}r}{\mathrm{d}v_{\mathrm{rel}}} \approx 0.1\ \mathrm{s}$

In case of negative slope it can be seen as an “in-build” range prediction in the same order of the needed processing time after the measurement.

B Implementation of Ergodic Stochastic Single-Point Model

To simulate the receiving power distributions from objects in the short range area of radar, ergodic stochastic single-point model is used. In each simulation cycle, a reflecting point is generated on the surface of each object in the short range area.

The receiving power from such a point is equal to $S_{\mathrm{P}}(\theta_{\mathrm{obj}})/60$, where $S_{\mathrm{P}}(\theta_{\mathrm{obj}})$ is the total receiving power that can be received from the object to be modeled at its momentanious heading angle (modeled in Section 6.4).

The position of such a reflecting point is identified stochastically by a probability density function. According to the ergodicity, the probability density function should be equal to the normalized receiving power distribution and calculated as follows:

$$p(\phi) = \frac{P_{\mathrm{Gauss}}(\phi)}{S_{\mathrm{P}}(\theta_{\mathrm{obj}})} \tag{B-1}$$

where $P_{\mathrm{Gauss}}(\phi)$ is the receiving power distribution from the object (modeled in Section 6.4). Since the receiving power distribution is modeled two-dimensionally in this work, the position of the reflecting point in elevation angle is not taken into consideration.

Since $P_{\mathrm{Gauss}}(\phi)$ is modeled by a Gaussian distribution, as mentioned in Section 6.4, and $S_{\mathrm{P}}(\theta_{\mathrm{obj}})$ is constant for a certain object heading angle, $p(\phi)$ is a Gaussian function as well. In this way, the azimuth position of the reflecting point can be generated by Box-Muller method as follows:

$$\phi_{\mathrm{ref}} = k\sqrt{-2\ln U_1}\cos(2\pi U_2) + \phi_0 \tag{B-2}$$

where k is the scale factor calculated in Equation 6-14; ϕ_0 is the peak position modeled in Section 6.4; U_1 and U_2 are two independent standard random numbers.

After repeat generating such reflecting points for 60 times and accumulating their "receiving power" with respect to their azimuth position. A representation of the receiving power distribution over azimuth angle can be achieved.

C Measurement for Radiation Pattern

To obtain the influence of the radiation pattern on receiving power, an measurement of corner reflector by the radar to be modeled at different azimuth angles is executed. Each measurement takes 30 s.

The receiving power (in dB) at different azimuth angle and its variation are shown in Table C.1:

Table C.1 Measured receiving power from corner reflector and its variation at different azimuth angles

Azimuth angle	0°	0.5°	1°	1.5°	2°	2.5°	3°	3.5°	4°
Receiving power	-8.861	-11.935	-15.236	-10.862	-12.964	-12.683	-10.846	-12.261	-12.518
Variation	0.002	0.003	0.023	0.005	0.021	0.006	0.012	0.005	0.006

Azimuth angle	4.5°	5°	5.5°	6°	6.5°	7°	7.5°	8°	8.5°
Receiving power	-17.317	-20.1	-17.387	-17.66	-13.721	-17.153	-15.874	-18.413	-17.867
Variation	0.024	0.033	0.011	0.01	0.003	0.006	0.008	0.009	0.024

Azimuth angle	9°	9.5°							
Receiving power	-11.397	-13.332							
Variation	0.002	0.004							

The receiving power is plotted in

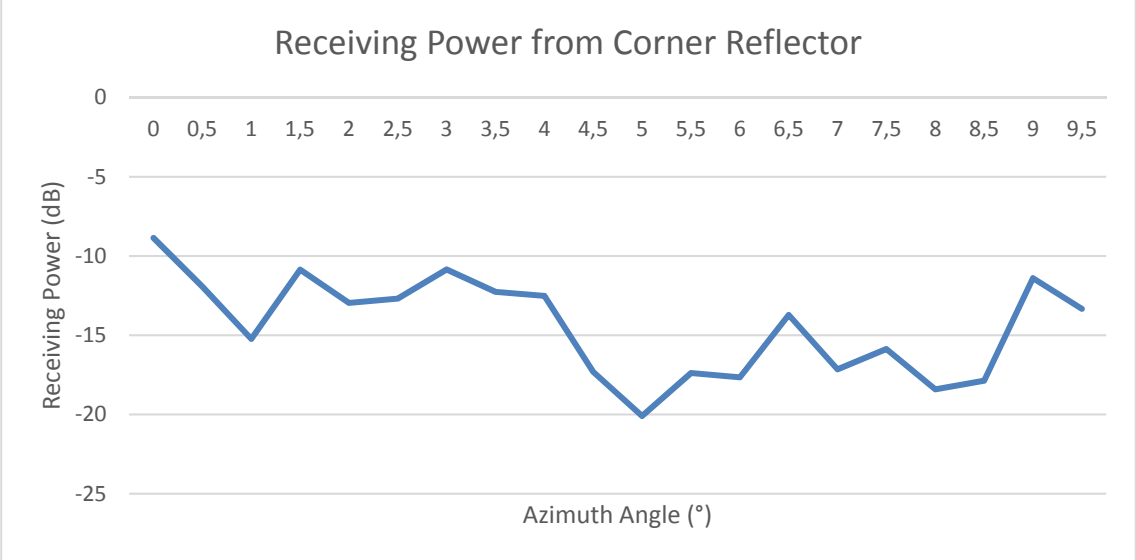

Figure C.1:

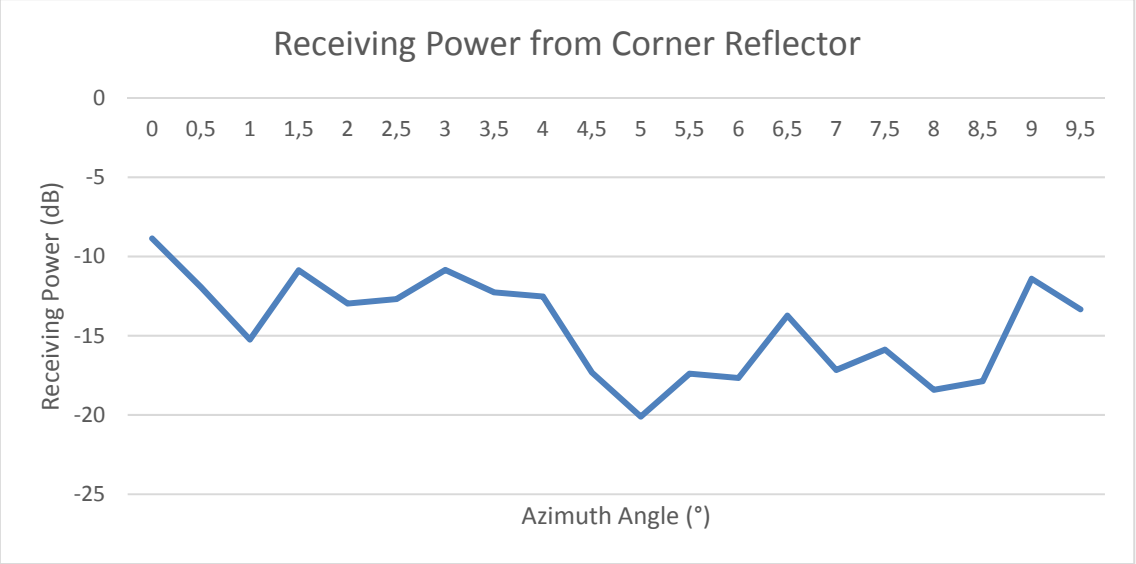

Figure C.1 Receving Power from Corner Reflector

D Measurement of Object Reflectivity in Long Range Area

According to Qin[95], the RCS information of the clusters measured by the sensor to be modeled is used for identifying the object reflectivity in long range, because a vehicle in such a range is normally detected as one point. Further investigation and modeling of the reflectivity distribution over azimuth angle are not necessary.

However, due to the rotation of the vehicle in the experiment, a significant difference between the relative velocity of different parts of the vehicle could exist. Because of the occupancy of different velocity bins, the object can be detected as more than one clusters (separation capability). To measure the total reflectivity of the object, the RCS of all these clusters should be taken into consideration. With another word, the RCS of a cluster will be accumulated to the total object reflectivity, as long as the cluster stays in a range between the minimum and the maximum range of the vehicle, and meanwhiles at an azimuth angle between the minimum and the maximum azimuth angle of the vehicle (without considering its velocity).

Since the experiment is executed on an empty open field, nothing besides the vehicle to be measured can provide a significant high RCS for detection. For this reason, the accumulation of the RCS described above will not cause much measurement error.

Thus, the RCS of an object can be calculated as follows:

$$RCS_{\mathrm{obj}} = 10 \cdot \lg\left(\sum_{i=1}^{N_{r,\phi}} 10^{\frac{RCS_i}{10}}\right) \tag{D-1}$$

where RCS_i is the RCS of the i-th cluster. $N_{r,\phi}$ is the number of the clusters, which stay in a range between the minimium and the maximium range of the vehicle, and meanwhile at an azimuth angle between the the minimium and the maximium azimuth angle of the vehicle. Because the RCS is measured in dB, an unit convertion to mW is necessary before the accumulation.

[95] Qin, L.: Master's Thesis, Untersuchung der Reflexionseigenschaften (2016).

E Measurement of Object Reflectivity in Short Range Area

Due to the limitation of the sensor data interface, the RCS distribution over azimuth angle is not available. To measure the reflectivity distribution of the object, the receiving power in the peaklist, which is available through the sensor data interface, should be used. The peaks in the peaklist from the sensor to be modeled is one-to-one corresponding to the cells in the cell-volume described in Section 4.1. Therefore, the signal power received by the sensor in each cell can be directly obtained.

Just like the measurement of object reflectivity in the long range area, the influence of the object rotation should be eliminated. The receiving power of all the relative velocity bins in the same range-azimuth cell is accumulated.

$$P_{\mathrm{R1}}(r,\phi) = \sum_{i=1}^{N_v} P_{\mathrm{R}}(r,\phi,v_i) \tag{E-1}$$

where P_{R} is the receiving power in a certain cell; N_v is the number of relative velocity bins in each range-azimuth cell; v_i is the relative velocity of the *i*-th relative velocity bin.

After that, the range-azimuth cells, whose ranges are between the maximum and the minimum range of the vehicle to be measured are taken out. The receiving power of the ones of them, which share the same azimuth angle bin, is accumulated again.

Thus, the azimuth angle-dependent receiving power can be obtained:

$$P_{\mathrm{R2}}(\phi) = \sum_{i=1}^{N_r} P_{\mathrm{R1}}(r_i,\phi) \tag{E-2}$$

where N_r is the number of the range-azimuth cells, whose range are between the maximum and the minimum range of the vehicle to be measured; r_i is the range of the *i*-th range bin.

F Simulation of RCS of Different Vehicles in Long Range

According to the method introduced in Section 6.3, the RCS of different vehicles in 70 m is modeled and shown in Figure F.1:

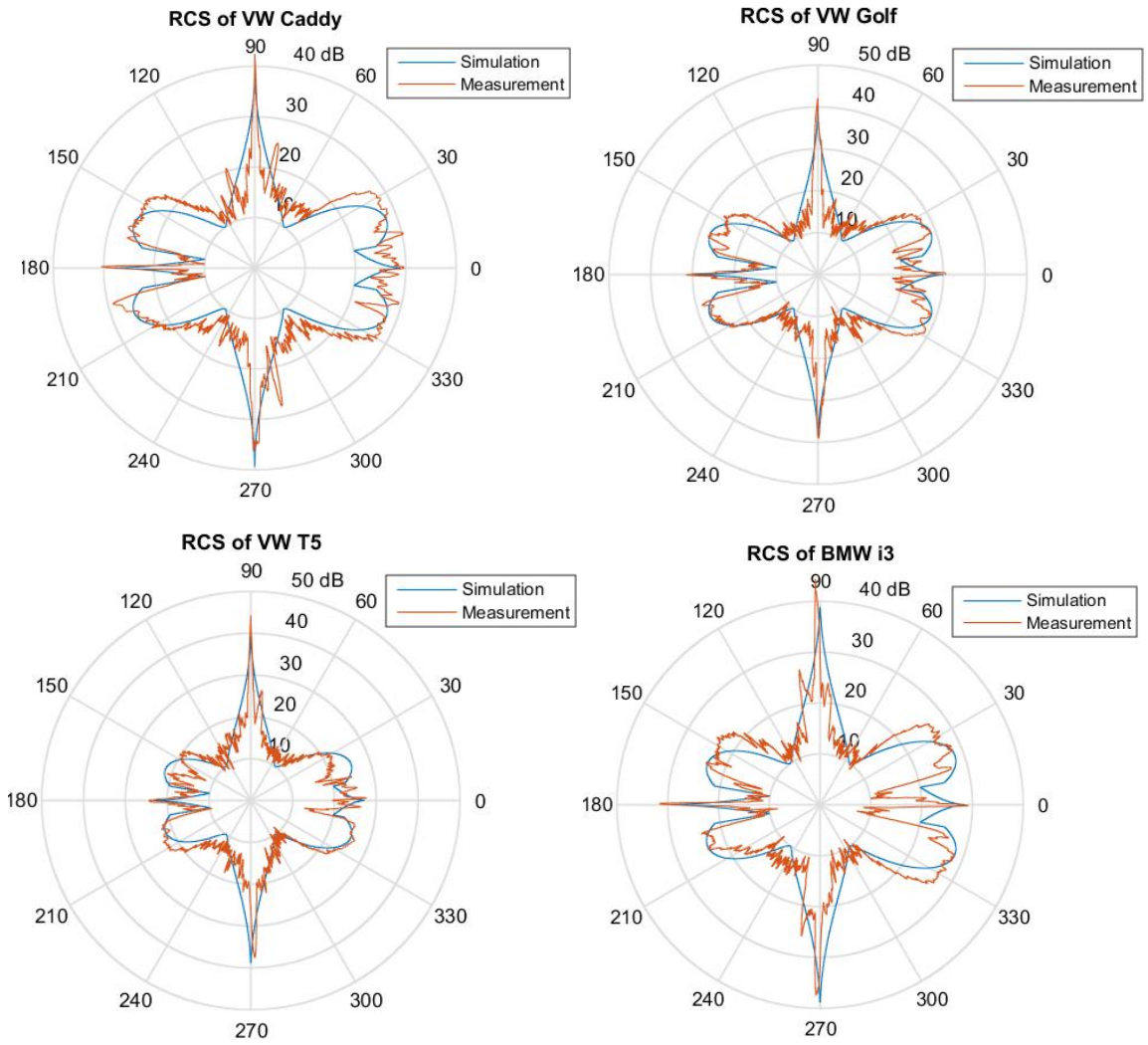

Figure F.1 RCS of different vehicles in 70 m at different heading angles

Under the assumption that all vehicles have symmetric geometry and material usage with respect to their longitudinal axes, the RCS of a vehicle should be symmetric with respect to the 0°-180° line in Figure F.1. The unsymmetry in Figure .1 can be considered as caused by measurement errors or noise.

As shown in Figure F.1, the RCS of most vehicles can be represented by the simulation well. However, the RCS of BMW i3 at a heading angle of 0° reduces more quickly than

the other three vehicles with the increasing heading angle. This phenomenon is considered as a special reflectivity characteristic of BMW i3, which cannot be described in a generic way. This phenomenon indicates the necessity of model validation when modeling the reflectivity of some vehicles with special geometric characteristics by the generic model in this work.

G Simulation of Receiving Power Distribution from Different Vehicles in Short Range

According to the method introduced in Section 6.4, the receiving power distribution from different vehicles can be generically represented by three parameters: $P_{\max}$, S_{P} and ϕ_0. These parameters can be modeled respectively. Since the ϕ_0-models are only based on geometric parameters of vehicles, which are independent of the measured data, an enumeration of these models is not necessary. The models of $P_{\max}$ and S_{P} for different vehicles in a range of 20 m and at a azimuth angle of 0° are shown as follows.

Figure G.1 shows the modeling of $P_{\max}$ for the vehicles: VW Caddy, VW Golf, BMW i3 and VW T5 in a range of 20 m and at a azimuth angle of 0°.

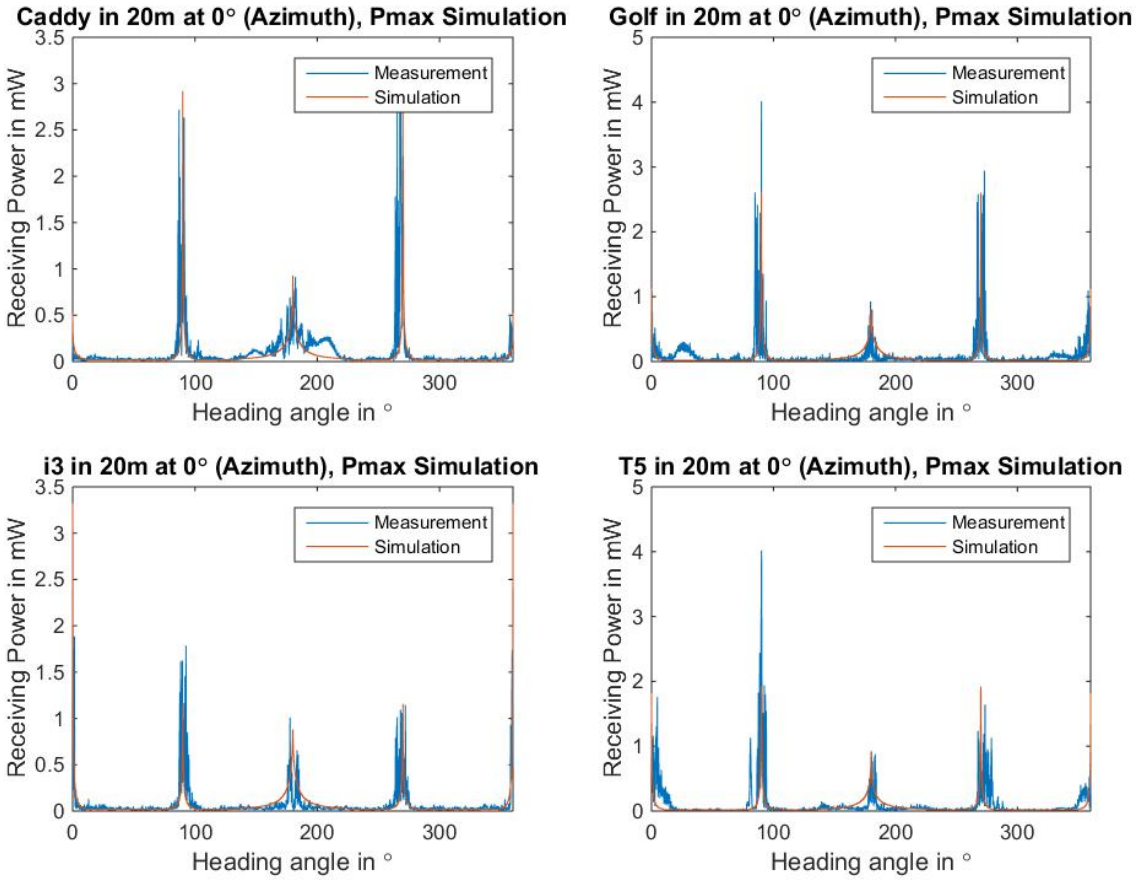

Figure G.1 Modeling of Pmax for different vehicle (r = 20 m, ϕ = 0°)

Figure G.2 shows the modeling of S_{P} for the vehicles: VW Caddy, VW Golf, BMW i3 and VW T5 in a range of 20 m and at a azimuth angle of 0°.

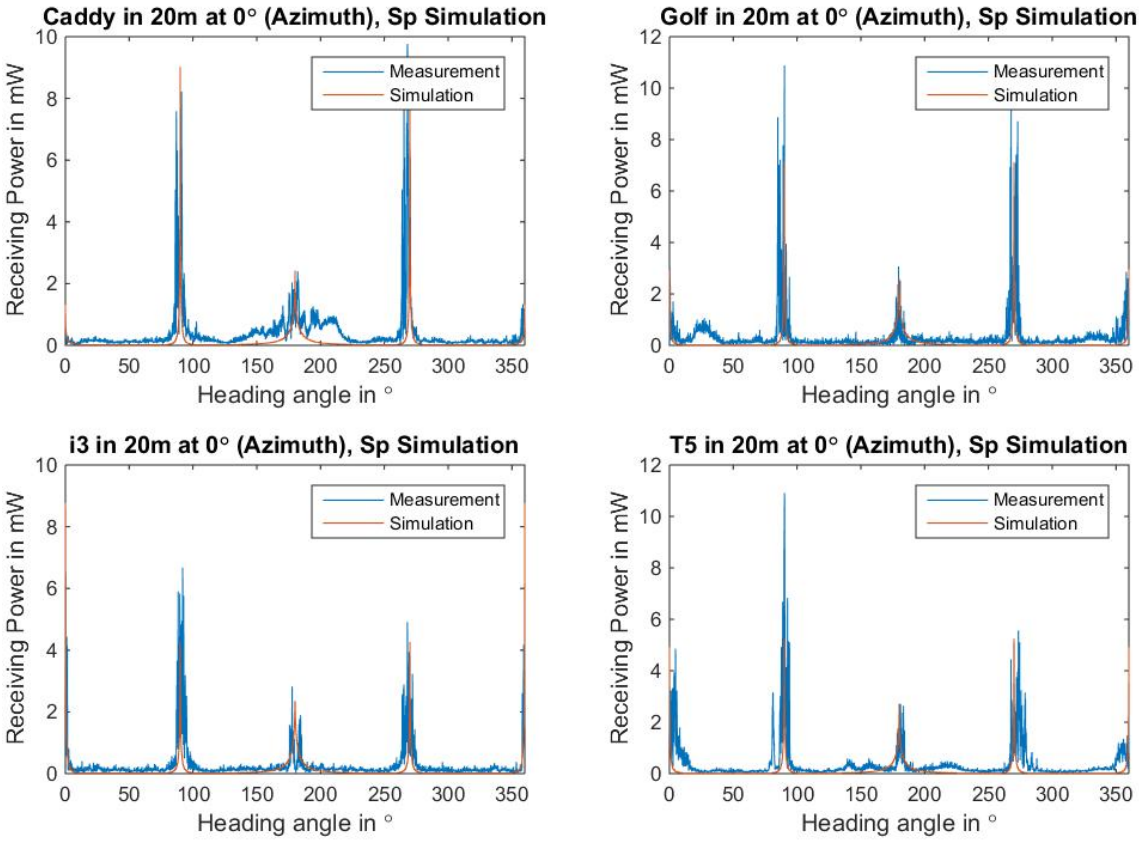

Figure G.2 Modeling of S_p for different vehicle (r = 20 m, ϕ = 0°)

Bibliography

Aeberhard, M. et al.: Lessons Learned from Automated Driving (2015)
Aeberhard, Michael; Rauch, Sebastian; Bahram, Mohammad; Tanzmeister, Georg; Thomas, Julian; Pilat, Yves; Homm, Florian; Huber, Werner; Kaempchen, Nico: Experience, Results and Lessons Learned from Automated Driving on Germany's Highways, in: IEEE Intelligent Transportation Systems Magazine (1), Issues 7, pp. 42–57, 2015

Andres, M.: Diss., Charakterisierung komplexer Ziele (2015)
Andres, Markus: Charakterisierung komplexer Ziele für breitbandige Automobile 77/79 GHz-Radarsensoren, Dissertation Universitat Ulm, 1. Edition, Cuvillier, E, Göttingen, Niedersachs, 2015

Baake, U. et al.: Testing and Simulation-based Validation (2014)
Baake, Uwe; Wüst, Klaus; Maurer, Markus; Lutz, Albert: Testing and Simulation-based Validation of ESP Systems for Vans, in: ATZ worldwide (2), Issues 116, pp. 30–35, 2014

Barton, D. K.: Radar system analysis and modeling (2004)
Barton, David K.: Radar system analysis and modeling, Artech House, Boston, Mass. [u.a.], 2004

Bartsch, A. et al.: Pedestrian recognition (2012)
Bartsch, A.; Fitzek, F.; Rasshofer, R. H.: Pedestrian recognition using automotive radar sensors, in: Advances in Radio Science, Issues 10, pp. 45–55, 2012

Bernsteiner, S. et al.: Radarsensormodell für den virtuellen Entwicklungsprozess (2015)
Bernsteiner, Stefan; Magosi, Zoltan; Lindvai-Soos, Daniel; Eichberger, Arno: Radarsensormodell für den virtuellen Entwicklungsprozess, in: ATZelektronik (2), Issues 10, pp. 72–79, 2015

Blackman, S. S.: Multiple-target tracking (1986)
Blackman, Samuel S.: Multiple-target Tracking with Radar Applications, Artech House, Dedham, MA, 1986

BMW: BMW 7er Limousine : Fahrerassistenz (2017)
BMW AG: BMW 7er Limousine : Fahrerassistenz; http://www.bmw.de/de/neufahrzeuge/7er/limousine/2015/fahrerassistenz.html, 2017, Access 12.10.2017

Buddendick, H.; Eibert, T. F.: Radio Channel Simulations (2005)
Buddendick, H.; Eibert, T. F.: Radio Channel Simulations Using Multiple Scattering Center Models, in: 2005 IEEE 61st Vehicular Technology Conference, 2005

Burgmeier, T.: BUMAT Drehbühnen Autodrehbühnen (2017)
Burgmeier, Timo: BUMAT Drehbühnen Autodrehbühnen; http://www.bumat.com/d/produkte/drehbuehnen/drehbuehnen.html, 2017, Access 13.10.2017

Cambridge Dictionary: Performance (2017)
Cambridge Dictionary: Performance Meaning in the Cambridge English Dictionary; http://dictionary.cambridge.org/dictionary/english/performance, 2017, Access 13.10.2017

Cao, P. et al.: Perception Sensor Modeling (2015)
Cao, Peng; Wachenfeld, Walther; Winner, Hermann: Perception Sensor Modeling for Virtual Validation of Automated Driving, in: it - Information Technology (4), Issues 57, 2015

Cook, R. L. et al.: Distributed Ray Tracing (NY : ACM, 1984)
Cook, Robert L.; Porter, Thomas; Carpenter, Loren: Distributed Ray Tracing, in: Christiansen, Hank (Ed.): Proceedings of the 11th annual conference on Computer graphics and interactive techniques, ACM, New York, NY, NY : ACM, 1984

Daimler: Mercedes-Benz Intelligent Drive (2017)
Daimler AG: Mercedes-Benz Intelligent Drive; https://www.mercedes-benz.com/de/mercedes-benz/innovation/mercedes-benz-intelligent-drive/, 2017, Access 12.10.2017

Darms, M. et al.: Classification and tracking (2008)
Darms, Michael; Rybski, Paul; Urmson, Chris: Classification and tracking of dynamic objects with multiple sensors for autonomous driving in urban environments, in: Intelligent Vehicles Symposium, 2008 IEEE, IEEE Xplore, [Piscataway, N.J.], 2008

Diewald, F.: Diss., Objektklassifikation und Freiraumdetektion (2013)
Diewald, Fabian: Objektklassifikation und Freiraumdetektion auf Basis bildgebender Radarsensorik für die Fahrzeugumfelderfassung, Dissertation Universität Ulm, Universität Ulm, 2013

Donges, E.: Aspekte der aktiven Sicherheit (1982)
Donges, Edmund: Aspekte der aktiven Sicherheit bei der Führung von Personenkraftwagen, in: AUTOMOB-IND (2), Issues 27, 1982

Donges, E.: Driver Behavior Models (2016)
Donges, Edmund: Driver Behavior Models, in: Winner, Hermann et al. (Eds.): Handbook of Driver Assistance Systems, Springer International Publishing, Cham, 2016

dSPACE: ASM Traffic (2017)
dSPACE GmbH: ASM Traffic; https://www.dspace.com/shared/data/pdf/2017/dSPACE_ASM_Traffic_Product_information_2017_English.pdf, 2017, Access 12.10.2017

Fuchs, F.: Diss., Entwicklung und Verifikation eines RCS-Rechenmodells (2001)
Fuchs, Frank: Entwicklung und Verifikation eines RCS-Rechenmodells basierend auf den finiten Differenzen im Zeitbereich (FDTD) mit dem Ziel der Hybridisierung mit der Physikalischen Optik (PO), Dissertation Universität des Saarlandes, DLR, Köln, 2001

Geduld, G.: Lidarsensorik (2012)
Geduld, Georg: Lidarsensorik, in: Winner, Hermann; Hakuli, Stephan; Wolf, Gabriele (Eds.): Handbuch Fahrerassistenzsysteme [Elektronische Ressource], Vieweg+Teubner Verlag, Wiesbaden, 2012

Gubelli, D. et al.: Ray-tracing Simulator for Radar (2013)
Gubelli, Demetrio; Krasnov, Oleg A.; Yarovyi, Olexander: Ray-tracing Simulator for Radar Signals Propagation in Radar Networks, in: 2013 European Radar Conference, 2013

Gupte, S. et al.: Detection and classification of vehicles (2002)
Gupte, S.; Masoud, O.; Martin, R.F.K.; Papanikolopoulos, N. P.: Detection and classification of vehicles, in: IEEE Transactions on Intelligent Transportation Systems (1), Issues 3, pp. 37–47, 2002

Hanke, T. et al.: Generic Architecture for Simulation (2013)
Hanke, T.; Hirsenkorn, N.; Dehlink, B.; Rauch, A.; Rasshofer, R.; Biebl, E.: Generic Architecture for Simulation of ADAS Sensors, in: 2013 IEEE Nuclear Science Symposium and Medical Imaging Conference (2013 NSS/MIC), 2013

Hirano, T.: FDTD (2017)
Hirano, Takuichi: FDTD; http://www.takuichi.net/em_analysis/fdtd/fdtd.html, 2017, Access 12.10.2017

Hirsenkorn, N. et al.: A Non-parametric Approach (2015)
Hirsenkorn, N.; Hanke, T.; Rauch, A.; Dehlink, B.; Rasshofer, R.; Biebl, E.: A Non-parametric Approach for Modeling Sensor Behavior, in: 2015 16th International Radar Symposium (IRS), 2015

Hirsenkorn, N. et al.: Virtual Sensor Models (2016)
Hirsenkorn, Nils; Hanke, Timo; Rauch, Andreas; Dehlink, Bernhard; Rasshofer, Ralph; Biebl, Erwin: Virtual Sensor Models for Real-time Applications, in: Advances in Radio Science, Issues 14, pp. 31–37, 2016

IPG: CarMaker (2015)
IPG Automotive GmbH: CarMaker; https://ipg-automotive.com/de/, 2015, Access 13.01.2015

IPG: CarMaker (2017)
IPG Automotive GmbH: CarMaker; https://ipg-automotive.com/de/produkte-services/simulation-software/carmaker/, 2017, Access 12.10.2017

IPG: Complex Scenarios for the Future (2017)
IPG Automotive GmbH: Complex Scenarios for the Future of Autonomous Driving; https://press.ipg-automotive.com/fileadmin/user_upload/content/Download/Press_Release/2017/20170612_IPG_Automotive_PR_Sensormodels_EN.pdf, 2017, Access 12.10.2017

ISO/TC 204: ISO 17387:2008 (2008)
ISO/TC 204 Intelligent transport systems: ISO 17387:2008 Intelligent transport systems - Lane change decision aid systems (LCDAS) - Performance requirements and test procedures, 2008

ISO/TC 204: ISO 15622:2010 (2010)
ISO/TC 204 Intelligent transport systems: ISO 15622:2010 Intelligent transport systems - Adaptive Cruise Control systems - Performance requirements and test procedures, 2010

ISO/TC 204: ISO 15623:2013 (2013)
ISO/TC 204 Intelligent transport systems: ISO 15623:2013 Intelligent transport systems - Forward vehicle collision warning systems - Performance requirements and test procedures, 2013

ISO/TC 22/SC 32: ISO 26262-1:2011 (2011)
ISO/TC 22/SC 32 Electrical and electronic components and general system aspects: ISO 26262-1:2011 Road vehicles -- Functional safety -- Part 1: Vocabulary, 2011

Johnston, D. V.; Tarjan, P. N.: CS348b Final Project (2006)
Johnston, Douglas V.; Tarjan, Paul N.: CS348b Final Project: Ray-tracing Interference and Diffraction; https://graphics.stanford.edu/wikis/cs348b-06/DougJohnston/FinalProject?action=AttachFile&do=get&target=diffraction-JohnstonTarjan.pdf, 2006, Access 12.10.2017

Kajiya, J. T.: The Rendering Equation (NY : ACM, 1986)
Kajiya, James T.: The Rendering Equation, in: Evans, David C. (Ed.): Proceedings of the 13th annual conference on Computer graphics and interactive techniques, ACM, New York, NY, NY : ACM, 1986

Kammel, S. et al.: Team AnnieWAY's autonomous system (2008)
Kammel, Sören; Ziegler, Julius; Pitzer, Benjamin; Werling, Moritz; Gindele, Tobias; Jagzent, Daniel; Schröder, Joachim; Thuy, Michael; Goebl, Matthias; Hundelshausen, Felix v.; Pink, Oliver; Frese, Christian; Stiller, Christoph: Team AnnieWAY's autonomous system for the 2007 DARPA Urban Challenge, in: Journal of Field Robotics (9), Issues 25, pp. 615–639, 2008

Khammari, A. et al.: Vehicle detection combining gradient analysis (2005)
Khammari, A.; Nashashibi, F.; Abramson, Y.; Laurgeau, C.: Vehicle detection combining gradient analysis and adaboost classification, in: 2005 IEEE intelligent transportation systems conference, IEEE, 2005

Köhler, M. et al.: Feasibility of automotive radar (2013)
Köhler, Mike; Hasch, Jürgen; Blöcher, Hans L.; Schmidt, Lorenz-Peter: Feasibility of automotive radar at frequencies beyond 100 GHz, in: International Journal of Microwave and Wireless Technologies (01), Issues 5, pp. 49–54, 2013

Kühn, M.; Hannawald, L.: Driver Assistance and Road Safety (2016)
Kühn, Matthias; Hannawald, Lars: Driver Assistance and Road Safety, in: Winner, Hermann et al. (Eds.): Handbook of Driver Assistance Systems, Springer International Publishing, Cham, 2016

Li, Q. et al.: A Sensor-Fusion Drivable-Region (2014)
Li, Qingquan; Chen, Long; Li, Ming; Shaw, Shih-Lung; Nuchter, Andreas: A Sensor-Fusion Drivable-Region and Lane-Detection System for Autonomous Vehicle Navigation in Challenging Road Scenarios, in: IEEE Transactions on Vehicular Technology (2), Issues 63, pp. 540–555, 2014

Li, Y.: Master's Thesis, Modellierung der Unebenheit (2015)
Li, Yong: Modellierung der Unebenheit der realistischen Fahrbahnen für die Untersuchung der Ausbreitung der Strahlen von Kfz-Umfeldsensoren, Master's Thesis
TU Darmstadt, Darmstadt, 2015

Lincoln: 2017 Lincoln MKZ Technology Features (2017)
The Lincoln Motor Company: 2017 Lincoln MKZ Technology Features - Lincoln Motor Company™ -Luxury Cars - Lincoln.com; https://www.lincoln.com/luxury-cars/mkz/2017/features/technology/, 2017, Access 12.10.2017

Liu, D. S.-M.; Hsu, C.-W.: Ray-Tracing Based Interactive Camera Simulation (2013)
Liu, Damon S.-M.; Hsu, Che-Wei: Ray-Tracing Based Interactive Camera Simulation, in: IARP (ed) International Conference on Machine Vision Applications (MVA), pp. 383–386, 2013

Ludloff, A.: Praxiswissen Radar und Radarsignalverarbeitung (2008)
Ludloff, Albrecht: Praxiswissen Radar und Radarsignalverarbeitung, Vieweg + Teubner, Wiesbaden, 2008

Majek, K.; Bedkowski, J.: Range Sensors Simulation (2016)
Majek, Karol; Bedkowski, Janusz: Range Sensors Simulation Using GPU Ray Tracing, in: Burduk, Robert et al. (Eds.): Proceedings of the 9th International Conference on

Computer Recognition Systems CORES 2015, Advances in Intelligent Systems and Computing volume 403, Springer, [Cham], 2016

Marx, B. J.: Diss., Bewertungsverfahren für die Radareigenschaften (2014)
Marx, Benjamin J.: Bewertungsverfahren für die Radareigenschaften von Personenkraftwagenkarosserien Benjamin Jakob Marx, Dissertation TU Darmstadt, VDI-Verl., Düsseldorf, 2014

NETZSCH: Peak Separation (2017)
NETZSCH: Peak Separation - NETZSCH Analysieren & Prüfen; https://www.netzsch-thermal-analysis.com/de/produkte-loesungen/software/netzsch-advanced-software/peak-separation/, 2017, Access 13.10.2017

Oxford Dictionaries: Definition of perception (2017)
Oxford Dictionaries: Perception | Definition of perception in English by Oxford Dictionaries; https://en.oxforddictionaries.com/definition/perception, 2017, Access 12.10.2017

Qin, L.: Master's Thesis, Untersuchung der Reflexionseigenschaften (2016)
Qin, Longwen: Untersuchung der Reflexionseigenschaften von Fahrzeugen für Kfz-Radars, Master's Thesis
TU Darmstadt, Darmstadt, 2016

Reuter, S.: Diss., Multi-object tracking (2014)
Reuter, Stephan: Multi-object tracking using random finite sets, Dissertation Universität Ulm, Universität Ulm, 2014

SAE: Levels of Driving Automation (2017)
SAE International: Automated Driving - Levels of Driving Automation are Defined in New SAE International Standard J3016; https://www.sae.org/misc/pdfs/automated_driving.pdf, 2017, Access 12.10.2017

Schneider, R.: Diss., Modellierung der Wellenausbreitung (1998)
Schneider, Robert: Modellierung der Wellenausbreitung für ein bildgebendes Kfz-Radar von Robert Schneider, Dissertation Universität Fridericiana Karlsruhe, 1998

Schöner, H.-P.: Challenges and Approaches for Testing (2016)
Schöner, Hans-Peter: Challenges and Approaches for Testing of Highly Automated Vehicles, in: Langheim, Jochen (Ed.): Energy Consumption and Autonomous Driving, Lecture Notes in Mobility, 1. Edition, Springer International Publishing, Cham, 2016

Schubert, R. et al.: Simulation of Sensor Models (2014)
Schubert, Robin; Mattern, Norman; Bours, Roy: Simulation of Sensor Models for the Evaluation of Advanced Driver Assistance Systems, in: ATZ worldwide (9), Issues 3, pp. 26–29, 2014

Skolnik, M. I.: Radar Handbook (2008)
Skolnik, Merrill I. (Ed.) Radar Handbook Ed. in Chief Merrill I. Skolnik, McGraw Hill, New York [u.a.], 2008

Stewart, C. et al.: A neural clustering approach (1994)
Stewart, Clayton; Lu, Yi-Chuan; Larson, Victor: A neural clustering approach for high resolution radar target classification, in: Pattern Recognition (4), Issues 27, pp. 503–513, 1994

Tarko, V.: What Is Ergodicity? (2017)
Tarko, Vlad: What Is Ergodicity?; http://news.softpedia.com/news/What-is-ergodicity-15686.shtml, 2017, Access 13.10.2017

TASS: New in PreScan (2017)
TASS International: New in PreScan; https://www.tassinternational.com/new-prescan, 2017, Access 12.10.2017

TASS: PreScan (2017)
TASS International: PreScan; https://www.tassinternational.com/prescan, 2017, Access 12.10.2017

TESIS: Sensorsimulation (2017)
TESIS DYNAware Technische Simulation Dynamischer Systeme GmbH: Sensorsimulation: Physikalische Echtzeitsimulation von ADAS-Sensoren; https://www.tesis-dynaware.com/kompetenzen/fahrerassistenzsysteme/sensorsimulation.html, 2017, Access 12.10.2017

Thrun, S. et al.: Stanley - The robot that won (2006)
Thrun, Sebastian; Montemerlo, Mike; Dahlkamp, Hendrik; Stavens, David; Aron, Andrei; Diebel, James; Fong, Philip; Gale, John; Halpenny, Morgan; Hoffmann, Gabriel; Lau, Kenny; Oakley, Celia; Palatucci, Mark; Pratt, Vaughan; Stang, Pascal; Strohband, Sven; Dupont, Cedric; Jendrossek, Lars-Erik; Koelen, Christian; Markey, Charles; Rummel, Carlo; van Niekerk, Joe; Jensen, Eric; Alessandrini, Philippe; Bradski, Gary; Davies, Bob; Ettinger, Scott; Kaehler, Adrian; Nefian, Ara; Mahoney, Pamela: Stanley, in: Journal of Field Robotics (9), Issues 23, pp. 661–692, 2006

TÜV SÜD: Functional Safety (2018)
TÜV SÜD: Functional Safety; https://www.tuv-sud.com/activity/focus-topics/functional-safety, 2018, Access 15.02.2018

Villa-Martinez, H.: Accelerating Algorithms for Ray Tracing (2006)
Villa-Martinez, Hector.: Accelerating Algorithms for Ray Tracing; https://www.researchgate.net/publication/287646188_Accelerating_Algorithms_for_Ray_Tracing, 2006, Access 12.10.2017

VIRES: VTD - VIRES Virtual Test Drive (2017)
VIRES Simulationstechnologie GmbH: VTD - VIRES Virtual Test Drive; https://vires.com/vtd-vires-virtual-test-drive/, 2017, Access 12.10.2017

VIRES: Virtual Test Drive User Manual (2017)
VIRES Simulationstechnologie GmbH: Virtual Test Drive User Manual, 2017

Wachenfeld, W.; Winner, H.: Die Freigabe des autonomen Fahrens (2015)
Wachenfeld, Walther; Winner, Hermann: Die Freigabe des autonomen Fahrens, in: Maurer, Markus et al. (Eds.): Autonomes Fahren, Springer Vieweg, 2015

Waymo: Journey – Waymo (2017)
Waymo: Journey – Waymo; https://waymo.com/journey/, 2017, Access 12.10.2017

wendweb: BASELABS Models in PreScan (2017)
wendweb GmbH: BASELABS Models for better sensor simulation in PreScan | BASELABS; https://www.baselabs.de/baselabs-models-for-prescan/, 2017, Access 12.10.2017

Winner, H.: Radarsensorik (2009)
Winner, Hermann: Radarsensorik, in: Winner, Hermann; Hakuli, Stephan; Wolf, Gabriele (Eds.): Handbuch Fahrerassistenzsysteme [Elektronische Ressource], Vieweg+Teubner, Wiesbaden, 2009

Winner, H.: Automotive Radar (2016)
Winner, Hermann: Automotive Radar, in: Winner, Hermann et al. (Eds.): Handbook of Driver Assistance Systems, Springer International Publishing, Cham, 2016

Winner, H. et al.: Handbook of Driver Assistance Systems (2016)
Winner, Hermann; Hakuli, Stephan; Lotz, Felix; Singer, Christina (Eds.) Handbook of Driver Assistance Systems, Springer International Publishing, Cham, 2016

Winner, H.; Schopper, M.: Adaptive Cruise Control (2016)
Winner, Hermann; Schopper, Michael: Adaptive Cruise Control, in: Winner, Hermann et al. (Eds.): Handbook of Driver Assistance Systems, Springer International Publishing, Cham, 2016

Xu, R.; Wunsch, D. C.: Clustering (2009)
Xu, Rui; Wunsch, Donald C.: Clustering, Wiley [u.a.], Hoboken, N.J. [u.a.], 2009

Own Publications

Cao, P., Wachenfeld, W., Winner, H.: Perception Sensor Modeling for Virtual Validation of Automated Driving, in: it-Information Technology 57(4), 243–251 (2015)

Weitzel, A.; Winner, H.; Cao, P.; Geyer, S.; Lotz, F.; Sefati, M.: Absicherungsstrategien für Fahrerassistenzsysteme mit Umfeldwahrnehmung. Berichte der Bundesanstalt für Straßenwesen Fahrzeugtechnik, Heft F98, Bergisch Gladbach, 2014

Supervised Students‘ Work

Qin, L., Mechanical and Process Engineering: Untersuchung der Reflexionseigenschaften von Fahrzeugen für Kfz-Radars. Master's Thesis Nr. 612a/16, 2016

Su, C., Mechanical and Process Engineering: Bewertung und Weiterentwicklung einer HiL-Umgebung für die Validierung einer Automotiven Applikation. Master's Thesis Nr. 591/15, 2015

Yu, X., Mechanical and Process Engineering: Entwicklung eines Testfall-Generierungsframeworks für die Validierung einer Automotiven Applikation. Master's Thesis Nr. 590/15, 2015

Albert, J., Mechanical and Process Engineering: Bewertung der Validität eines statistischen Sensormodells für Kfz-Radars. Bachelor's Thesis Nr. 1230/15, 2015

Jung, L., Mechanical and Process Engineering: Untersuchung und Modellierung der Reflexionsfähigkeit von Fahrzeugen im Fernbereich für Kfz-Radar. Bachelor's Thesis Nr. 1216/15, 2015

Wang, C., Mechanical and Process Engineering: Analyse und Vergleich der Objektdiskretisierungskonzepte für die Repräsentation der Reflexionseigenschaften eines Objekts im Fahrumfeld. Master's Thesis Nr. 577/15, 2015

Nauth, M., Business Engineering – Technical Field of Studies Mechanical Engineering: Untersuchung der Reflexionsfähigkeit von Fahrzeugen im Nahbereich für Kfz-Radar. Bachelor's Thesis Nr. 1214/15, 2015

Li, Y., Mechanical and Process Engineering: Modellierung der Unebenheit der realistischen Fahrbahnen für die Untersuchung der Ausbreitung der Strahlen von Kfz-Umfeldsensoren. Master's Thesis Nr. 569/15, 2015

Li, O., Mechatronics: Weiterentwicklung der Testcase-Matrix für die virtuelle Absicherung der Umfeldsensorik. Master's Thesis Nr. 567/15, 2015

Serifsoy, D., Mechanical and Process Engineering: Ermittlung des Entwicklungszustands der strahlbasierenden Umfeldsensierung in Fahrsituationen und Analyse der Modellierungsmöglichkeit. Study Thesis Nr. 1207/14, 2014

Wang, M., Mechanical and Process Engineering: Entwicklung eines Referenzsystems für die statischen und dynamischen Tests eines Umfeldsensormesssystems. Master's Thesis Nr. 552/14, 2014

Heide, D., Mechanical and Process Engineering: Definition und Entwicklung der für Anwendungen entscheidenden Testcases der Umfeldsensoren in einem realistisch simulierten Fahrumfeld. Master's Thesis Nr. 545/14, 2014

Yu, X., Mechanical and Process Engineering: Development and Verification of the Interface between a Perception Sensor Model and the Virtual Automobile Testing Environment. IREP Project, 2014

Wang, L., Traffic and Transport: Entwicklung und Inbetriebnahme eines adaptierbaren Messsystems für die Untersuchung der Ausbreitung elektromagnetischer Wellen im Fahrumfeld. Master's Thesis Nr. 540/13, 2013

Curriculum Vitae

Personal details

Name:	Peng Cao
Date of Birth:	09.07.1986
Place of Birth:	Shanghai, PR China

Schooling

2001 – 2004	Kongjiang High School, Shanghai, PR China

Studies

2004 – 2009	Study of Automotive Engineering Tongji University, Shanghai, PR China Degree: BACHELOR OF ENGINEERING (B. Eng.)
2009 – 2012	Study of Mechanical and Process Engineering Technical University Darmstadt, Germany Degree: MASTER OF SCIENCE (M.Sc.)

Work experience

2012 – 2017	Research Associate at the Institute of Automotive Engineering of Technical University Darmstadt